THE DIURNAL CIRCULATION OF THE THERMOSPHERE

by

C. PABLO LAGOS

B. S., Universidad Nacional Mayor de
San Marcos, Lima, Peru
(1964)

M. S., Massachusetts Institute of Technology
(1967)

SUBMITTED IN PARTIAL FULFILLMENT OF THE
REQUIREMENTS FOR THE DEGREE OF
DOCTOR OF PHILOSOPHY

at the

MASSACHUSETTS INSTITUTE OF TECHNOLOGY
(October, 1969)

Signature of Author.....
Department of Meteorology, 27 October 1969

Certified By.....
Thesis Supervisor

Accepted By.....
Chairman, Departmental Committee on Graduate Students

THE DIURNAL CIRCULATION OF THE THERMOSPHERE

by

C. Pablo Lagos

Submitted to the Department of Meteorology on 27 October 1969 in partial fulfillment of the requirement for the degree of Doctor of Philosophy.

ABSTRACT

Two studies of the thermospheric physics and dynamics are considered. In the first study a comprehensive theoretical discussion of the nature of energy sources and of the general theory of gravity-tidal wave motions in the neutral gas is given. We consider motions which are of planetary scale in the horizontal and which have time scales of order of a day or longer. For time scale of one day we derive equations which generalize the usual equations for atmospheric tides and may be used to describe the diurnal circulation of the thermosphere. Motions are classified as thermally, thermal--electromagnetically, and electromagnetically driven, according to which driving force is most important. Motions are further classified by the relative importance of viscosity and heat conduction as inviscid, transition, and diffusive regimes. For large ion drag, typical of high solar activity, we define a "thermal geoplasma regime" which describes the balance between the thermal forcing and the ion drag in the momentum equation. This motion regime is fully studied.

The dissipative processes of viscosity, heat conduction, and ion drag are briefly discussed. The physics of diabatic heating sources as they occur in the thermosphere are discussed in some detail from the macroscopic and microscopic points of view. Ionization heating efficiency for neutral particles is found to be as large as 85% and for electrons as low as 2% above 200 km. A simple and useful expression

for Joule heating in terms of neutral and drift velocities is derived. It is found that Joule heating, heating by viscous dissipation, corpuscular heating, and chemical heating can only be as large as one tenth of solar heating.

In the second study the "thermal geoplasma motion regime" forced by solar heating and infrared cooling is integrated numerically in the forced region and analytically outside the forced region. The analytical study reduces to the solution of a fourth order ordinary differential equation whose solutions are coefficients of spherical harmonics. Power series solutions satisfying the condition of no flux at $z = \infty$ are obtained. Another solution satisfying the boundedness condition for small z is obtained in integral form. The two solutions are matched at the upper and lower boundaries of the numerical integration region. The results further establish that adiabatic heating and cooling by vertical motions is the "second heat source" of Harris & Priester.

Thesis Supervisor: Reginald E. Newell
Title: Professor of Meteorology

TABLE OF CONTENTS

LIST OF FIGURES

LIST OF TABLES

PART I. THEORETICAL CONSIDERATIONS

1. INTRODUCTION

1.1 The General Circulation of the Atmosphere

The study of the general circulation of the atmosphere is the description and explanation of the characteristic properties of all circulation patterns which ever occur in the atmosphere.

The circulation patterns include the long-term time and zonally averaged circulations, synoptic features such as cyclones, anticyclones, and the jet streams, long and ultra-long waves, and tidal and gravity waves. From these, only the long-term and synoptic circulations have received more attention in the general circulation of the lower atmosphere. Long and ultra-long waves have received more attention in weather prediction. Because of a minor amount of the total energy contained in the tidal and gravity wave, they have not been considered at all in the general circulation of the lower atmosphere. Only in the thermosphere is the gravity-tidal motion a dominant feature.

The circulation pattern is described by the field of motion, temperature, radiation, and other thermodynamic variables.

There seems to be no question that the driving force of the circulation is the solar radiation. The absorption of this radiation takes place throughout the atmosphere. Most of the radiation lies

in the visible region and reaches the earth surface where it is absorbed and which in turn is transmitted to the overlying atmosphere. The remaining solar energy in the ultraviolet, soft and hard x-rays, and infrared regions is absorbed by the atmospheric gases. Some of this energy is reflected or scattered back to space and plays no further role in the energy balance of the atmosphere.

The incoming solar energy is more intense in low than in high latitudes, and the net result is therefore a considerable excess of heating in low latitudes, which causes a cross-latitude pressure gradient. It follows that horizontal and vertical motions must develop and consequently the atmosphere possesses a circulation to allow a transport of energy across each latitude.

This circulation must possess a direct meridional cell to transport the required amount of energy poleward. Since this cell would also transport angular momentum poleward, there must be easterly surface winds in low latitudes and westerlies in higher latitudes. But such a single meridional cellular circulation is not observed. The real atmosphere contains eddy structures which have been extensively described in the literature. The role of the eddies represent one of the most important aspects of the general circulation of the lower atmosphere. The energy of the eddies in the

form of available potential energy is gained from the zonally averaged circulation by transporting energy toward latitudes of lower temperature, and kinetic energy is returned to the zonal flow by eddies transporting angular momentum toward latitudes of higher angular velocity. The gain of kinetic energy from the eddies by the mean flow has been considered as a new physical phenomenon and discussed extensively by Starr (1968).

The description and explanation of the general features of the general circulation in the lower atmosphere as revealed by observation is discussed in detail by Lorenz (1967). Newell (1968) has reviewed and discussed the pertinent main features of the general circulation of the atmosphere above 60km.

1.2 Atmospheric Tides

The formulation of the dynamical tidal theory in connection with the oscillation of the ocean and the lower atmosphere, where the dissipative effect of viscosity, heat conduction and ion drag can be neglected, was first presented by Laplace (1799, 1825). The solution of the so-called Laplace's tidal equation has been extensively studied after the elegant treatment of Hough (1897, 1898), who first obtained solutions in terms of spherical harmonics. A detailed

review of the derivation and discussion of the tidal equations are given by Wilkes (1949) and Siebert (1961). The discussion includes both gravitational lunar tide and gravitational and thermal solar tides. Further calculation and investigation of Laplace's tidal equations are presented by Kato (1966), Lindzen (1966b, 1967b) and Longuet-Higgins (1967), among others. A somewhat different derivation of the classical atmospheric tidal equation has been presented by Dickinson (1966) and Flattery (1967), based on the primitive equations of meteorology. A more specialized article on lunar tides has been written by Matsushita (1967).

The observed diurnal density variation in the thermosphere indicates that the oscillation has strong thermal origin, that is, the main thermal drive for the diurnal oscillation is the absorption of the extreme ultraviolet solar radiation. It will become clear from the present study that the theory of the diurnal bulge can be interpreted as an extension of the diurnal tidal theory of the lower atmosphere.

1.3 Motivation and Statement of the Problem

To begin with the study of the diurnal circulation of the thermosphere, one certainly would start with the description of the

general behaviour of the wind and temperature fields, and the neutral and ionized constituents. Having established from observation what the general features of the circulation are, one would proceed with theoretical studies searching for the explanation. To do this we would employ our experience with the analogous circulation of the lower atmosphere or else we would develop new procedures to provide deeper physical insight to the problem at hand.

We would be, however, far behind if we followed systematically this procedure. There are practically no observations on a global scale that can be used for obtaining the statistical properties of the circulation. A somewhat detailed picture of the fields of neutral gas density has only emerged from the analysis of satellite drag measurements above 100km. There is also some very scarce data on composition and temperature obtained with high altitude rockets. The statistics of these data has revealed five different effects on the neutral gas density, which are:

1) the diurnal variation

2) variation with geomagnetic activity

3) the 27-day variation

4) the semiannual variation

5) variation with solar cycle

Detailed discussion of these effects are given by Jacchia (1967), Jacchia and Slowey (1967), Keating and Prior (1967), Harris and Priester (1967), and Priester et al. (1967).

To attempt an explanation of the physical behavior of the thermosphere we further require the knowledge of the temperature and wind fields. The temperature can be derived from density fields, and the wind fields, due to lack of observations, can only be derived indirectly. Here we compute these fields theoretically and investigate their role. From our experience in dynamical meteorology we know that the thermosphere must possess a circulation, since a state of no motion would be incompatible with the poleward temperature gradient which radiative processes alone would demand. We expect that these large-scale motions will play a significant role in most of the problems that remain to be solved.

The present study, therefore, is motivated by the lack of theoretical description which can explain properly several time-varying features of the earth's upper atmosphere. Among these are the discrepancy between the phase and amplitude of the diurnal bulge deduced from the analysis of satellite drag measurements (Jacchia and Slowey, 1967) and the results of the quasi-static diffusion model when the extreme ultraviolet solar radiation is the only heat source (Harris and

Priester, 1962, 1965; Mahoney, 1966), and the disagreement between the small latitudinal temperature gradient observed by Jacchia and Slowey (1967) and the large equator-to-pole temperature difference at the equinox and the winter solstice calculated by Lagos and Mahoney (1967) using a quasi-static diffusion model. Theoretical explanation of the observed semi-annual variation in the thermospheric density is still lacking (Harris and Priester, 1969), and many features of the interaction between the upper atmospheric heating during magnetic storms by Joule dissipation of ionospheric currents and the subsequent density changes remain unsolved. The problem is of fundamental importance to the aeronomer because of the implications of the motion field in modifying the neutral and ionized density distribution and the ionospheric currents associated with such motions; and because such motion will supply sources of energy through large-scale circulation, which in turn will have significant geophysical effects at these altitudes.

It has been previously suggested that motion would account for the phase-amplitude discrepancy (Newell, 1966; Lindzen, 1966a; Lagos and Mahoney, 1967), and the latitudinal variance (Newell, 1966; Lagos and Mahoney, 1967). Geisler (1966, 1967) Kohl and King (1967), Bramley (1967) and Rishbeth (1967) have undertaken the task of

calculating the motion field of the neutral thermospheric gas in connection with its possible effects on the ionization distribution in the ionospheric F region. Volland (1966, 1967) and Lindzen (1967a) have also computed the horizontal wind system and indicated that horizontal advection of heat would possibly account for the "second heat source" postulated by Harris and Priester which was required in order to bring into agreement the calculated and observed variation of the diurnal bulge. May (1966), however, has pointed out that a mean zonal wind can only decrease the amplitude but does not change the phase of the diurnal bulge. More recently, Lagos (1967, 1968) and Dickinson, Lagos, and Newell (1968) have shown by scale analysis and by an initial-boundary value, two-dimensional numerical model that adiabatic heating by vertical motion plays an important role in the diurnal oscillation of the thermosphere. When this effect is included in the dynamical study, the diurnal phase discrepancy discussed above disappears. Furthermore, it was shown that horizontal advection of heat has negligible effect on the phase of the diurnal bulge.

Our previous numerical studies, however, have certain shortcomings such as neglect of ion drag and the two-dimensional approximation. From the studies of Lindzen (1967a) and Geisler (1966, 1967) it is known that neglect of ion drag can result in horizontal and hence

vertical wind amplitudes that are overestimated by a factor of 3 or greater. Motions are of a global nature with strong horizontal coupling. Neglect of meridional velocities in the continuity equation may result in further overestimation of vertical velocities if the divergence of the north-south motions cancels the divergence of the east-west motions. Hence, the actual vertical velocity may differ considerably in amplitude and phase from that obtained using a two-dimensional model. The concomitant adiabatic heating would, therefore, change, and our result that adiabatic warming associated with the vertical motion gives the proper "second heat source" should be considered accidental. These uncertainities will remain unless these approximations are lifted.

Our next task is therefore, to remedy the deficiency discussed above by retaining ion drag and extending the numerical studies to three dimensions on a spherical earth. The hydrodynamic system of equations is now greatly complicated and can be numerically tractable only if some other terms in the momentum equation are disregarded. Hence, we are forced to consider in our analytical and numerical studies the simplest yet consistent system of equations which retains ion drag and describes the coupling between the equation of motion and the thermodynamic equation on a spherical earth. In this

system, the horizontal momentum equation is replaced by the balance of pressure gradient force with ion drag force, and the vertical momentum equation is replaced by the hydrostatic approximation. The thermodynamic equation is exact to a first order approximation, however.

1.4 Scope of the Present Study

This work will be concerned with the formulation and discussion within the framework of modern dynamical meteorology of the general theory of gravity-tidal wave motions in the thermosphere. The diurnal circulation, therefore, will be properly described.

Two main subjects of the thermosphere are considered: The theoretical and the analytical and numerical part. In the first part we present the system of governing equations and introduce some useful approximations. Viscosity, heat conduction, and ion drag are retained in the formulation and discussion of the equations. The nature of several sources of energy and the relevant physical parameters are critically reviewed and some new ideas are introduced. These are discussed in the next six chapters and represent the first most comprehensive theoretical study on the subject. An application is presented in the remaining chapters, dealing with a discussion of analytical solutions and the numerical simulation of the circulation in

the middle thermosphere based on the approximate set of equations outlined at the end of last section. The role of vertical motion as a source and sink of heat through adiabatic compression and expansion of magnitude comparable to solar heating is further established.

The theoretical formulation of the equations uses the logarithm of pressure as an independent variable instead of height. This transformation of the vertical coordinate has been used by many writers in order to simplify the formulation of many atmospheric problems. In dynamic meteorology pressure is used as a vertical coordinate in the theory of vertical motions (Bjerknes et al., 1910), in the theory of quasi-static wave motions in autobarotropic layers and in the theory of turbulent motions (Bjerknes et al., 1933). This method has been extended and proved to be valid for any hydrostatic system (Eliassen, 1949), and used in the analysis of geostrophic motion (Phillips, 1963). In the theory of atmospheric tides the pressure and the logarithm of pressure as the vertical cooridnate has been also introduced successfully (Flattery, 1967, Dickinson, 1966, 1968). Under this transformation, the equations of motion and continuity are simpler than in the usual form. Thus, density drops out in the horizontal equation of motion if viscosity is not included, and the equation of continuity expresses that the three-dimensional velocity field is solenoidal.

The vertical structure equation of the tidal theory for a non-isothermal atmosphere is much simpler if the logarithm of pressure, rather than altitude, is used as the vertical coordinate (Dickinson and Geller, 1968).

In the thermosphere we not only obtain a simpler continuity equation, but as indicated by the model computations of Mahoney (Mahoney, 1966), the constituent partial pressures, mean molecular weight, mean specific heat, and solar heating at constant solar declination, can be expected to vary much less on constant pressure surfaces than on constant height surfaces, for a given composition in the lower thermosphere. We can also expect that the electron density in the F-region will vary much less on constant pressure surfaces than on constant height surfaces.

In summary:

Chapter 2 presents the hydromagnetic equations for the thermosphere. The hydromagnetic approximation is based on the concept of a single-component, electrically conductive but neutral fluid interacting with an external magnetic field. The mechanical motion of the system can then be described in terms of the usual hydrodynamic variables of density, velocity, and pressure. At low-frequency oscillation of the fluid compared to the mean ion gyrofrequency, the description in terms of a single fluid will be valid. Thus,

our analysis of the thermospheric motion with further assumptions will be restricted to: a) use of a continuum Newtonian fluid model, that is, a fluid model whose stress components are linear functions of the rate of strain components; b) the mean molecular weight and mean specific heat depend only on pressure; and c) the perturbations are in hydrostatic balance. The theory then becomes a generalization of theories of dynamical meteorology and tidal theory for the lower atmosphere.

The usual continuum Newtonian fluid theory of atmospheric motions may be employed so long as:

1) the mean free path of gas molecules is small compared to the typical distance scales of the motion and the collision frequency of the plasma particles is large enough.

2) local departure of the fluid molecules from a Boltzman velocity distribution are small so that pressure density, temperature and other thermodynamic variables may be defined and the equations of equilibrium thermodynamics apply.

Both of these assumptions can be readily justified up to the base of the exosphere (roughly 500km) for atmospheric motions with a horizontal scale of at least 10^3km and appear to be approximately valid to altitudes twice as great, provided

planetary horizontal scales of motion are considered. It must be noted also that a continuum fluid model approach has been employed to discuss flow past the magnetosphere at several earth radii altitude (Spreiter, Summers and Alksne, 1966).

The concept of hydrostatic balance can be extended to heights of roughly 500 km (cf. Anderson and Francis, 1966) by correcting for particles with escape trajectories, but at such levels the mean free paths become greater than the radius of the earth and the collective behaviour implicit in a fluid model is gone completely.

In chapter 3 we discuss the scaling assumptions of the hydromagnetic equations for use in the study of thermospheric dynamics. We shall exhibit in a systematic fashion the lowest order balances that occur in the governing equations for different ranges of relevant nondimensional parameters. The procedure of dimensional analysis used here is analogous to that employed in earlier studies of dynamical meteorology (Charney, 1947; Burger, 1958; Charney and Stern, 1962; Phillips, 1963; and Pedlosky, 1964) and in the theory of rotating fluids (Greenspan, 1964). We then nondimensionalize the govern-

ing equations for motions with a horizontal scale the radius of the earth and with a vertical scale assumed to be an atmospheric scale height. Other important parameters introduced include a time scale, a Rossby number measuring amplitude of nonlinear advections, an Ekman number determining the relative importance of viscosity, a flux tube drift velocity, ratio of ion collision to gyrofrequency and a parameter measuring the ionization density.

In chapter 4 we take the Rossby number to be small and classify various possible motion regimes according to the values assumed by the other nondimensional parameters. For very small Ekman numbers we define an "inviscid regime," for Ekman number of order one, a "transition region," and for very large Ekman numbers, a "diffusive regime." The inviscid regime motions match below to motions of the lower atmosphere. The diffusive regime motions match above to motions of the exosphere where gas collisions become negligible and the usual laws of continuum single fluid model breaks down. For small time scales applicable to longitudinal asymmetric motions with periods of a day or less but greater than the period of buoyancy oscillations, we follow the terminology applied to motions of the lower atmosphere in referring to the motion as "gravity-tidal waves." For larger time scales applicable to longitudinally averaged

motions, we obtain various other approximate systems of equations according to the relative importance of the thermal and electromagnetic driven forces which are implied by different scalings. One such a motion regime is the thermal geoplasma regime which describes the balance between the thermal forcing and the ion drag in the horizontal momentum equation, and which forms the basis for the numerical study.

In chapter 5 we discuss the mathematical formulation of the physically-meaningful boundary conditions required for specification of well-posed problems in thermospheric dynamics. In chapter 6 we discuss the physics of the dissipative processes of viscosity, heat conduction and ion drag. The time and space dependence of the magnitude of ion drag for various ionization profiles and model atmospheres is presented.

In chapter 7 we review and discuss the present knowledge of the diabatic heating and cooling as it appears in the thermosphere. We discuss the relevant photochemistry of the neutral and ionized constituent in the thermosphere and outline the correct procedure to calculate the heating efficiencies for the neutral and electron gas components. The values obtained are compared with current values available in the literature. Other heating sources which we discuss

briefly include Joule heating, heating by viscous dissipation, corpuscular heating and chemical heating.

In chapter 8 we describe the procedure to develop the numerical model for the diurnal circulation in the middle thermosphere. By neglecting viscosity, coriolis force, and inertia in the momentum equation, the system of equations is easily reduced to a fourth-order differential equation in the z co-ordinate, the coefficients of which depend on e^{-z}, and where the dependent variables are coefficients of Legendre Polynomials. Consequently, all hydrodynamical variables and forcing functions are represented in terms of spherical harmonics. The differential equation is integrated numerically in the transition region and analytically above and below this region. Conditions at the upper and lower boundary of the numerical integration are supplied by matching the analytical solutions to the numerical solution. The numerical procedure is also outlined.

Chapter 9 summarizes the principal results obtained from the model calculations when different parameters are changed systematically. In chapter 10 we discuss the results of velocity and temperature fields and briefly indicate the most important conclusions which can be deduced from our theoretical analysis and model calculations.

2. THE DYNAMIC EQUATIONS WITH VISCOSITY, HEAT CONDUCTION, AND DRAG

In this chapter we present the general equations that govern a large class of fluid systems, such as an electrically conducting Newtonian fluid, where viscosity, heat conduction, and electrodynamic effects are present. These equations are used to derive the primitive equations of dynamical meteorology, which have been taken as the starting point for the study of thermospheric dynamics. The plasma nature of the thermosphere introduces an additional complication. The plasma has three components, and there is a coupling between the motion of the electrons, that of the ions, and that of the molecules. These couplings make the derivation of the governing equations very complicated. At very low frequency oscillations that involve the motion of the fluid, the system can be described in terms of a single conductive fluid with the usual hydrodynamic variables of density, velocity, and pressure. At these low frequencies the displacement current in Ampere's law is neglected and the approximation lies in the magnetohydrodynamics domain. Thus in addition to the gas dynamics equations which determine the density, pressure, velocity, and temperature, we must also use the Maxwell equations in order to obtain the strengths of the electric and magnetic fields. We note that when a conductor moves in a magnetic field, an induced electrical field is

generated in accordance with Faraday's law. In the thermosphere, the source of this electrical field is either the dynamo field in the E-region which drives the motion of electrons and ions in the F-region or lies in the magnetosphere. Consistent with the magnetohydrodynamics approximation, an additional term, $\underset{\sim}{J} \times \underset{\sim}{B}$ (the pondermotive force acting on the conducting medium), will appear in the momentum equations, and a term $\underset{\sim}{J} \cdot (\underset{\sim}{E} + \underset{\sim}{V} \times \underset{\sim}{B})$ in the energy equation.

2.1 The Exact One-component Gas Dynamic Equations

For a rotating spherical coordinate system (λ, ϕ, r), where λ, ϕ and r represent longitude, latitude and altitude respectively, these equations are:

The equation of motion:

$$\rho \frac{dv}{dt} + 2\rho \underset{\sim}{\Omega} \times \underset{\sim}{v} = -\nabla P - \rho g + \underset{\sim}{J} \times \underset{\sim}{B} + \nabla \cdot \underset{\sim}{\Pi} \tag{2.1}$$

The equation of mass continuity: (2.2)

$$\frac{\partial \rho}{\partial t} + \nabla \cdot (\rho \underset{\sim}{v}) = 0$$

The energy equation (see Appendix I for derivation of this equation):

$$\rho T \frac{ds}{dt} = \nabla \cdot (K \nabla T) + \underset{\sim}{J} \cdot (\underset{\sim}{E} + \underset{\sim}{V} \times \underset{\sim}{B}) + \Phi + \rho q \tag{2.3}$$

the equation of state:

$$P = R \rho T \tag{2.4}$$

Maxwell's equations:

$$\nabla \times \underset{\sim}{B} = \underset{\sim}{J} \tag{2.5}$$

$$\nabla \times \underset{\sim}{E} = - \frac{\partial \underset{\sim}{B}}{\partial t} \tag{2.6}$$

where, for a Newtonian fluid,

$$dIV \underset{\sim}{\Pi} = - \nabla \times \nabla \times \mu \underset{\sim}{V} - \underset{\sim}{V} \nabla^2 \mu + \nabla \mu \times (\nabla \times \underset{\sim}{V}) + \frac{1}{3} \mu \nabla (\nabla \cdot \underset{\sim}{V}) \tag{2.7}$$

$$- \frac{2}{3} \nabla \cdot \underset{\sim}{V} \mu + \nabla \nabla \cdot (\mu \underset{\sim}{V})$$

$$\Phi = (\underset{\sim}{\Pi} \cdot \nabla) \cdot \underset{\sim}{V} \tag{2.8}$$

$$\frac{d}{dt} = \frac{\partial}{\partial t} + \underset{\sim}{V} \cdot \nabla \tag{2.9}$$

$$\nabla = \frac{\mathbf{i}}{r \cos \phi} \frac{\partial}{\partial \lambda} + \frac{\mathbf{j}}{r} \frac{\partial}{\partial \phi} + \mathbf{k} \frac{\partial}{\partial r} \tag{2.10}$$

and where

v = vector velocity

t = time

p = thermodynamic pressures

T = Temperature

s = entropy

ρ = density

g = acceleration of gravity

$\underset{\sim}{J} \times \underset{\sim}{B}$ = pondermotive force per unit volume due to the magnetic field

$\underset{\sim}{B}$ = magnetic field

$\underset{\sim}{E}$ = electric field

$\underset{\sim}{J}$ = electric current density

Φ = viscous dissipation function

$\underset{\sim}{\Pi}$ = viscous stress tensor

Ω = rate of rotation of the earth

K = thermal conductivity coefficient

μ = dynamic viscosity coefficient

q = diabatic heating rate per unit mass

$\underset{\sim}{J}\ (\underset{\sim}{E}+\underset{\sim}{V}\times\underset{\sim}{B})$ = Joule heating

R = R^*/m, where R^* = universal gas constant

m = mean molecular weight

In these equations and definitions we have used the MKSQ (meter-kilogram-second-coulomb) units. The electromagnetic fields in the fluid are described by (2.5) and (2.6). For electrically neutral plasma, as is the case in the thermosphere to a high degree or accuracy, the electrical charge density is zero and consequently the two divergence Maxwell's equations are $\nabla \cdot D = O$ and $\nabla \cdot B = O$. We have neglected the displacement current $\partial \underset{\sim}{D}/\partial t$ in (2.5) according to the MHD approximation. Since the thermospheric plasma is not ferromagnetic, the magnetic permeability is unity. Next we need to specify a relation between the current density $\underset{\sim}{J}$ and fields $\underset{\sim}{E}$ and $\underset{\sim}{B}$. This relationship is given Ohm's law:

$$\underset{\sim}{J} = \boldsymbol{\sigma} \cdot (\underset{\sim}{E} + \underset{\sim}{V} \times \underset{\sim}{B}) \tag{2.11}$$

where $\boldsymbol{\sigma}$ is the electric conductivity tensor. In the energy equation which is derived in Appendix I, we find that the thermodynamic pressure, the internal energy and the reversible work done by the fluid include mechanical and magnetic components. However, the magnetic component has a zero net contribution to the entropy, and hence, the general equation for gas dynamics applies with an additional term due to Joule heating.

2.2 The One-component Gas Primitive Equations

The solution of the system (2.1) - (2.6) is a formidable task and we don't intend to do this here, but rather to systematically derive another approximate, and hence more tractable consistent set of equations. To simplify the problem we shall restrict the analysis to motions with perturbation densities and vertical pressure gradient hydrostatically balanced. The assumption of hydrostatic balance implies the neglect of the vertical acceleration, the vertical component of the coriolis force, the viscous force and the ion drag, in the third component of the momentum equation. To justify this approximation it is necessary to reduce the hydrodynamic system of equations to an equation in a single variable with and without the hydrostatic approximation and see under what conditions the hydrostatic solution will be accurate. It follows from this analysis that if the time scales of the vertical forces and acceleration are large compared to the buoyancy time scale, which is approximately 10^2 sec, then hydrostatic balance is justified. Ion drag time scales, for typical values of the ionospheric parameters, are 10^3 sec or greater. Planetary scale motions with periods of several hours or greater and with vertical length scale of one scale height should be in hydrostatic balance. We then use $z = \log (p_o/p)$ as a vertical coordinate, where p is the total pressure of the fluid and p_o is some

reference pressure to be later specified. The vertical component of the momentum equation is then the hydrostatic relation

$$\frac{\partial \phi}{\partial z} = RT \tag{2.12}$$

where ϕ is geopotential and T the gas temperature. As indicated by the model computations of Mahoney, the mean molecular weight and mean specific heat, can be expected to vary much less on constant pressure surfaces than on constant height surfaces, for a given composition of the lower thermosphere to be constant and neglect the horizontal fluctuation of m and c_p compared to perturbations on T and take $m = m(z)$ and $c_p = c_p(z)$ to be specified z-dependent parameters to account for the variable composition in z. This will allow us to treat the thermosphere as a single component gas with height dependent molecular weight. In Figs. 2.1 - 2.2 we sketch the vertical variation of mean molecular weight and the specific heat at constant pressure as obtained from the models of Mahoney.

Let D be a typical vertical distance scale of thermospheric motions and assume motions have a horizontal scale $\underline{a}$, where $\underline{a}$ is the mean radius of the earth. Then let us define the parameter δ by

$$\delta = D/a \tag{2.13}$$

since, as discussed in chapter I, continuum equations only apply up

to altitudes of 1000 km, or so, even for planetary scale motions we can without further restriction assume $\delta << 1$.

Neglecting terms of 0 (δ) we may make the following approximations, originally stated by Phillips (1963); "The radial distance from the center of the earth is approximately constant so that a) gravity g is uniform, b) geopotential surfaces are approximately spherical, and c) the horizontal metric coefficients are sensibly independent of the distance from the center of the earth". Furthermore, we may assume that diffusive transfer of heat and momentum depends only on the vertical gradient of the temperature and motion fields respectively. For planetary scale motion this approximation should be valid up to about 500 km. At this and higher altitudes the motion can choose its own scale height so that the horizontal component of diffusive terms is important and must be retained.

Let the eastward, nortward velocities, and the vertical motion parameter be

$$u = a \cos\varphi \dot{\lambda}, \quad v = a\dot{\varphi}, \quad w = \dot{z} \tag{2.14}$$

The equations of motion and conservation of mass may then be written

$$\frac{du}{dt} + \frac{1}{a\cos\varphi}\frac{\partial\phi}{\partial\lambda} - v\sin\varphi\,(2\Omega + \dot{\lambda}) = F_{\lambda I} + F_{\lambda v} \qquad (2.15)$$

$$\frac{dv}{dt} + \frac{1}{a}\frac{\partial\phi}{\partial\varphi} + u\sin\varphi(2\Omega + \dot{\lambda}) = F_{\varphi I} + F_{\varphi v} \qquad (2.16)$$

$$\frac{1}{a\cos\varphi}\left[\frac{\partial u}{\partial\lambda} + \frac{\partial}{\partial\varphi}(v\cos\varphi)\right] + \frac{\partial w}{\partial z} - w = 0 \qquad (2.17)$$

$$\frac{d}{dt} = \left(\frac{\partial}{\partial t} + \frac{u}{a\cos\varphi}\frac{\partial}{\partial\lambda} + \frac{v}{a}\frac{\partial}{\partial\varphi} + w\frac{\partial}{\partial z}\right) \qquad (2.18)$$

Above 100 km the electromotive forces or the so-called iondrag forces $F_{\lambda I}$, $F_{\varphi I}$ are of the following form, the derivation of these expressions are given in appendix II,

$$\left.\begin{aligned} F_{\lambda I} &= \frac{n_i\, i / n_n}{1 + \rho_+^2}\left((u_d - u) + \rho_+(v_d - v)\sin I\right) \\ F_{\varphi I} &= \frac{n_i\, i / n_n}{1 + \rho_+^2}\left((v_d - v)\sin^2 I - {}_{+}(u_d - u)\sin I\right) \end{aligned}\right\} \qquad (2.19)$$

where we use the definitions

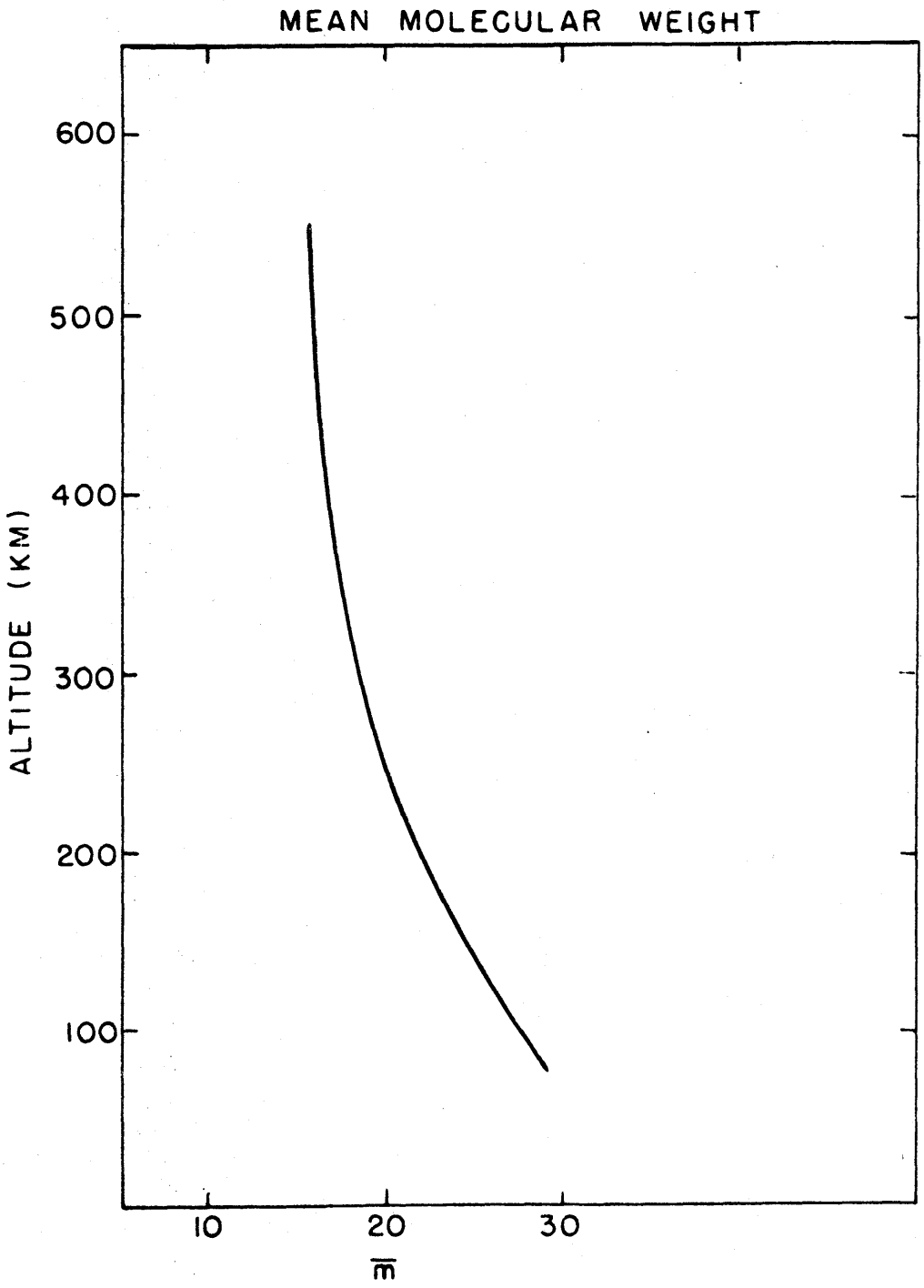

Fig. 2.1. Vertical variation of mean molecular weight.

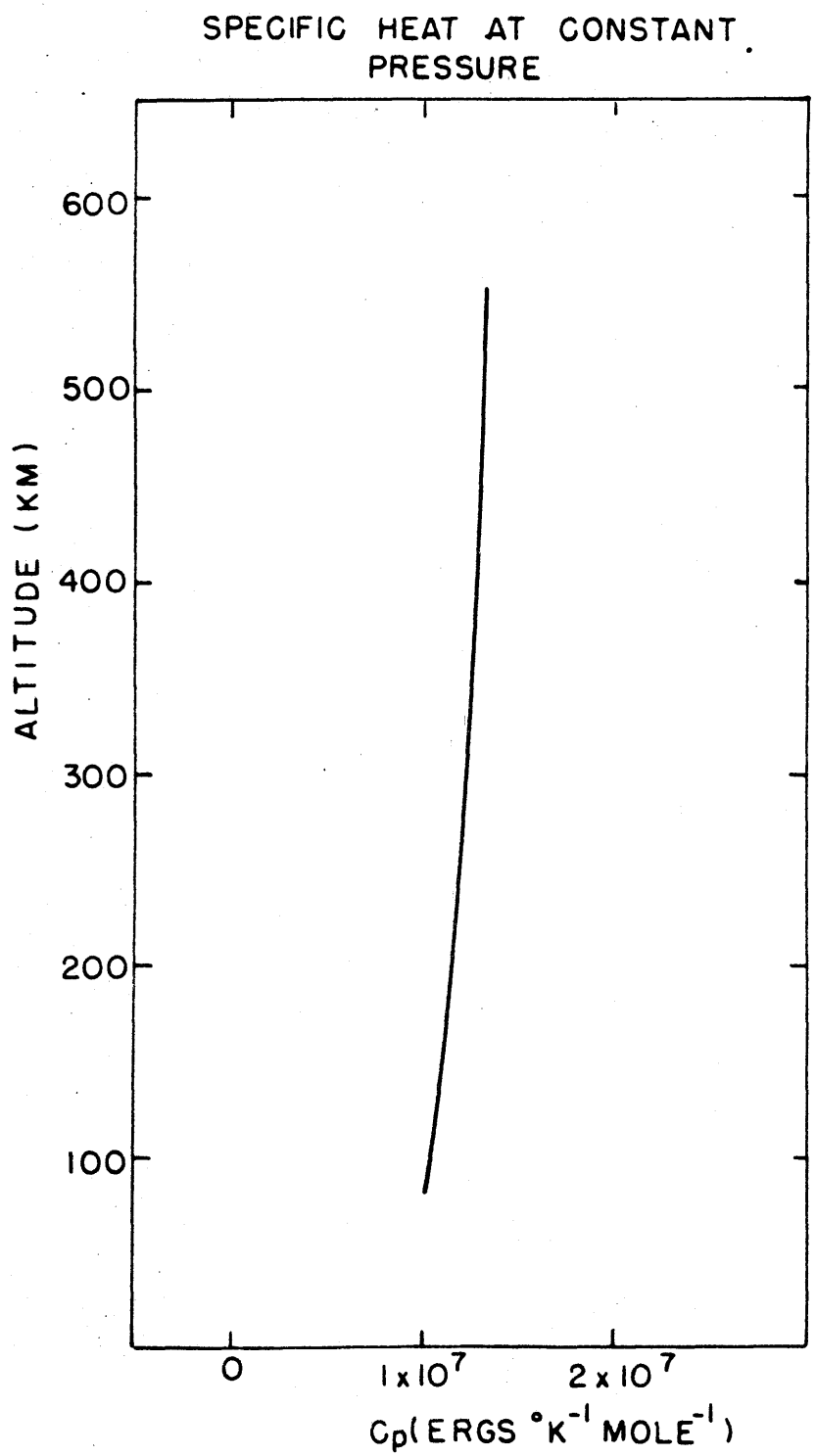

Fig. 2.2. Vertical variation of specific heat at constant pressure.

$\rho_+ = \nu_i/\omega_i$

ν_i = the frequency of ion-neutral collisions per ion

ω_i = the mean ion gyrofrequency, $\frac{n_i}{\rho_i} q \, |\underset{\sim}{B}| \simeq 200 \text{ sec}^{-1}$;

where q is the ionic charge, and $\underset{\sim}{B}$ the magnitude of the earth's magnetic field.

n_i = number density of ionized molecules

n_n = number density of neutral molecules

ρ_i = density of ionized molecules

I = magnetic dip angle, ($\tan I = \tan 2 \phi_m$, where ϕ_m is the magnetic latitude.)

u_d, v_d = the components in the λ and ϕ directions of the flux tube drift velocity $\underset{\sim}{E} \times \underset{\sim}{B} / |\underset{\sim}{B}|^2$ where $\underset{\sim}{E}$ is the net electric field due to polarization in the ionosphere or magnetosphere.

The viscous forces $F_{\lambda v}$, $F_{\phi v}$, to a first approximation are of the form

$$F_{\lambda v} = \frac{1}{\rho H} \frac{\partial}{\partial z} \frac{\mu}{H} \frac{\partial u}{\partial z}$$

$$F_{\phi v} = \frac{1}{\rho H} \frac{\partial}{\partial z} \frac{\mu}{H} \frac{\partial v}{\partial z} \qquad (2.20)$$

where $H = RT/g$ is the atmospheric scale height.

The energy equation (3.3) may be written

$$c_p \frac{dT}{dt} - \frac{1}{\rho} \frac{dP}{dt} = Q + \dot{q}_{cond} \qquad (2.21)$$

Here $\dot{q}_{cond}$ denotes the conductive heating and Q denotes all other forms of heating per unit masses.

Q is written as

$$Q = \dot{q}_{SR} + \dot{q}_{IR} + \dot{q}_{JE} + \dot{q}_{DS} + \dot{q}_{EX} \qquad (2.22)$$

where

$\dot{q}_{SR}$ = heating by solar radiation

$\dot{q}_{IR}$ = cooling by infrared radiation

$\dot{q}_{JE}$ = Joule heating

$\dot{q}_{DS}$ = heating by molecular dissipation

$\dot{q}_{EX}$ = any other externally specified heating, such as corpuscular heating, heating by chemical recombination.

Since the temperature dependence of $\dot{q}_{IR}$ is negligible, as we shall see later, we assume here that $\dot{q}_{SR}$, $\dot{q}_{IR}$, and $\dot{q}_{EX}$ are externally specified, and take $q^{(e)} = \dot{q}_{SR} + \dot{q}_{IR} + \dot{q}_{EX}$.

The conductive heating, to a first approximation is taken to be given by

$$\dot{q}_{cond} = \frac{1}{\rho H} \frac{\partial}{\partial Z} \frac{K}{H} \frac{\partial T}{\partial Z} \tag{2.23}$$

We note that the coupling between the electromagnetic and mechanical effect in the momentum equation are via the drift velocity $\underset{\sim}{V}_d$. An explicit expression for the drift velocity can be obtained, but this will not be necessary since we shall only be restricted in this work to thermally forced motions. Finally we note that the adiabatic heating given by - $\rho^{-1} dp/dt$ can alternatively be written as - $R(z)wT$.

3. THE NON-DIMENSIONAL EQUATIONS

3. 1 Scaling Assumptions

We shall analyze motion characterized by the following scales

horizontal scale = a

vertical scale = D

time scale = $1/2\ \epsilon\ \Omega$

scale of maximum horizontal velocity = C

where a is the radius of the earth, and where we now take D to be order of magnitude of a scale height, and C is taken to be order of magnitude of 100 m/sec or less. ϵ is a dimensionless parameter. It is equal to unity for the time scale of longitudinal asymmetric motions, and much smaller than one for the time scale of longitudinal average motions.

From the relevant dimensions of the problem at hand, we may form the following nondimensional parameters. We have the Rossby number R_o

$$R_0 = c/2\Omega a \sim 1/10 \qquad (3.1)$$

which describes the ratio of the motion velocity to the earth's velocity of rotation. Also we have the Prandtl number, which we denote

$$\mathcal{P} = c_p \mu_o / K_o \sim .4 \qquad (3.2)$$

describing the ratio of viscosity to heat conduction, and the Ekman number E

$$E = \xi \mu_o / \rho_o 2 \Omega H_o \sim [10^6 p_o(mb)]^{-1} \qquad (3.3)$$

which measures the ratio of viscous to Coriolis forces. Furthermore, we take $\tilde{\mu} = H_o \mu / (\mu_o H)$ and $\tilde{K} = H_o K / (K_o H)$ to be 0(1) nondimensional viscosity and heat conduction coefficients. Here μ_o and K_o are μ and K evaluated at some reference level z_o. It will be convenient to divide the factor $n_i \nu_i / n_n$ in (2.19) by 2Ω to define a nondimensional ion drag coefficient

$$N_i = (n_i / n_n) \nu_i / 2\Omega \sim 5 \cdot 10^{-6} n_i \qquad (3.4)$$

Typically, the ion number densities in the ionosphere are in the range 10^5 to 10^6 / cm^3, hence $N_i \sim 0(1)$.

The hemispheric average of the external heating $q^{(e)}$ gives diabatic heating rates of $0[(2\Omega)^3 a^2/c_p] \sim 100$ deg/hr. and deviations from this hemispheric average will be assumed to give diabatic heating rates of ~ 10 deg/hr. Let $\bar{\bar{q}}^{(e)}$, $\bar{q}^{(e)''}$, and $q^{(e)'}$ be, respectively, the hemispheric average, the longitudinal average deviation from this average, and the deviation from the longitudinal average of the heating $q^{(e)}$. The nondimensional heating

of order unity is denoted Q and written

$$Q = Q_o + R_o \bar{Q}_1 + R_o Q_1' \tag{3.5}$$

where we use the definitions

$$\left.\begin{matrix} Q_o(z,t) \\ \bar{Q}_1(\varphi,z,t) \\ Q_1'(\lambda,\varphi,z,t) \end{matrix}\right\} = \frac{R_{oo}/C_{p_o}}{(2\Omega)^3 a^2} \left\{\begin{matrix} \bar{\bar{q}}^{(e)} \\ \bar{q}^{(e)} \\ q^{(e)'} \end{matrix}\right. \tag{3.6}$$

and R_{oo} is R evaluated at z_o. According to (3.5), the deviation heating is $0(R_o)$ smaller than the mean heating, giving a consistent perturbation expansion, with the equations for the hemispheric mean state of lower order than the deviation equations. The deviation temperatures and geopotentials observed in the upper thermosphere are considered $0(R_o)$ of a mean reference state, but the calculated deviation heating rates are actually found to be as large as the hemispheric mean rate.

3.2 The Nondimensional Equations

When the governing equations are written so that dependent and independent variables are nondimensional and of order unity, information concerning the amplitudes of these variables is relegated to the nondimensional parameters of the problem. We obtain the relevant small parameters in which solutions to the governing equations can be expanded. The equations of Section 2.2 are written in terms of nondimensional starred variables and are the same as those given in Dickinson, Lagos and Newell (1968). We use the following definitions

$$t = (2\epsilon\Omega)^{-1} t^* \qquad u = 2a\Omega u^* \qquad v = 2a\Omega v^* \qquad w = 2\Omega w^*$$

$$R_{00} T = (2\Omega a)^2 T^* \qquad \phi = (2\Omega a)^2 \phi^* \qquad u_g = C u_g^* \qquad v_g = C v_g^*$$

The nondimensionalized atmospheric velocities are measured relative to the earth's rotational velocity.

We now may use the above definitions to write equations (2.12), (2.15), (2.16), (2.17), (2.21), and (2.24) respectively as

$$\frac{\partial \phi^*}{\partial z} = R^* T^* \tag{3.7}$$

$$\epsilon \frac{\partial u^*}{\partial t^*} + M^\lambda - \sin\varphi v^* + \frac{1}{\cos\varphi}\frac{\partial \phi^*}{\partial \lambda} = N_i F^*_{\lambda I} + E F^*_{\lambda V} \qquad (3.8)$$

$$\epsilon \frac{\partial v^*}{\partial t^*} + M^\varphi + \sin\varphi u^* + \frac{\partial \phi^*}{\partial \varphi} = N_i F^*_{\varphi I} + E F^*_{\varphi V} \qquad (3.9)$$

$$\frac{1}{\cos\varphi}\frac{\partial u^*}{\partial \lambda} + \frac{1}{\cos\varphi}\frac{\partial}{\partial \varphi}(v^*\cos\varphi) + \frac{\partial w^*}{\partial z} - w^* = 0 \qquad (3.10)$$

$$\epsilon \frac{\partial T^*}{\partial t^*} + \mathcal{H} = \frac{E}{\pi} e^z \frac{\partial}{\partial z}\left(\tilde{K}\frac{\partial T^*}{\partial z}\right) + Q_0 + R_0 Q_1 \qquad (3.11)$$

where we use the definitions,

$$M^\lambda = \frac{u^*}{\cos\varphi}\frac{\partial u^*}{\partial \lambda} + v^*\frac{\partial u^*}{\partial \varphi} - \tan\varphi u^* v^* + w^*\frac{\partial u^*}{\partial z}$$

$$M^\varphi = \frac{u^*}{\cos\varphi}\frac{\partial v^*}{\partial \lambda} + v^*\frac{\partial v^*}{\partial \varphi} + \tan\varphi u^{*2} + w^*\frac{\partial v^*}{\partial z}$$

$$F^*_{\lambda I} = (1+\beta_+^2)^{-1}\left[(R_0 U_g^* - u^*) + \sin I\,\beta_+ (R_0 U_g^* - v^*)\right]$$

$$F^*_{\varphi I} = (1+\beta_+^2)^{-1}\left[(R_0 U_g^* - v^*)\sin I - \beta_+ (R_0 U_g^* - u^*)\sin I\right]$$

$$F^*_{\lambda v} = e^z \frac{\partial}{\partial z}\left(\tilde{\mu}\,\frac{\partial u^*}{\partial z}\right)$$

$$F^*_{\varphi v} = e^z \frac{\partial}{\partial z}\left(\tilde{\mu}\,\frac{\partial v^*}{\partial z}\right)$$

$$\mathcal{H} = c_p^*\left[\frac{u^*}{\cos\varphi}\frac{\partial T^*}{\partial \lambda} + v^*\frac{\partial T^*}{\partial \varphi} + w^*\left(\frac{\partial T}{\partial z} + \frac{R}{c_p}T^*\right)\right]$$

$$R^* = R/R_{00}$$

$$c_p^* = c_p/c_{p_0}$$

$$Q_1 = \bar{Q}_1 + Q'$$

In order for (3.7) - (3.11) to represent a closed system of differential equations, it is necessary to prescribe the heating, the drift velocity, and the ion number density. These parameters, which in general may depend on motions, are here assumed known. Assuming now that the Rossby number defined by (3.1) characterizes the amplitude of the atmospheric velocities, we seek solutions to (3.7) - (3.11) expressed as an asymptotic power series in R_o.

$$\left.\begin{aligned} u^* &= R_0 u_1 + R_0^2 u_2 + \cdots \\ v^* &= R_0 v_1 + R_0^2 v_2 + \cdots \\ \phi^* &= \phi_0 + R_0 \phi_1 + R_0^2 \phi_2 + \cdots \\ T^* &= T_0 + R_0 T_1 + R_0^2 \phi_2 + \cdots \\ w^* &= R_0 w_1 + R_0^2 w_2 + \cdots \end{aligned}\right\} \qquad (3.12)$$

Substituting (3.12) into (3.7) - (3.11), using the definitions of Section 3.1, and requiring that terms multiplied by a given power of Rossby number separately must satisfy the equations, we obtain a sequence of linear partial differential equations. Implicit in this procedure is the assumption that all parameters and variables are now 0 (1) except the Rossby number R_o, which is a small parameter.

The lowest order system is

$$\begin{aligned} \frac{\partial \Phi_0}{\partial \lambda} &= 0 \\ \frac{\partial \Phi_0}{\partial \varphi} &= 0 \\ \frac{\partial \Phi_0}{\partial z} &= R^* T_0 \\ -\frac{E}{\pi} e^z \frac{\partial}{\partial z}\left(\tilde{\kappa} \frac{\partial T_0}{\partial z}\right) &= Q_0(z) \end{aligned} \tag{3.13}$$

We shall assume that any boundary conditions applied to (3.13) will be independent of x, y and t so that T_0 and Φ_0 will depend only on z. These resulting dependent variables will then be hemispheric averages or standard atmosphere.

The first system is

$$\left.\begin{aligned} &\epsilon \frac{\partial u_1}{\partial t^*} + N u_1 - E e^z \frac{\partial}{\partial z}\left(\tilde{\mu} \frac{\partial u_1}{\partial z}\right) - N v_1 \beta_* \sin I - \sin\varphi v_1 + \frac{1}{\cos\varphi} \frac{\partial \Phi_1}{\partial \lambda} \\ &\qquad = N(u_d + \beta_* v_d \sin I) \\ &\epsilon \frac{\partial v_1}{\partial t^*} + N v_1 \sin^2 I - E e^z \frac{\partial}{\partial z}\left(\tilde{\mu} \frac{\partial v_1}{\partial z}\right) + N u_1 \beta_* \sin I + \sin\varphi u_1 + \frac{\partial \Phi_1}{\partial \varphi} \\ &\qquad = N(v_d \sin^2 I - \beta_* u_d \sin I) \\ &\frac{1}{\cos\varphi} \frac{\partial u_1}{\partial \lambda} + \frac{1}{\cos\varphi} \frac{\partial}{\partial \varphi}(v_1 \cos\varphi) + \frac{\partial w_1}{\partial z} - w_1 = 0 \\ &\frac{\partial \Phi_1}{\partial z} - R^* T_1 = 0 \\ &\epsilon c_p^* \frac{\partial T_1}{\partial t^*} - \frac{E}{\pi} e^z \frac{\partial}{\partial z}\left(\tilde{\kappa} \frac{\partial T_1}{\partial z}\right) + w_1 S = Q_1 \end{aligned}\right\} \tag{3.14}$$

where we use $N = N_i \left(1 + \rho_+^2\right)^{-1}$, $S = c_p\left(\frac{dT_0}{dz} + \frac{R}{c_{p_0}} T_0\right)$

The parameter $S \sim 1$ for a 1000 deg K isothermal atomic oxygen atmosphere. The first order system provides an approximate model for the description of motions of the neutral gas in the thermosphere. Equation (3. 14) has been written so all forcing terms, assumed known, occur on the right-hand side. The higher order equations have a left-hand side similar to (3. 14) but their right hand sides contain forcing by nonlinear terms of lower order. Knowing the solution of (3. 14) we can solve the second order system, and by further iteration, we can solve the higher order systems.

4. CLASSIFICATION OF MOTION REGIMES

4.1 The Nature of Nondimensional Parameters

Motions described by the system (3.14) will depend primarily on the choice of parameters ϵ, E, N, ρ_+, and (u_d, v_d), since the parameters η, S, can vary in the thermosphere but little from their mean values. We shall now introduce a number of scaling assumptions based on the observed range of values assumed by the parameters, and use these assumptions to derive various simple systems of equations. These systems are intended to be useful for theoretical rather than practical applications. For the latter usage, some of the approximations assumed should and can easily be relaxed.

Since we are considering motions with a time scale of one day or larger we take $\epsilon \leq 1$. Noticing that a typical average value for ion number density in the thermosphere is $10^5/cm^3$, we assume that the nondimensional parameter $N \sim 0(1)$. Let us assume that R_o, which describes the importance of nonlinear terms, is much less than one. We see from Figs. 7.3 that $\rho_+ << 1$ except in the region in which $E << 1$ where we can assume $\rho_+ \sim 0(1)$. Also we assume here $\sin I \simeq 1$, which is valid for middle and high latitudes.

Given the above restrictions we now have as free parameters ϵ , E , (u_d , v_d) which describe respectively the time scale of motion, the magnitude of heat conduction and viscosity, and the magnitude of "magnetospheric convection" drives. Three general classes of motion may be distinguished according to the magnitude of (u_d , v_d). These are class I, thermally driven motions, where $u_d , v_d \ll 1$, class II, thermal-electromagnetically driven motions, where $u_d , v_d = 0(1)$, and class III, electromagnetically (or plasma) driven motion, where $u_d , v_d \gg 1$. For class I, we may neglect the drive resulting from plasma motions which accompany motions of magnetic field tubes, while for class III, the plasma motions are assumed to be aprimary drive for the neutral gas. The studies of Geisler (1966), Lindzen (1967a), Lagos (1967), Dickinson, Lagos, and Newell (1968) assume class I motions to occur, while studies of Kato (1956), Axford-Hines (1961), Hines (1965), Dougherty (1963), De Witt and Akasofu (1964), and Rishbath et al. (1965), have examined the possible importance of class III motions.

We have assumed for derivation of our equation two nondimensional time variables according to the value of ϵ . For $\epsilon \sim 1$ we have a short time variable t^* , which is of the order of a day. This

time scaling is appropriate for the discussion of diurnal motions. For $\epsilon \ll 1$ (say $\epsilon \sim R_o$), on the other hand, we have a long time variable. This time scale, which is longer than a day, is appropriate for the study of zonally symmetric motions. For the discussion of long time scale motions, we again start with (3.7) - (3.11) and use the $R_o t^*$ time variable. Assuming again (3.12), we obtain equations equivalent to (3.13) and(3.14) except that the time derivative terms are deleted. Thus we can classifythe motions according to these time scales as (1) gravity-tidal waves for $\epsilon = 1$, which would be forced by Q_1, and (2) meteorological scale motions for $\epsilon \tilde{=} R_o$ forced by $\bar{Q}_1$.

The Ekman number E increases with height approximately as e^{z_o}. Hence, specification of the parameter E specifies a reference level. Using the discussion of Yanowitch (1967), the following levels are so defined

a) $E \ll 1$, the inviscid regime ($p > 10^{-2}\mu b$)

b) $E \sim 1$, the transition regime ($10^{-4}\mu b \leq p \leq 10^{-2}\mu b$)

c) $E \gg 1$, the diffusive regime ($p < 10^{-4}\mu b$)

As noted above, we take $\varsigma_+ \ll 1$ for b) and c) and $\varsigma_+ = 1$ for a).

The pressure levels for which in practice these regimes

occur depend on the assumed values for vertical scale of disturbance. The values given in parentheses above are roughly estimated using the scaling of this paper (see Table 3).

4.2 The Inviscid Regime

The inviscid regime thermospheric motions are given to first order by

$$
\left.
\begin{aligned}
&\epsilon \frac{\partial u_1}{\partial t^*} + N u_1 + N v_1 \beta_* - \sin\varphi v_1 + \frac{1}{\cos\varphi} \frac{\partial \phi_1}{\partial \lambda} = N(u_d + \beta_* v_d) \\
&\epsilon \frac{\partial v_1}{\partial t^*} + N v_1 - N u_1 \beta_* + \sin\varphi u_1 + \frac{\partial \phi}{\partial \varphi} = N(v_d - \beta_* u_d) \\
&\epsilon \frac{\partial T_1}{\partial t^*} + w_1 S = Q_1 \\
&\frac{1}{\cos\varphi} \frac{\partial u_1}{\partial \lambda} + \frac{1}{\cos\varphi} \frac{\partial}{\partial \varphi}(v_1 \cos\varphi) + \frac{\partial w_1}{\partial z} - w_1 = 0 \\
&\frac{\partial \phi_1}{\partial z} = R^* T_1
\end{aligned}
\right\} \quad (4.1)
$$

Eq. (4.1) with $\epsilon = 1$ describes class II gravity-tidal wave motions. To describe class I motions we simple omit u_d and v_d in the first two equations. To describe class III motions we simply omit ϕ_1 in (4.1). For class III motions the momentum equations are decoupled from the thermodynamic equation . In order to study

meteorological scale motions, we note that $\epsilon \cong R_o$, and therefore, to a first approximation we neglect the time differentiated terms.

Eq. (4.1) should be valid below about 150km altitude. If we consider motions below 100km, we may further make the assumption that $N \ll 1$ to justify the omission of ion drag terms. With this additional assumption, the first five equations in (4.1) represent the usual linearized primitive equations of dynamical meteorology. To obtain the equivalent form of geostrophic scale analysis discussed by Phillips (1963) for motions of the lower atmosphere, we simply modify the first five equations of (4.1) so that $S \sim \epsilon$, $Q_1 \sim \epsilon$, $\epsilon \cong R_o$, $N \ll 1$, and the horizontal scale $\sim \epsilon$ a .

4.3 The Transition Regime

For transition region motions, we take $E = 1$, and obtain to first order

$$\left.\begin{aligned}
&\epsilon \frac{\partial u_1}{\partial t^*} + N_i u_1 - e^z \frac{\partial}{\partial z}\left(\tilde{\mu} \frac{\partial u_1}{\partial z}\right) - \sin\varphi v_1 + \frac{1}{\cos\varphi} \frac{\partial \phi_1}{\partial \lambda} = N_i U_d \\
&\epsilon \frac{\partial v_1}{\partial t^*} + N_i v_1 - e^z \frac{\partial}{\partial z}\left(\tilde{\mu} \frac{\partial v_1}{\partial z}\right) + \sin\varphi u_1 + \frac{\partial \phi_1}{\partial \varphi} = N_i V_d \\
&\frac{1}{\cos\varphi} \frac{\partial u_1}{\partial \lambda} + \frac{1}{\cos\varphi} \frac{\partial}{\partial \varphi}(v_1 \cos\varphi) + \frac{\partial w_1}{\partial z} - w_1 = 0
\end{aligned}\right\} \quad (4.2)$$

$$\left.\begin{aligned} \frac{\partial \Phi_1}{\partial z} &= R^* T_1 \\ \epsilon \frac{\partial T_1}{\partial t^*} - e^z \frac{\partial}{\partial z}\left(\tilde{K} \frac{\partial T_1}{\partial z}\right) + w_1 S &= Q_1 \end{aligned}\right\} \qquad (4.2)$$

Eq. (4.2) with $\epsilon = 1$ describes class II motions. Again we omit u_d and v_d for class I motion and Φ_1 for class III motion in (4.2). The gravity-tidal wave motion is appropriate to describe the thermospheric diurnal bulge. For meteorological scale motions, we simply omit the time differentiated terms since they are multiplied by R_o. The resultant system of equations is appropriate to the study of the seasonal and long time thermospheric motions, and can easily be modified to describe the meridional circulation of the thermosphere.

4.4 The Diffusive Regime

The diffusive regime motions to first order are simply given by

$$\left.\begin{aligned} E e^z \frac{\partial}{\partial z}\left(\tilde{\mu} \frac{\partial u_1}{\partial z}\right) &= 0 \\ E e^z \frac{\partial}{\partial z}\left(\tilde{\mu} \frac{\partial v_1}{\partial z}\right) &= 0 \\ E e^z \frac{\partial}{\partial z}\left(\tilde{K} \frac{\partial T_1}{\partial z}\right) &= 0 \\ \frac{\partial \Phi_1}{\partial z} &= R^* T_1 \\ \frac{1}{\cos\varphi}\frac{\partial u_1}{\partial \lambda} + \frac{1}{\cos\varphi}\frac{\partial}{\partial \varphi}(v_1 \cos\varphi) - \frac{\partial w_1}{\partial z} - w_1 &= 0 \end{aligned}\right\} \qquad (4.3)$$

Eq. (4.3) describes motions of class I and II. To describe class III motions, (4.3) is modified so that $N_i U_d$ and $N_i V_d$ appears in the right hand side of the first two equations. Eq. (4.3) together with appropriate boundary conditions, such as the requirement of no heat, momentum, and mass fluxes at infinity establishes that, to the order that (3.14) holds, U_i, V_1, W_1 and T_1 are constant with z. At very high altitudes, however, the vertical and horizontal components of diffusive terms balance, as discussed in section 2.2.

4.5 The Thermal Geoplasma Regime

To insure the validity of the scale analysis, it was necessary that the nondimensional ion drag coefficient N_i defined by (3.4) be of 0 (1) or less. An interesting motion regime results if this restriction is violated. This would be the case if the ion number density is greater than $2 \cdot 10^5$. Typical values for the ion concentration above 25km at daytime is 10^6. This number will increase by a factor of 2 at the equinoxes in middle latitudes and by about a factor of 5 at sunspot maximum. This will result in ion drag dominating in the momentum equations. For $E \sim 0(1)$ and $N_i \sim 0(R_o^{-1})$ it is easily shown that ion drag term will balance the pressure gradient to zeroth and first order approximations in the momentum equation.

$N_i \sim (R_o^{-1})$ or larger will occur within 1.5 to 2 scale heights above and below the F-region peak, for the period described above (i.e. daytime, sunspot maximum and at the equinox).

We shall, therefore, call the Thermal Geoplasma Regime that mode of motion in which the horizontal component of the ion drag force is balanced, or nearly balanced, by the geopotential pressure gradient force. This mode of motion is somewhat equivalent to the geostrophic motion, the approximate balance between the coriolis force and the horizontal pressure gradient force, in the lower atmosphere.

The thermal geoplasma regime motions to first order are simply described by the system of equation

$$\left.\begin{aligned}
\frac{1}{\cos\varphi}\frac{\partial \phi_1}{\partial \lambda} &= N_i(u_d - u_1)\\
\frac{\partial \phi_1}{\partial \varphi} &= N_i(v_d - v_1)\\
\frac{1}{\cos\varphi}\frac{\partial u_1}{\partial \lambda} + \frac{1}{\cos\varphi}\frac{\partial}{\partial \varphi}(v_1\cos\varphi) + \frac{\partial w_1}{\partial z} - w_1 &= 0\\
\frac{\partial \phi_1}{\partial z} &= R^* T_1\\
\epsilon\frac{\partial T_1}{\partial t^*} - e^z\frac{\partial}{\partial z}\left(\tilde{\kappa}\frac{\partial T_1}{\partial z}\right) + w_1 S &= \Phi_1
\end{aligned}\right\} \qquad (4.4)$$

Here again, ϵ will take the value of unity for gravity-tidal wave motions and the magnitude of R_o for meteorological scale motion.

Eq. (5.4) forms the basis for the numerical study discussed in chapter 8.

The above analysis into equations for inviscid, transition, diffusive, and thermal geoplasma motions has been made to show the different balances that will be important at different heights in the thermosphere. For actual application of these equations to real geophysical phenomena, it will probably be more convenient to use (3.14) as the only system valid at all heights rather than matching the solutions of (4.1) - (4.4). Finally, the above discussions are only valid for planetary scale motions. For motions with horizontal scale much smaller than the radius of the earth the R_o will no longer satisfy the relation $R_o \ll 1$, and therefore, nonlinear terms will need to be retained to first order if we wish to consider motions of smaller horizontal scale with amplitudes of the order of 100 m/sec as those commonly observed.

5. FORMULATION OF BOUNDARY CONDITIONS

5.1 Lateral Boundary Conditions

Before the systems of equations (3.14) or (4.1) - (4.4) can be solved, it is necessary to specify boundary conditions. The selection of our lateral boundary conditions will depend entirely on the manner in which the variables are represented. There are two alternatives: (1) we may represent the variables as discrete functions on a mesh which covers physical space, or (2) we may represent the variables by the coefficient of an expansion in orthogonal functions. For planetary scale motions, the grid point method contains serious difficulties when extended to cover the entire globe. We, therefore, choose the spectral representation, on the ground that it does not use any approximations for the evaluation of horizontal space derivatives, and though it does not eliminate entirely the necessity for truncation, it permits a rigid control over the resulting truncation errors.

The shape of the earth suggests that we represent the hydrodynamic variables in terms of spherical harmonics. This set has the advantage that no artificial lateral boundary conditions are necessary.

5.2 Vertical Boundary Conditions

The vertical boundary conditions are obtained from physical considerations. If we consider the thermosphere to extend from the mesopause to some very high level, we can ignore any effect of the surface of the earth and extend the lower and upper boundaries to infinity. This geometry suggests that the boundary conditions should be formulated for a vertically unbounded domain and then approximated by conditions on finite boundaries when numerical methods are used in modeling the thermosphere.

In the absence of sources and magnetic field each component of the momentum equation may be regarded as describing two viscous modes of motion, one growing and one decaying exponentially in z. Similarly the thermodynamic equation may be regarded as describing two heat conduction modes. When magnetic field is present in a weakly ionized gas, the collisions between charged and neutral particles will essentially provide the coupling between the electromagnetic and hydrodynamic forces giving rise to two further modes, the hydromagnetic modes, which remain when we neglect viscosity. Likewise as a result of coupling between motion and temperature perturbation, there will exist two additional modes. This last pair of modes will remain if we formally neglect viscosity, ion drag, and heat conduction,

and so may be regarded as the inviscid component of the motion. To summarize, we expect the vertical structure of solutions to be described by six dissipative, two hydromagnetic and two inviscid modes.

Four boundary conditions for $z \to \infty$ are then readily obtained. These are

$$\lim_{z \to \infty} \left\{ \begin{array}{l} \tilde{\mu} \dfrac{\partial u}{\partial z} \\ \tilde{\mu} \dfrac{\partial v}{\partial z} \\ \tilde{\kappa} \dfrac{\partial T}{\partial z} \\ e^{-z} w_1 \end{array} \right\} = 0 \qquad (5.1)$$

which implies the conditions of no vertical fluxes of heat, horizontal u or v momentum, or mass at very high levels. We will make little error if these conditions are applied at some level sufficiently high into the diffusive regime.

If we take all sources to vanish below some level, then a plausible requirement for $z \to -\infty$ is that all solutions decay "exponentially" in the downward direction below the level.

We would like to obtain four boundary conditions in z from this requirement. Three conditions follow directly. That is, we require below the source region that the three downward growing dissipative modes are identically zero.

First let us consider the situation when the inviscid modes are evanescent, that is, gravity waves or Rossby waves are not present in the inviscid equations. Then there will be one inviscid mode where energy density grows and one whose energy density decays exponentially with decreasing z. We take then as the fourth condition that the growing mode is absent below the source region. We now have a well posed problem for the region unbounded for a large negative z .

Secondly, let us assume the inviscid modes are wavelike. Then there will be two normal mode solutions, one mode propagating energy upward and one mode propagating energy downward. In order to insure that solutions at a lower boundary contain no inviscid mode that propagates energy upward, we select the normal mode solutions that give outward energy flux. If the influence of the lower atmosphere on the thermosphere is considered, we may explicitly specify waves coming upward from the lower atmosphere. A more detailed discussion of the mathematical formulation of boundary conditions will be examined when we apply the system of equations described in the last section to specific problems.

6. THE PHYSICS OF VISCOSITY, HEAT CONDUCTION AND ION DRAG COEFFICIENTS

Various thermodynamically irreversible processes that attenuate or alter the shape of any wavelike motion are present in the thermosphere. These irreversible processes are represented by viscosity, heat conduction and ion drag, which have indeed the most important effects. They represent small departures from an equilibrium distribution of energy and from an isotropic distribution of molecular velocities about their mean values, and are mainly due to the fact that molecules drift to new positions between collisions and require a few collisions before reaching the mean energy and momentum values characteristic of their new position.

When we consider a monatomic gas, a molecule exhibits a lag in taking up the translational energy appropriate to its new location. When, on the other hand, we consider a mixture of monatomic and diatomic molecules, we must introduce the rotational and vibratory energy and further molecular relaxation processes are to be considered, i. e. the lag of the molecule in taking up the energy of rotational degrees of freedom behind the taking up of the translational energy. The number of collisions required for a rotational energy of

the gas molecule to adjust to the equilibrium condition are very few, but a much larger number of collisions may be necessary to adjust the energy in the vibrational degrees of freedom.

Because the time constant of the dynamical processes we are concerned with is very large compared with the time constant of the relaxation process or lag, we may still use the concept of equilibrium thermodynamics (Goldstein, 1960) as long as we introduce viscosity, heat conduction, and ion drag, which are considered as thermodynamically irreversible processes, in the dynamic equations. Thus, the coefficients of shear viscosity, μ, heat conduction, K, and ion drag, $N_i (1 + \rho^2_+)^{-1}$, will describe the lag associated with the taking up of the translational energy in the adjustment of the molecules to equilibrium conditions. Similarly, the effect of relaxation processes associated with the internal degrees of freedom will be represented by a bulk viscosity, μ'. The relaxation times for dissociation, ionization, and recombination are taken as negligibly small compared with the characteristic time of the dynamical process we are concerned with.

6.1 Viscosity

For a perfect collision type gas the coefficient of shear viscosity, μ, is independent of density and is a function of tempera-

ture only. The temperature dependence of μ varies according to what molecular model is used (Chapman and Cowling, 1952). For example, from kinetic theory of gases the simplest model, rigid elastic spherical molecules, gives $\mu \propto T^{1/2}$. If the force between molecules of opposite type varies inversely as the ν^{th} power of their mutual distance, the temperature dependence of μ for point-centers of force and for a gas-mixture gives $\mu \propto T^{m}$ where $m = \frac{1}{2} + \frac{2}{\nu-1}$. Experiments show that the actual variation of viscosity coefficient with temperature is more rapid than $\mu \propto T^{1/2}$ (see references cited in Chapman and Cowling, 1952). This is because the collision cross-section, σ, gradually falls as temperature rises, since $\mu \propto \frac{T^{1/2}}{\sigma}$.

Thus far, the viscosity we are speaking of is of the molecular type. In dealing with planetary scale motions in which the velocities measured are averages of large spatial and temporal scales, it is more convenient to introduce a coefficient of turbulent or eddy viscosity in order to discuss the transfer of momentum. However, the nature of this parameter, generally speaking, is far from being understood. When this coefficient of eddy viscosity turns out to be systematically negative, the effects of the transport processes lies within a new physical phenomena (Starr, 1968) which cannot be treated by

analogy to molecular viscosity. Whether the actual thermospheric flow will exhibit negative viscosity effects is too early to speculate. Finally, due to the presence of ionized particles in the thermosphere, the coefficient of molecular viscosity will be systematically altered when magnetic and electric fields are present. In the present study we only consider the molecular viscosity of the neutral gas component.

6.2 Heat Conduction

The thermal conductivity, K, is connected with the coefficient of viscosity, μ, by an equation of the form $K \propto \mu c_v$, where c_v is the specific heat at constant volume, and its variation with temperature is in general approximately the same to the variation of μ.

For the thermospheric application the temperature dependence of the thermal conductivity and the coefficient of viscosity are not sufficiently well known. Power constant law ranging from 0.5 to 1 are being used. For example, Harris and Priester (1962) and Mahoney (1966) used the square-root law, Nicolet (1963) used $K \sim T^{3/4}$. Konowalow et al (1959) and Dalgarno and Smith (1962) have calculated the coefficients of thermal conduction and viscosity for atomic oxygen and found a temperature dependence, for $T < 350^{\circ}K$

(Konowalow et al) and for $100^{\circ}K \leq T \leq 100,000^{\circ}K$ (Dalgarno and Smith), of the form $\mu \sim K \propto T^{0.71}$. Figures 6.1 and 6.2 illustrate the vertical distribution of the mean values of μ and K when the square-root and 2/3's law are assumed. The mean temperature corresponds to average solar activity and is presented in Fig. 9.20.

If the presence of ions and electrons would have to be considered, then the thermal conductivity should be altered to take into account the thermoelectric and thermomagnetic effects. For weakly and fully ionized gases, the thermoelectric effect acts to reduce the effective coefficient of thermal conductivity. The thermomagnetic effect acts to reduce the heat flow in the direction perpendicular to both the electric and magnetic fields. These effects we do not include in the present study.

6.3 Ion Drag

We next describe the observational features about the space and time variation of several ionospheric parameters which comes into the ion drag coefficient, namely, the ion-neutral collision frequency (ν_i), the ion gyrofrequency (ω_i), and the ion concentration (n_i). Collision frequencies at ionospheric level are discuss-

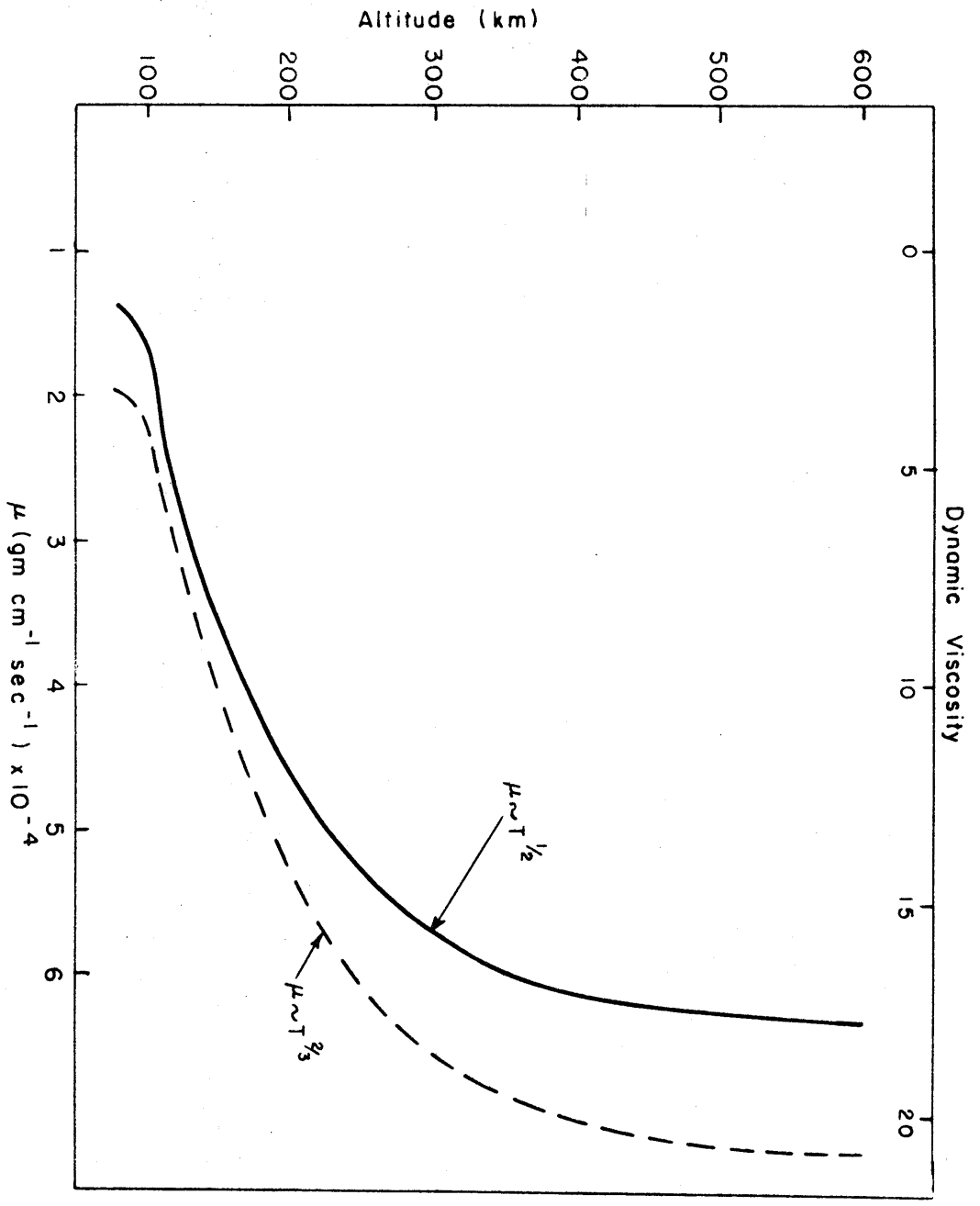

Fig. 6.1 Vertical distribution of mean dynamic viscosity for the square-root and 2/3th law of temperature dependence. —— Left scale – – – right scale.

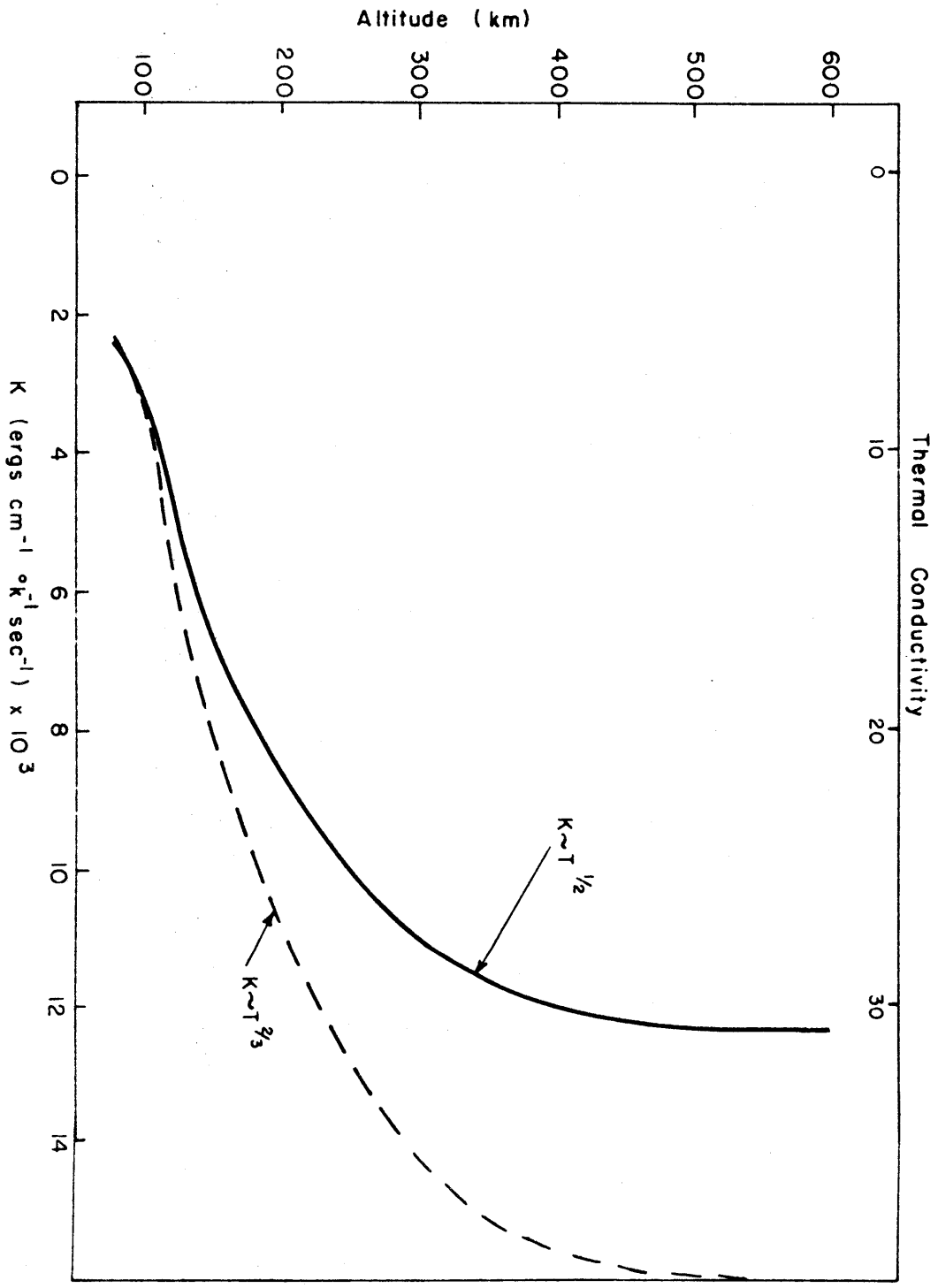

Fig. 6.2. Vertical distribution of mean thermal conductivity for the square-root and 2/3th law of temperature dependence. —— Left scale – – – right scale.

ed by Chapman (1956). Changes in collision frequency are due to changes in the concentration of ion and neutral particles and molecular weight. Hanson (1965) has calculated the ion-neutral collision frequencies for daytime, nighttime, sunspot maximum and sunspot minimum conditions, and we use these values. The daytime vertical distribution of the ν_i/ω_i ratios are shown in Figure 6.3. The electron and the ion densities are quite variable parameters in the ionosphere. The vertical electron density distribution is characterized by a large diurnal variation controlled partly by solar radiation and partly by transport processes due to horizontal and vertical wind systems, electromagnetic drifts, plasma diffusion etc. The diurnal variation pattern of electron density is different at different latitudes (diurnal anomaly) and depends on the season and sunspot activity. Seasonal, geographical and solar cycle variation of the electron density profile are discussed for example by Davis (1965). The dependence of the ionospheric F region on the solar cycle for summer and winter and for low, medium and high latitudes at noon, is illustrated in Figure 6.4.

The concentration of neutral particles for low and high solar activity has been obtained from Cospar International Reference Atmosphere (CIRA, 1965). Using the data from Figures (6.3) and (6.4) and the data for n_m, the dependence of the vertical distribution of the

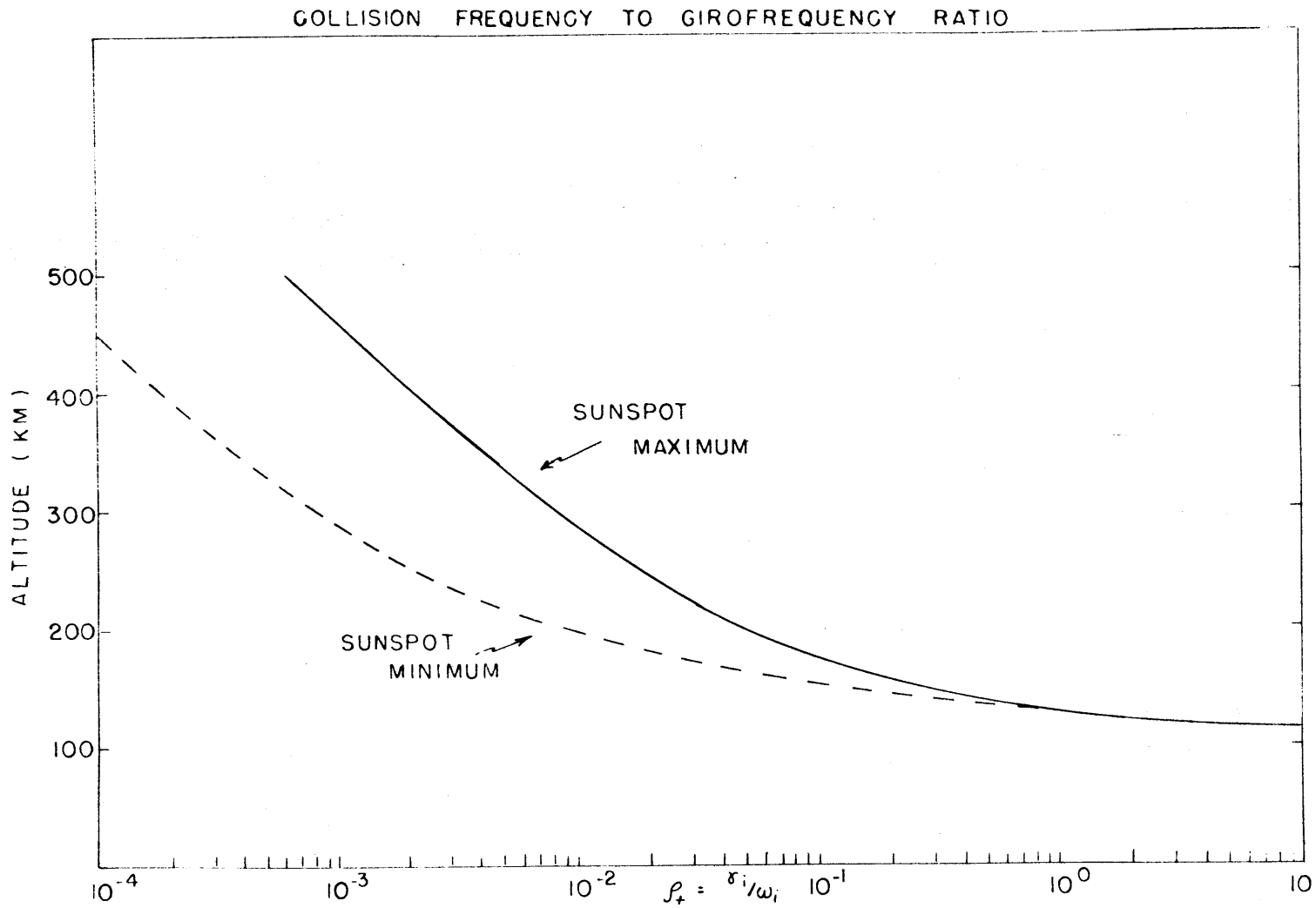

Fig. 6.3. Daytime vertical distribution of collision frequency to girofrequency ratio for sunspot maximum and minimum.

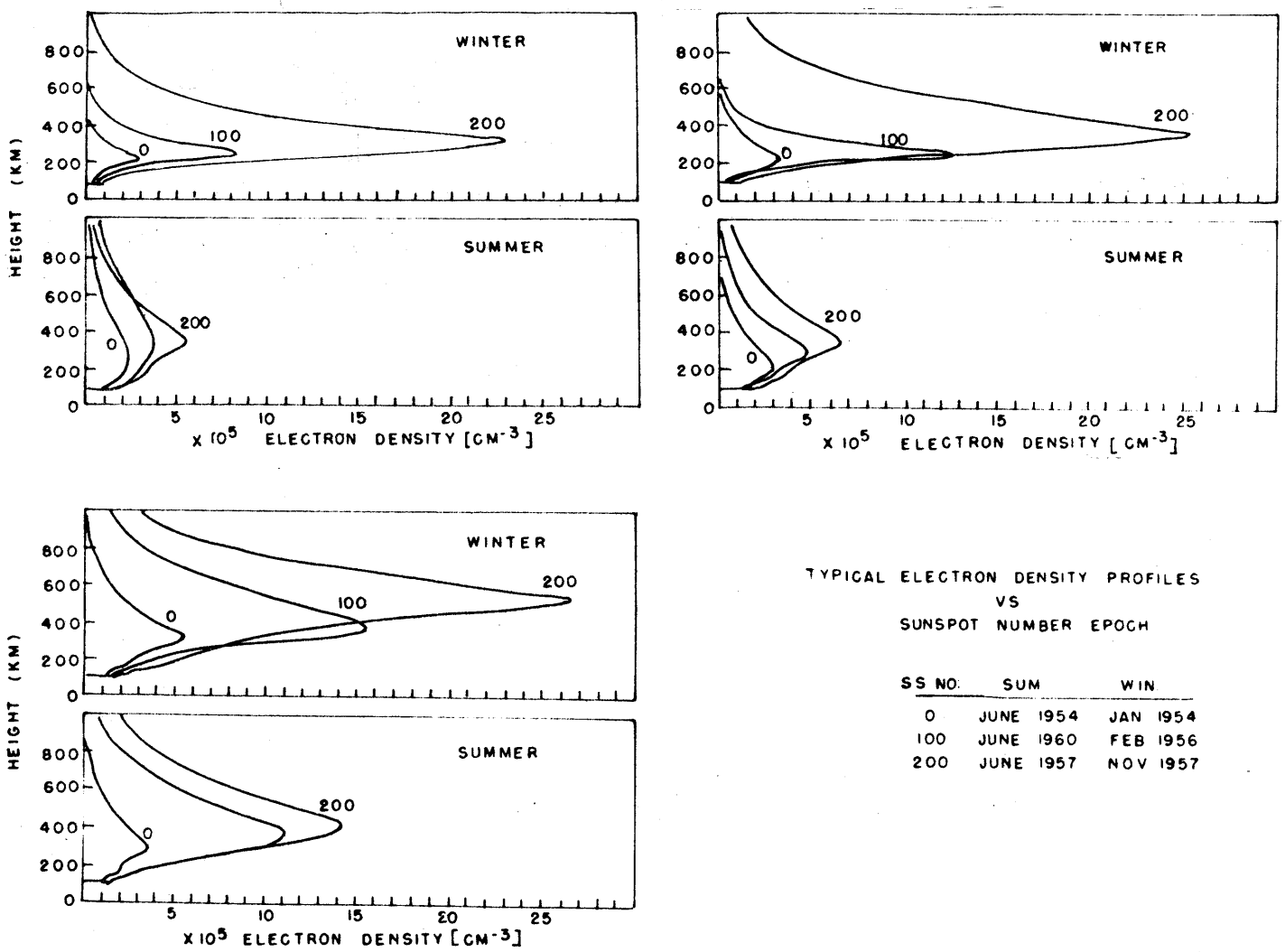

TYPICAL ELECTRON DENSITY PROFILES
VS
SUNSPOT NUMBER EPOCH

SS NO:	SUM	WIN
0	JUNE 1954	JAN 1954
100	JUNE 1960	FEB 1956
200	JUNE 1957	NOV 1957

Fig. 6.4. Variability of electron density with solar cycle for high (upper left), medium (upper right), and low (bottom left)latitudes (after Wright, 1962).

ion drag coefficient $N_i / (1 + \varsigma_+^2)$ on the sunspot activity are calculated for summer and winter conditions for middle latitude at noon. The results are shown in Figures 6.5 and 6.6. We have assumed here that ν_i / ω_i does not change with local time and season, and n_m does not change with season.

For actual application to the numerical study, in the region above about 15km, we find it more convenient to use the relation $\nu_i = 7 \cdot 10^{-10} n_m$ and $\varsigma_+ \ll 1$. Hence, the ion drag coefficient $N = N_i (1 + \varsigma_+^2)^{-1} = 7 \cdot 10^{-10} (2\Omega)^{-1} n_i \sim 5.10^{-6} n_i$. A set of vertical profiles of N is presented and discussed in chapters 9 and 10.

Viscosity and heat conduction play an increasingly important role at sufficiently large altitudes z, since the density roughly decreases exponentially as $z \to \infty$. Ion drag will also be important in the altitude range between 200 and 500km and especially at periods of maximum solar activity. The dissipative effect of these processes will damp the motion at high altitude. These damping processes and other additional effects of viscosity, heat conduction and ion drag will be further discussed in the next chapter.

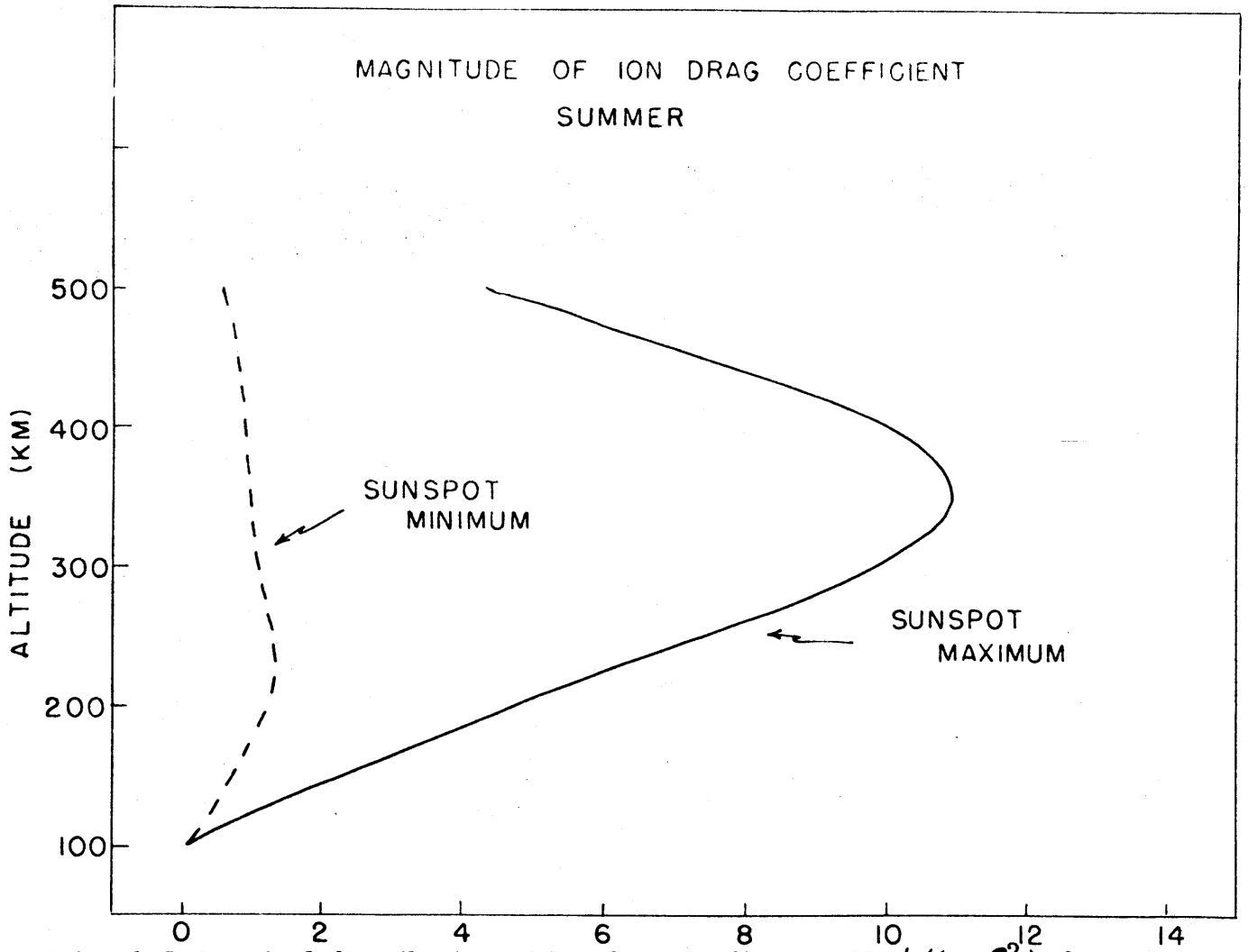

Fig. 6.5. Vertical distribution of ion drag coefficient $N_i / (1 + \rho_+^2)$ for sunspot maximum and minimum, middle latitude, and summer at noon.

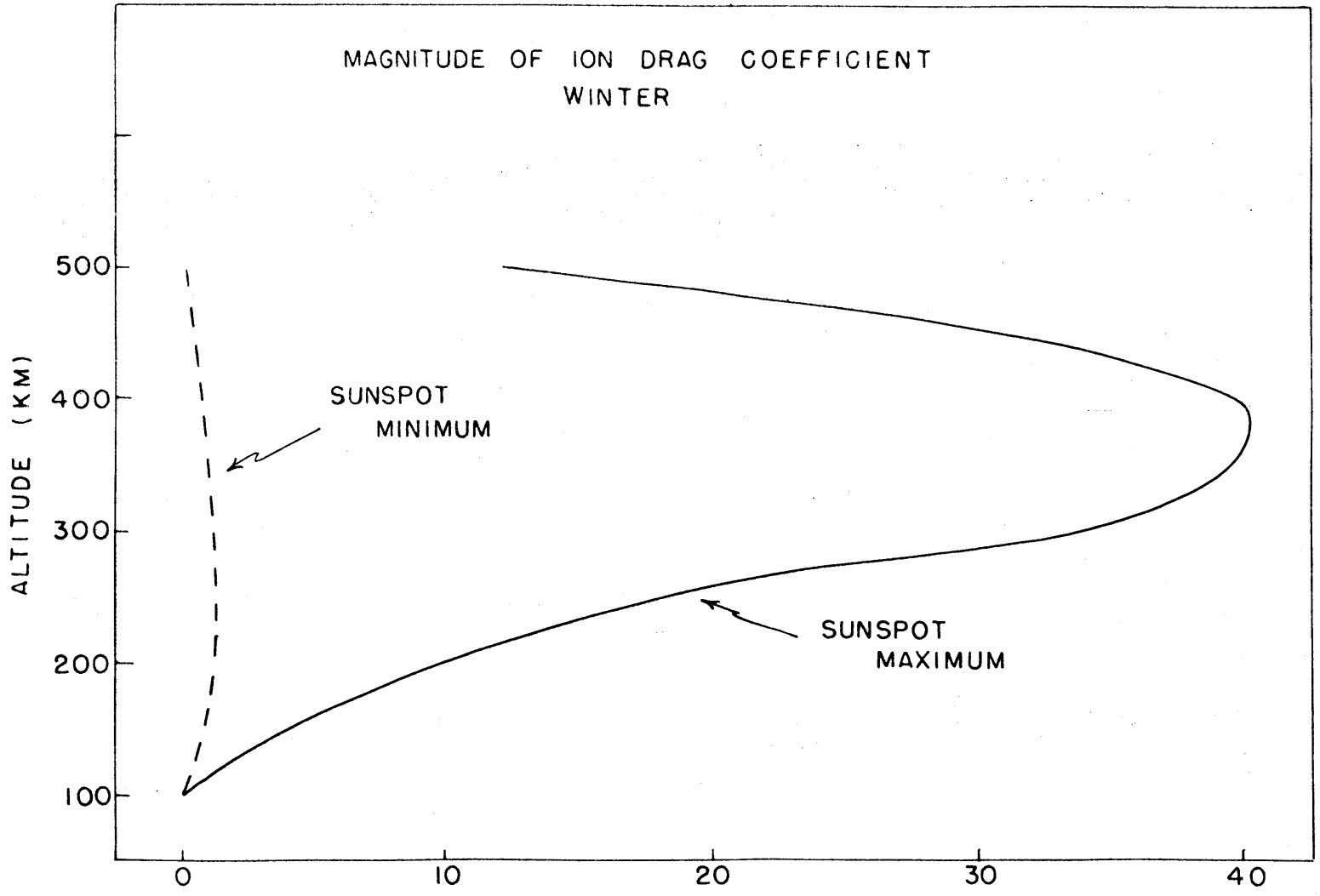

Fig. 6.6. Same as Fig. 6.5 but for winter.

7. THE PHYSICS OF DIABATIC HEATING

The most important diabatic processes, in the thermosphere, are associated with several modes of heating, each given a contribution to the generation of total potential energy. The modes of diabatic heating as defined in section 2.2, are:

(1) absorption of EUV solar radiation

(2) infrared radiation

(3) corpuscular heating

(4) chemical heating

7.1 Solar Heating

The major diabatic energy source of the thermosphere above 100 km can be considered to be the absorption of solar radiation in the spectral region for which $\lambda < 1800$ Å. Changes in the thermospheric temperature are due principally to the variation of EUV, as found by Bordeau et al. (1964). To obtain a quantitative description of this heating source, one needs the following information

(1) a precise description of the incoming extreme ultraviolet and soft X-ray spectrum, which gives solar photon flux as a function of wavelength.

(2) absorption and ionization cross sections for each spectral interval and for each component gas.

(3) a detailed description of the photo-chemical processes that follow the absorption of a photon of a given wave length by a given component.

(4) concentration and composition of the neutral gas.

Recent observational programs and the extensive progress made in developing instrumentation for measuring the EUV have been reviewed by Hinteregger (1965). Allen (1965) has reviewed and summarized previous tabulations of ionizing solar fluxes and cross section data and discussed their interpretation. Further details and references may be found in these papers. The following summary is sufficient for our purposes.

Almost all the radiation in the spectral region 40 Å to 1000 Å is absorbed in the 10^{-1} to 10^{-3} μb layer (radiation in the spectral region 30 Å - 40 Å is absorbed in the 1 to 10^{-2} μb layer, radiation in the spectral region 200 Å - 973 Å is absorbed in the 10^{-2} to 10^{-4} μb layer, and the 1215.7 Å radiation is absorbed below the 10^{-1} μb layer). We can associate E layer ionizing radiation with heating of the 10^{-1} to 10^{-2} μb layer, and F layer ionizing radiation with heating of the 10^{-2} to 10^{-3} μb layer. Allen suggests

that for solar photon fluxes of energy in the E and F layers, one uses

Layer	Flux in ergs/cm^2 sec
E	0.5 (1 + .0097R)
F	0.9 (1 + .0124R)

where R is the sunspot number. R ranges from a minimum of 0 at sunspot minimum to a mean value of 100 at sunspot maximum, and exceeded 300 at times during the IGY. The sunspot cycle variation of the EUV radiation is deduced from surface measurements of the maximum electron content of the E and F layers, and has not yet been verified by a long term satellite monitoring program. Several months data from OSO I showed a good correlation between EUV (40 Å to 400 Å) and 10.7 cm microwave radiation. In view of this correlation, it has been generally assumed that the 10.7 cm radiation is another index of the intensity of EUV. It has also been accepted that the 10.7 cm flux and the EUV is closely correlated with the sunspot number. Anderson (1965), however, has questioned the assumed close association between the 10.7 cm flux and the EUV on the ground that they do not vary the same way over a solar cycle.

The other major solar heat source for the thermosphere are photons in the Schumann Range continum, $1325 \text{ Å} \leq \lambda \leq 1775 \text{ Å}$.

These photons are absorbed primarily between the 1 and .01 μb levels. The measured energy flux is approximately 32 ergs/cm^2 sec, and is believed to have little dependence on the sunspot cycle since it originates in the solar photosphere.

The solar energy fluxes mentioned above may be compared with the solar constant, 1.4 x 10^6 ergs/cm^2 sec. The drastic effect that the EUV has on the thermosphere is a consequence of the thermosphere's very small mass. For example, 1 erg/cm^2 sec heat input absorbed uniformly above .01 μb gives a heating rate of roughly a thousand degrees per day.

Let us now discuss those aspects of thermospheric photochemistry which determine the distribution and the fraction of the photon energy which is absorbed and realized as in situ heating. The direct heating can be determined as the difference between total photon energy absorbed and the energy lost in chemical reactions or reradiated by longer wave-length photons.

First we consider the heating by the ionizing radiation. From the survey and tabulation by Hinteregger et al. (1965) we see that photons more energetic than 1027 Å can ionize O_2, those more energetic than 911 Å can ionize O, and those more energetic than 796 Å can ionize N_2. The ultimate chemical end products that result after

charge exchange, dissociative recombination, and radiation of less energetic photons are O_2 and N_2 molecules, O and N atoms. The net change of atomic versus molecular composition, is needed to compute the fraction of photon energy converted to chemical energy.

Atoms are produced from charged molecules by the dissociative recombination processes.

$$\left.\begin{aligned} O_2^+ + e &\rightarrow 2\,O \\ NO^+ + e &\rightarrow N + O \end{aligned}\right\} \qquad (7.1)$$

For a quantitative description of the rate of production of the atomic end products we require the rate of production of O_2^+ and NO^+ molecules. Donahue (1966) has discussed the relevant ionospheric reactions in the light of recent laboratory measurements of rate coefficients and of recent ionic composition measurements. The important charge exchange reactions are:

$$\left.\begin{aligned} N_2^+ + O &\rightarrow NO^+ + N \\ N_2^+ + O_2 &\rightarrow O_2^+ + N_2 \\ O^+ + N_2 &\rightarrow NO^+ + N \\ O^+ + O_2 &\rightarrow O_2^+ + O \end{aligned}\right\} \qquad (7.2)$$

Based on Donahue's discussion we estimate that the rate of

production of O_2^+ and NO^+ and hence O's and N's from ionization are roughly equal. The N's undergo the further reactions $N + O \rightarrow NO$, $NO + N \rightarrow N_2 + O$, which from the discussion of Nicolet (1965) would appear to take place on a shorter time scale than the time scale for diffusion or transport by motions. Assuming then that all the above reactions occur locally at the point of initial ionization, the net result will be that for each ion produced from N_2, O_2, or O there occur locally the "equivalent" chemical reaction

$$O_2 + 5.1 \text{ e. v.} \rightarrow 2\,O \qquad (7.3)$$

where the 5.1 e.v. is the dissociation energy of O_2. Reaction (7.3) is equivalent to the photochemical processes that gives the net change from molecules to atoms. Hence, for photons of wavelength less than 1027 $\mathring{A}$ the rate of production of chemical energy (loss of ionization energy) is given by 5.1 e.v. times the sum of photons per spectral interval and times the ions produced per photon. A small loss of ionization energy in the form of chemical energy occurs from direct dissociation $O_2 \rightarrow 2O$.

If some of the N and NO are transported away from their production site, the chemical energy production by the "equivalent" reactions

$$\left.\begin{array}{lcl} N_2 + 9.8 \text{ e.v.} & \rightarrow & 2N \\ NO + 6.5 \text{ e.v.} & \rightarrow & N + O \end{array}\right\} \qquad (7.4)$$

where the 9.8 e.v. and 6.5 e.v. are the dissociation energy of N_2 and NO respectively, and the transport of the N's and NO's should alos be taken into account. The error resulting from assuming only (7.3) to occur probably will not exceed the error in specifying the solar fluxes.

The largest energy loss above the lower thermosphere due to nonthermal radiational damping of excited states is by the 6300 $\mathring{A}$ dayglow. According to Dalgarno and Walker (1964) a maximum airglow emission of 50 kiloraleighs $\sim$ .1 erg/cm^2 sec is possible but observational evidence suggests that this is reduced by about a factor of two. We deduce an upper limit of about 5×10^{-2} ergs/cm^2 sec energy loss from nonthermal radiation above the 10^{-1} μb level. For a review of the major dayglow lines in the visible, cf. Wallace and McElroy (1966). See Krassofskij and Lefov (1965) for a general tabulation of the strength of thermospheric airglow lines.

Photons of wavelength greater than 1027 $\mathring{A}$ are significantly absorbed in the thermosphere only by molecular oxygen. Most of the absorption takes place in the Shumann-Range continuum 1325 $\mathring{A} \leq \lambda \leq$ 1775 $\mathring{A}$, where molecular oxygen is dissociated into atomic oxygen.

Eq. (7.3) also applies here, thus 5.1 e.v. of chemical energy is produced per photon absorbed.

Figure 7.1 shows schematically the major photochemical processes that take place in the thermosphere. Q_{CH} and Q_A are the chemical energy and the energy reradiated by longer wavelength photons respectively.

The following considerations are discussed further as other forms of heating.

(1) Much of the dissociation energy itself may also eventually go into heat. The oxygen atoms resulting from the dissociation of O_2 are transported downward in the thermosphere by diffusion and motions until the atmosphere is dense enough $1\ \mu$ b, that three body recombination can quickly occur. This energy would be released in the lower thermosphere. This is discussed under "chemical heating".

(2) Most of the heat energy obtained directly from an ionizing photon originally goes into the kinetic energy of the escaping electron. These photo-electrons quickly come into thermal equilibrium with the electron gas and more slowly with the ions and neutrals. However, the photo-electrons

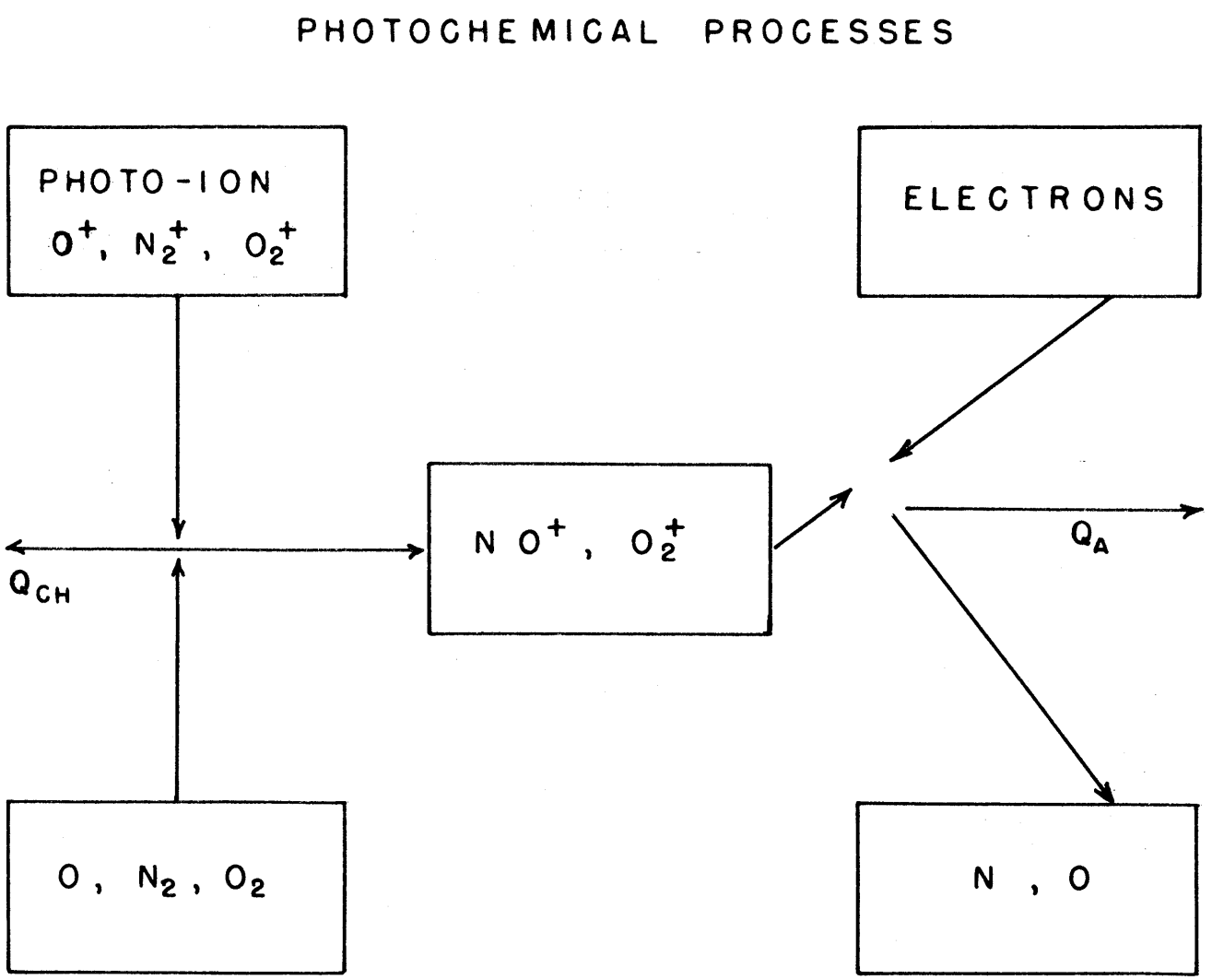

Fig. 7.1. Diagram of major thermospheric photochemical processes.

can travel a considerable distance up magnetic field lines before losing kinetic and chemical energy by collision, and hence being thermalized by the ambient electron gas in the congugate point. This nonlocal heating effect of the electron turns out to be negligible for the neutral gas heat budget.

7.2 Heating Efficiency in the Neutral Gas

The term heating efficiency factor, ε, used here is a nondimensional quantity which indicates the percentage of the total energy input that is transformed into heat, i.e. ε = (total input - loss) / total input. This parameter plays an important role in determining the heating rates and consequently the thermal structure of the neutral and ionized constituents in the thermosphere. Until now, its application to the thermosphere has been regarded as empirical only. The terms ε_N and ε_e will denote the neutral and electron heating efficiencies respectively. To estimate the value of ε_N we require a detailed description of the photochemical processes in the thermosphere, which we have discussed in the preceding section.

Let us first consider the heating efficiency due to the ionizing radiation. From the tabulation of the spectral intensity distribution

and ionizing efficiency (secondary ion production rate) of photons less than 1027 Å, we find an average photon energy of ~ 36 e.v. producing 1.3 ions/ photon. 6.6 e.v. (5.1 x 1.3) is expended to produce chemical energy, and a negligible amount of energy to produce airglow. The resulting mean heating efficiency is thus found to be 83%. This value is considerably higher than those used by other authors. Harris and Priester (1962) have assumed a heating efficiency of 38% and consider 70-90% an extremely high efficiency. Lasarev (1964) estimates that an average value for ε_N is between 40% and 60%, and probably nearer to 40%. Mahoney (1966) has estimated the value of ε_N to be 60%. It seems that only the heat energy obtained directly from ionizing photons adjusted empirically was included, and the energy lost in the photochemical processes was apparently neglected.

Since different wavelength photons are absorbed at different levels, the heating efficiency should vary with altitude. In order to obtain this distribution we require the knowledge of the total heat input, which we shall call ionization photon energy and denote by I_i, as a function of altitude or pressure. Using table 1, which presents the solar flux, cross sections, and secondary ion production rate, and table 2, which presents the composition data for average solar activity and noon condition as reported by Mahoney (1966), we calculate I_i

TABLE 1. Solar Flux (e.v.) and Cross Section (10^{-4} $gm^{-1}cm^2$)

(Å)	Flux (e.v.)	σ (O)	σ (O_2)	σ (N_2)	σ (IO_2)	σ (IN_2)	$\mathcal{M}$
1775-1725	6.98-7.19	0	0.32	0	0	0	1.0
1725-1675	7.19-7.40	0	1.62	0	0	0	1.0
1675-1625	7.40-7.63	0	4.14	0	0	0	1.0
1625-1575	7.63-7.87	0	9.79	0	0	0	1.0
1575-1525	7.87-8.13	0	15.06	0	0	0	1.0
1525-1475	8.13-8.41	0	21.28	0	0	0	1.0
1475-1375	8.41-9.02	0	26.92	0	0	0	1.0
1375-1325	9.02-9.36	0	10.92	0	0	0	1.0
1215.7	10.20	0	0.0156	0	0	0	1.0
1027-990	12.1-12.5	0	3.29	0.538	1.54	0	1.0
977.0	12.7	0	7.53	5.59	3.01	0	1.0
972.5	12.7	0	75.3	538.	33.9	0	1.0
990-911	12.5-13.6	0	13.8	6.95	8.02	0	1.0
911-840	13.6-14.8	10.8	18.5	9.75	12.4	0	1.0
840-810	14.8-15.3	12.0	49.0	7.21	17.1	0	1.0

TABLE 1 (continued)

(Å)	Flux (e.v.)	$\sigma(O)$	$\sigma(O_2)$	$\sigma(N_2)$	$\sigma(IO_2)$	$\sigma(IN_2)$	$\mathcal{M}$
810-796	15.3-15.6	12.4	75.3	14.5	26.4	0	1.0
796-740	15.6-16.8	12.7	46.7	53.6	23.5	33.1	1.0
740-630	16.8-19.7	32.4	60.6	54.4	48.4	48.8	1.0
630-460	19.7-27.0	47.8	57.6	51.9	52.7	46.9	1.0
460-370	27.0-33.5	43.7	45.0	36.6	44.2	35.5	1.0
370-310	33.5-40.0	34.7	40.3	19.1	40.3	19.1	1.0
303.8	40.8	36.9	36.7	1.08	36.7	1.08	1.0
310-280	40.0-44.3	34.6	35.2	1.05	35.2	1.05	1.0
280-240	44.3-51.7	27.6	27.5	8.35	27.5	8.35	1.1
240-205	51.7-60.5	19.7	19.7	6.39	19.6	6.39	1.3
205-165	60.5-75.1	12.4	12.4	4.52	12.3	4.52	1.9
165-138	75-90	7.91	7.91	3.01	7.91	3.01	2.4
138-103	90-120	4.14	4.14	1.94	4.14	1.94	3.1
103- 83	120-150	2.63	2.64	1.18	2.64	1.18	3.8
83-62	150-200	1.51	1.51	0.796	1.51	0.796	5.0
62-41	200-300	0.828	0.828	0.387	0.828	0.387	7.5
41-31	300-400	0.377	0.377	0.151	0.377	0.151	9.0

TABLE 2. Atmospheric Composition for Medium Solar Activity, 1200 Hours

N	Height	N(O)	$N(O_2)$	$N(N_2)$
1	.80000E 02	.75000E 11	.84308E 14	.31716E 15
2		.15000E 12	.29573E 14	.11125E 15
3	.91539E 02	.25000E 12	.98954E 13	.37226E 14
4		.50000E 12	.29758E 13	.11195E 14
5	.10590E 03	.50000E 12	.75626E 12	.28450E 13
6	.11854E 03	.19044E 12	.15878E 12	.69322E 12
7	.13712E 03	.74149E 11	.33305E 11	.16972E 12
8	.16315E 03	.30158E 11	.70605E 10	.42346E 11
9	.19779E 03	.12419E 11	.14479E 10	.10338E 11
10	.24175E 03	.51428E 10	.28155E 09	.24282E 10
11	.29419E 03	.21294E 10	.51207E 08	.54249E 09
12	.35303E 03	.85758E 09	.85028E 07	.11241E 09
13	.41613E 03	.33376E 09	.12995E 07	.21703E 08
14	.48174E 03	.12661E 09	.18765E 06	.39899E 07
15	.54868E 03	.47305E 08	.26234E 05	.71319E 06

from

$$I_i = \frac{\Sigma_\lambda \; F_\lambda \quad P_{i\lambda}}{P_T} \tag{7.5}$$

where F_λ and $P_{i\lambda}$ are the solar flux and photoelectron production rate at wavelength λ, and P_T is the total photoelectron production rate. Figure 7.2 shows this result. The magnitude of I_i ranges from 35 e.v., above about 250 km, to 170 e.v. around the 100 km level. The dependence of the heating efficiency due to ionization ε_N^i, on altitude is depicted in Fig. 7.3. The values obtained are seen to lie between 81% and 96%.

Let us now consider the heating efficiency due to absorption of the Schumann-Range photons. Again from the spectral intensity distribution we find an average photon energy of $\sim$ 8 e.v. and expenditure of 5.1 e.v. to produce chemical energy. The resulting heating efficiency per photon is $\sim$ 35%. The dissociation photon energy, I_d, as a function of altitude is also computed from tables 1, 2, and (7.5). The result is shown in Fig. 7.2. We find that the photon energy ranges from 7 to 11 e.v. The height dependence of the heating efficiency due to photodissociation, ε_N^d, is shown in Fig. 7.3. The value obtained is seen to lie between 30% and 36% above 100 km.

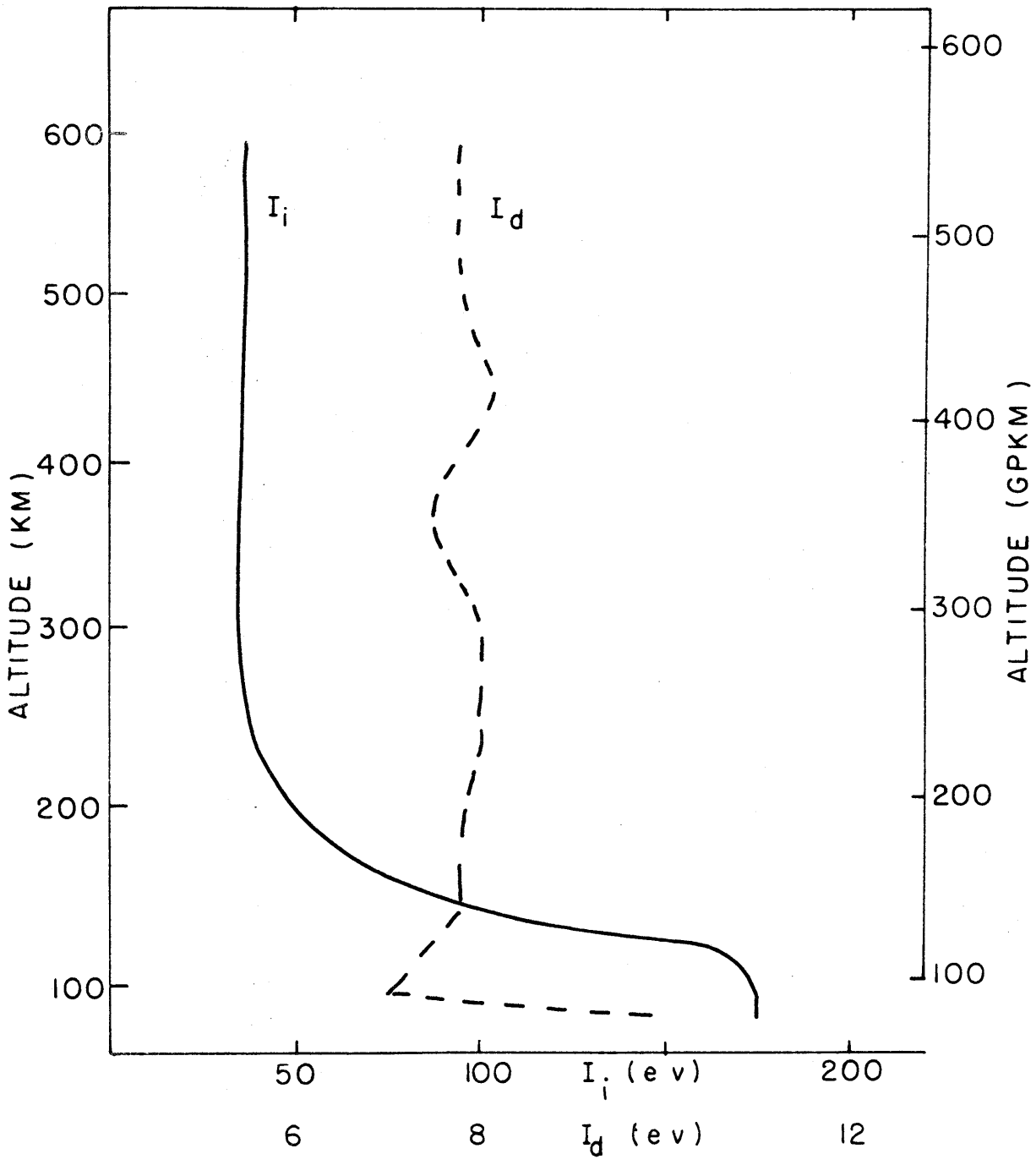

Fig. 7.2. Vertical distribution of ionization photon energy I_i and dissociation photon energy I_d.

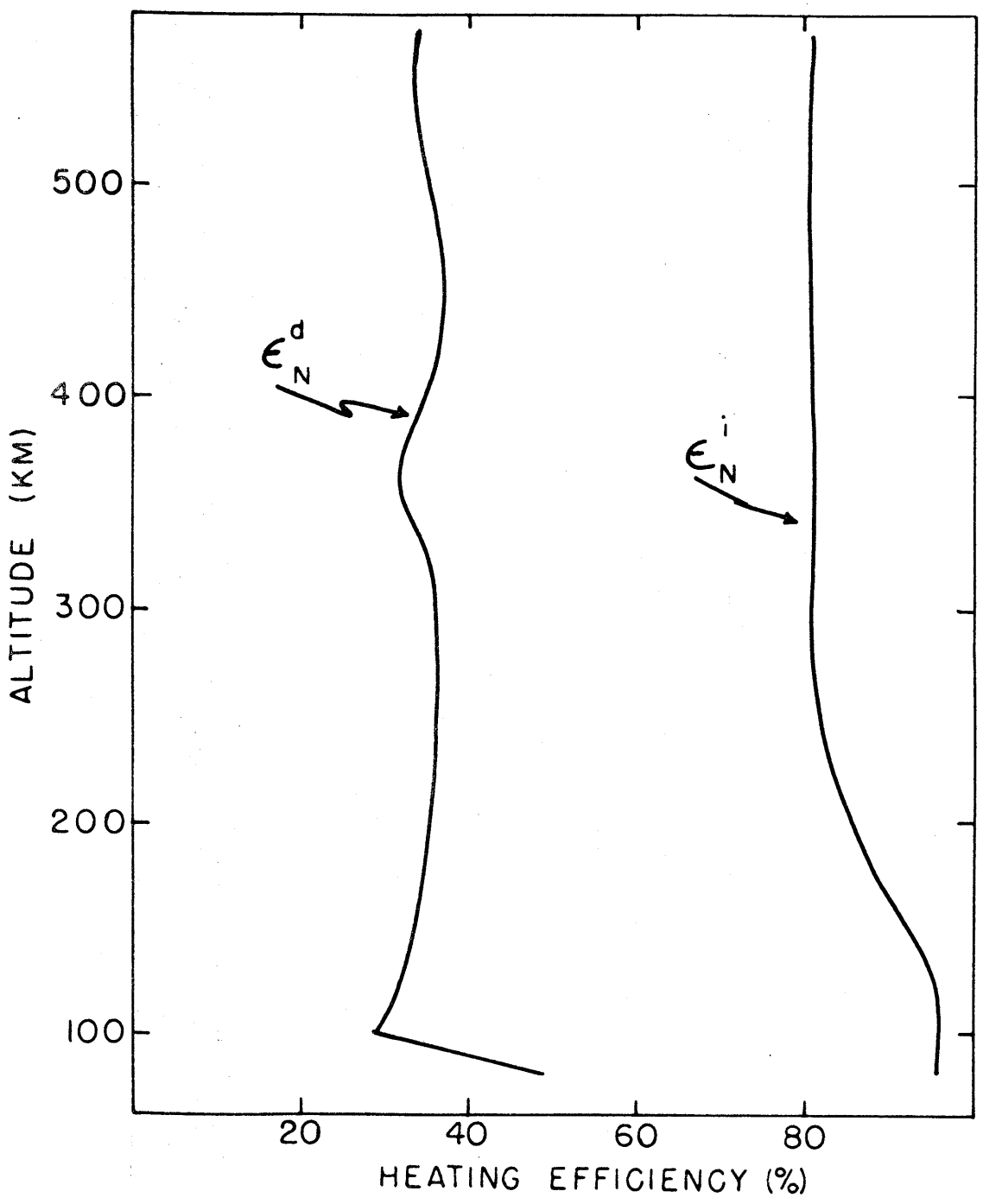

Fig. 7.3. Vertical distribution of ionization heating efficiency ϵ_N^i and dissociation heating efficiency ϵ_N^d for the neutral gas.

7.3 Heating Efficiency in the Ionosphere

Another important item which merits much study is the nature of the electron heating efficiency in the ionosphere. Just as the neutral heating efficiency plays an important role in determining the temperature structure of the thermosphere, so does the electron heating efficiency, ε_e, in determining the thermal structure of the electron gas. Determination of ε_e requires the detailed knowledge of the electron heating rate, i.e. the heat input to electrons, and the photoelectron production rate. Estimates of the value of ε_e and its altitude dependence given in the literature do not agree among themselves (Hanson, 1963; Hanson and Cohen, 1968; Nagy et al., 1969).

A detailed calculation and interpretation of the electron heating efficiency within the framework of ionospheric physics is beyond the scope of the present work. The following summary will be sufficient for our purposes.

We have already computed the ionization photon energy I_i, which required the knowledge of P_T and computed from tables 1 and 2. We next define the photoelectron heating energy coefficient, E_{phe}, as

$$E_{phe}\,(e.v.) = I_i - \bar{\Phi}_i \,, \qquad (7.6)$$

where $\bar{\Phi}_i$ is the average ionization potential for O, O_2 and N_2, and which we take to be $\sim$ 15 e.v. The electron heat input, Q_e, can be computed indirectly, by assuming that under local equilibrium, the heat input and loss must balance. The heat loss can be computed from the heat transfer to ions and neutrals. The heat transfer is fulfilled by means of elastic and inelastic collisions with neutral particles and elastic collision with ions.

The electron-ion-neutral energy flow in a mixture of O, O_2, N_2, e, O^+, NO^+, and O_2^+, in the ionosphere is presented in Fig. 7.4. Under the above assumption we would require the following relation to hold,

$$\begin{aligned} Q_e &= Q_{ei} + Q_{eN} \\ Q_{iN} &= Q_i + Q_{ei} \sim Q_{ei} \\ I_i &= Q_e + Q_i + Q_N + Q_s \end{aligned} \tag{7.7}$$

where Q_s is the rate of photoelectron lost to the magnetosphere by diffusion and escape. There is no estimates of Q_i, but this component must be very small compared to Q_{ei}. The process of slowing down the photoelectrons by neutral particles, Q_N, and the subsequent emission of the dayglow has been discussed by Dalgarno et al. (1969).

The electron-ion energy flow by means of elastic collision, measured in e.v./cm^3 sec, is (Dalgarno et al., 1967),

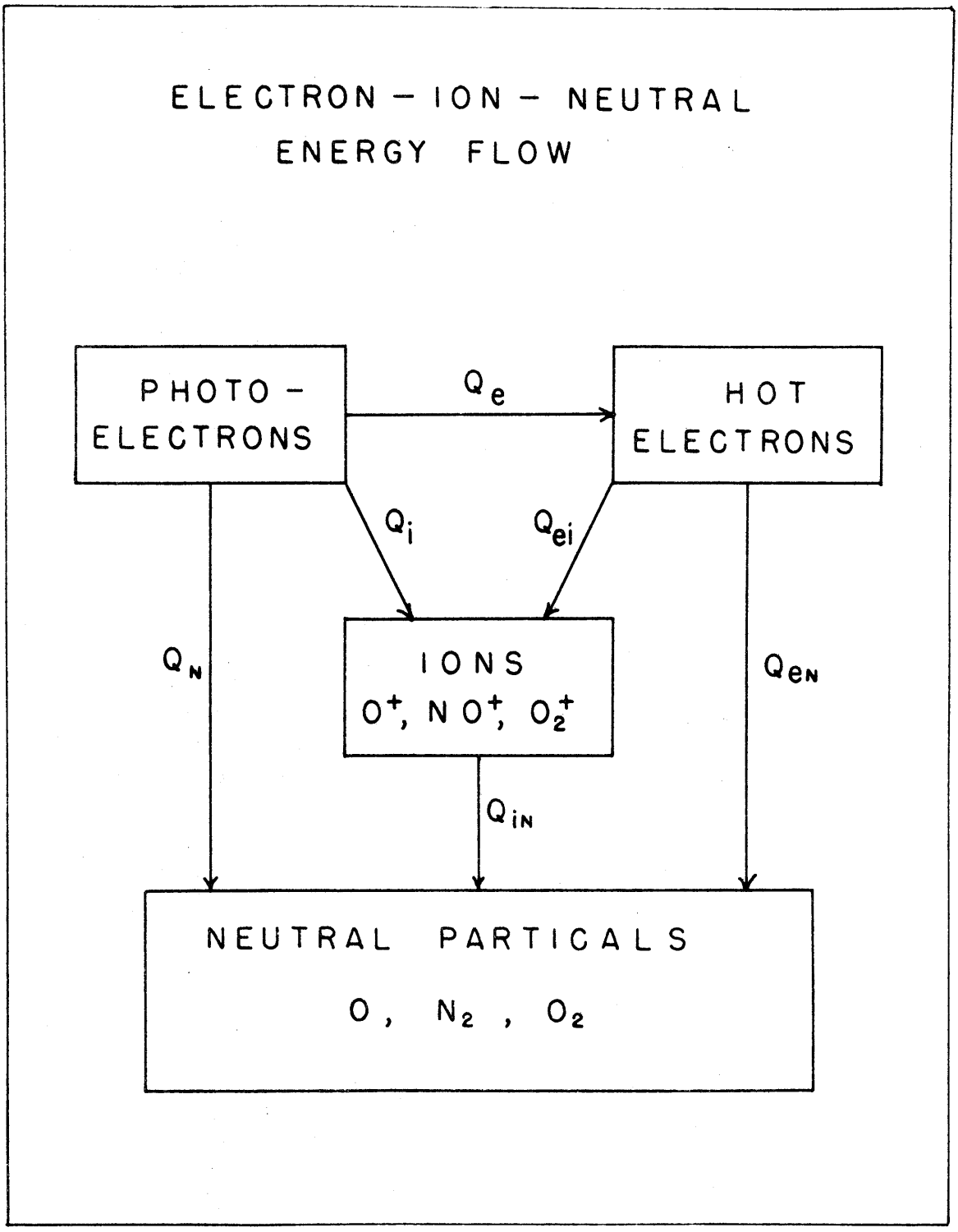

Fig. 7.4. The electron-ion-neutral energy flow in a mixture of O, O_2, N_2, e, NO^+, and O_2^+, in the ionosphere.

$$Q_{ei} \cong 5 \times 10^{-7} \, n_e^2 \, (T_e - T_i)/T^{3/2} \tag{7.8}$$

Here we have assumed that the O^+ ions dominate and that $n(O^+) \quad n_e$.

The rate at which the electron gas loses heat to the neutral by means of elastic collision is

$$\begin{aligned} Q_{en}^I = {} & 3.74 \times 10^{-18} \, n_e \, n(0) T_e^{\frac{1}{2}} \, (T_e - T_n) \\ & + 1.21 \times 10^{-18} \, (1 + 3.6 \times 10^{-2} \, T_e^{\frac{1}{2}}) \, n_e \, n(O_2) \, T_e^{\frac{1}{2}} (T_e - T_n) \\ & + 7.75 \times 10^{-16} \, (1 + 1.27 \times 10^{-4} T_e) \, n_e \, n(N_2)(T_e - T_n) \\ & + 2.3 \times 10^{-17} \, n_e \, n(H_e) \, T_e^{\frac{1}{2}} \, (T_e - T_n) \text{ e.v./cm}^3\text{sec} \end{aligned} \tag{7.9}$$

The terms for electron-neutral collision for O and O_2 were taken from Banks (1966), for N_2 from Dalgarno et al. (1963), and for H_e from Dalgarno et al. (1967). Electron cooling processes by rotational excitation of O_2 and N_2 have been included in (7.9), however, cooling by vibrational excitation is not. Electron cooling by excitation of atomic oxygen to ^1D level from the ground level has been neglected. The electron cooling arising from electron-impact-induced transition amongst the fine-structure levels of O, denoted here Q_{en}^{fs}, is adopted from the calculation of Dalgarno and Degger (1968).

In order to calculate Q_{ei} and Q_{en}^I we need to know n_e, T_e, T_i, and the composition and temperature of the neutral atmosphere. A sample of this calculation is presented below. We adopt here the

values of Q_{ei}, n_e, and T_e given by McClure (1969) for Jicamarca, Perú, for August 17, 1965, and use the same model of neutral atmosphere. The values of Q_{en}^{I} so obtained, together with Q_{en}^{II} and Q_{ei}, and the resulting Q_e are shown in Fig. 7.5. We note that Q_{en}^{I} is systematically smaller than Q_{en}^{II}, and Q_{en} smaller than Q_{ei}, except in the region below about 280 km.

Next, we define the electron heating energy coefficient, E_{eh}, as the ratio of the electron heating rate to the total photoelectron production rate,

$$E_{eh} \text{ (e.v.)} = Q_e / P_T \qquad (7.10)$$

and the "electron heating efficiency", ε_e, as the ratio of the electron heating energy coefficient to the photoelectron heating energy coefficient,

$$\varepsilon_e \text{ (\%)} = E_{eh} / E_{phe} \qquad (7.11)$$

Note that E_{eh}, as defined here, is equivalent to the parameter originally defined as electron heating efficiency. These three quantities are presented in Fig. 7.6. We first note that the value of E_{eh}, and hence ε_e, is smaller than those found by other authors. A maximum value of 1.4 e.v. is reached by E_{eh} at about 260 km. Secondly, we see that E_{eh} or ε_e does not increase monotonically with alti-

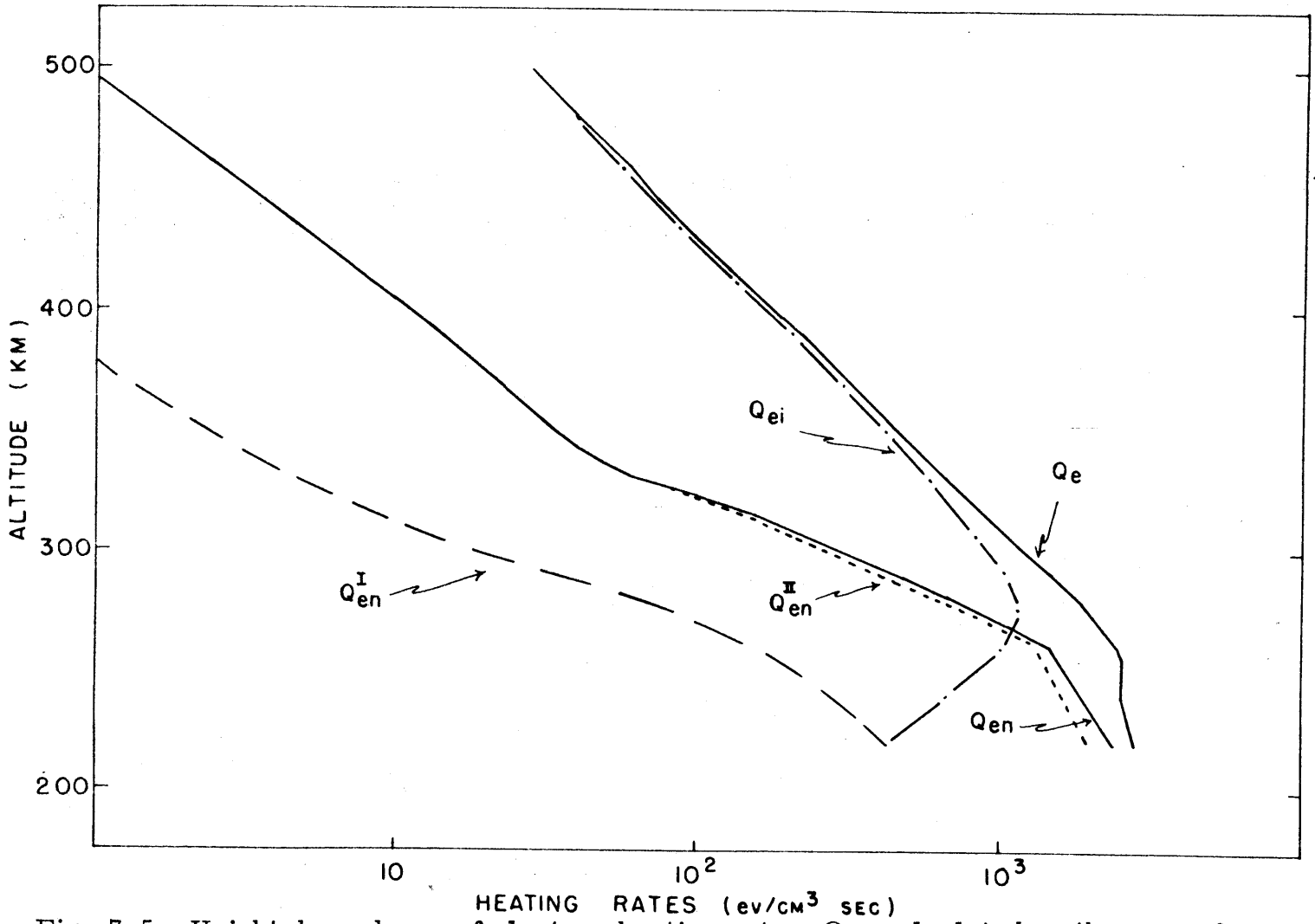

Fig. 7.5. Height dependence of electron heating rates Q_e calculated as the sum of electron-ion Q_{ei} and electron-neutral Q_{en} heating rates.

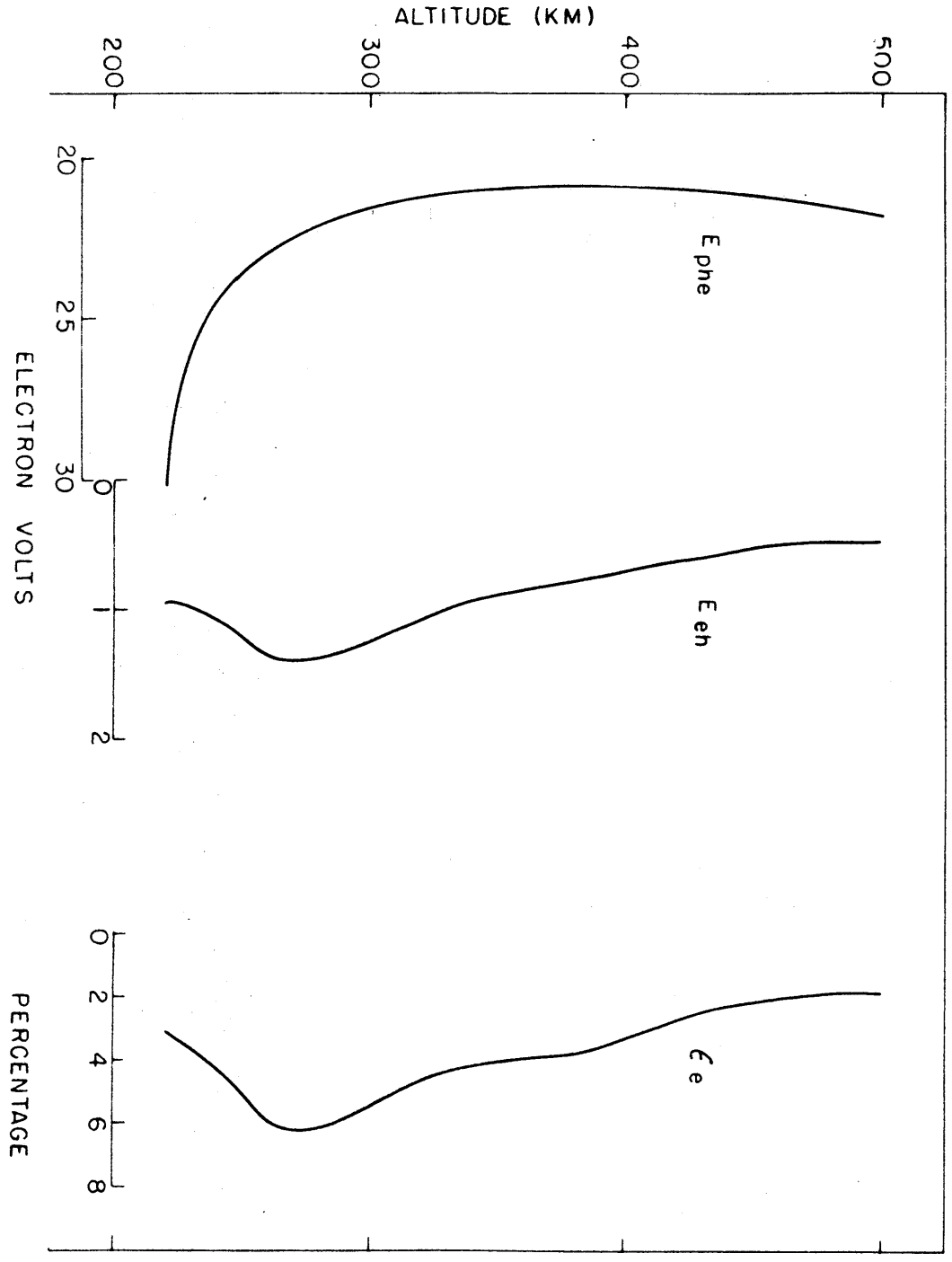

Fig. 7.6. Height dependence of photoelectron heating energy coefficient E_{phe}, electron heating energy coefficient E_{eh}, and electron heating efficiency ϵ_e.

tude as previous results (c. f. Hanson and Cohen, 1968). These differences arise, and the uncertainty in ε_e will remain, mainly from the uncertainties in the rate of total photoelectron production which are available for heating the electron gas and the electron heating rate. The values of P_T used here are 2.5 times larger than those used by Hanson and Cohen (1968) at about 300 km, whereas Q_e's used here are about 3 times smaller than those used by Hanson and Cohen at 300 km. Probably a significant amount of photoelectrons will diffuse and escape outward from the ionosphere (Nisbet, 1968), and consequently change the values of E_{eh} and ε_e.

The microscopic view treated in this section is useful not only for describing the heating processes in the thermosphere, but it is also more rigorous than the macroscopic description treated in sections 7.1 and 7.2. More work remains to be done to fully understand the physics associated with the heating processes. The present discussion is intended to be only a preliminary study.

7.4 Infrared Cooling

The radiation budget above 80 km is accomplished by the EUV solar heating and infrared heating primarily by atomic oxygen. In the lower thermosphere from 10 to .1 μb layer, the infrared thermal emission by CO_2, O_3 and H_2O are not yet very well understood,

primarily because the concentration of these trace substances is not known. Recent studies of the infrared radiative cooling in the 30 to 110 km region, which are due to CO_2, O_3, and H_2O were computed by Kuhn and London (1969). They found that the radiative heating and cooling rates corresponding to the 15 μ CO_2 band are of some importance at the base of the thermosphere. This cooling is approximately $12^{o}K$/day over the winter pole and decreases to $2^{o}K$/day over the summer pole. At the mesopause there is convergence of radiative energy leading to a heating of about $4^{o}K$/day over the summer pole and a weak cooling of about $4^{o}K$/day over the winter pole.

Above the .1 μ b level the only significant infrared cooling process is the 62 line of atomic oxygen (Bates, 1951; Nicolet, 1960). The ground state of atomic oxygen is ^3P_J with $J = 2$, $J = 1$, and $J = 0$. The energy levels of the last two lie 0.020 and 0.028 e.v. above the first one respectively. The statistical weight and the Einstein coefficient for the transition $^3P_1 - {}^3P_2$ are 3 and 8.9×10^{-5}/sec respectively. The corresponding magnitudes for the transition $^3P_0 - {}^3P_1$ are 1 and 1.7×10^{-5}/sec, hence, only the first transition is energetically significant and this gives rise to the 62 μ line.

The rate of heat lost per unit volume due to the 62 μ line has been given by Bates (1951) as

$$\dot{q}_{IR} = f(\gamma, T)\, n(O) \times 10^{-18} \text{ ergs cm}^{-3} \text{ sec}^{-1} \qquad (7.12)$$

where $f(\gamma, T)$ depends on optical path length from some z to ∞ and temperature. For an optically thin atmosphere, Bates gives the expression for $f(\gamma, T)$ as

$$f(O,T) = \frac{-1.67 \exp(-228/T)}{1 + 0.6 \exp(-228/T) + 0.2 \exp(-325/T)} \cdot \qquad (7.13)$$

Numerically one obtains from (7.13)

Temperature	f (O, T)
∞	.93
2,000	.88
1,500	.86
1,000	.83
500	.76
250	.51

which disagree with numerical values given by Nicolet (1960) but agrees with Hunt and VanZandt (1961).

Above the .01 μ b level the atmosphere may be regarded as optically thin to 62 μ radiation.

Bates gives, for the optical thickness, the expression

$$\gamma = 9.4 \times 10^{-17} \int_{z_o}^{\infty} \frac{(1 - \exp(-228/T))}{T^{1/2}}\, n(O, {}^3P_2)\, dz. \qquad (7.14)$$

Assuming a mean temperature, one obtains from (7.14)

$$\tau \simeq C\, M(O, {}^3P_2) \qquad (7.15)$$

where $M(O, {}^3P_2)$ is the column density of $O({}^3P_2)$ and C takes the following values

Mean Temperature	C
1000	6.6×10^{-19}
800	8.5×10^{-19}
600	12.0×10^{-19}
400	20.0×10^{-19}
200	45.0×10^{-19}

Observations indicate a column density of roughly 5×10^{-16} O's above the .01 μ b level, given an optical depth of .1 for a mean temperature of 400°K.

Current models of the lower thermosphere indicate the presence of 2 to 5×10^{17} cm^{-2} atomic oxygen atoms between .01 and 1 μ b, and about 1 to 2×19^{17} cm^{-2} between 1 and 10 μ b. The actual concentration of atomic oxygen is probably quite variable and the values quoted above may be within a factor of two larger or smaller. Thus, (7.12) overestimates the radiational cooling rate in the lower thermosphere because of the assumption that the atmosphere is optically thin to 62 μ .

A similar conclusion has been reached by Craig and Gille (1969) who have integrated numerically the equation of radiative transfer for the CIRA 1965 model atmosphere. Their results show that in the region 80 - 230 km (7.12) overestimate the cooling, with error over 50% below 130 km. Below 100 km they found a region of radiative warming, but the temperature change produced was very small. The fluctuation of the infrared cooling by CO_2 around its mean value, in a time scale of a day, is generally very small in the lower thermosphere. The error introduced by neglecting the fluctuation in infrared cooling by CO_2 and the reabsorption of the 62 μ line is no worse than the error caused by the neglect of the horizontally variable energy transfer due to downward diffusion of atomic oxygen and the dissipation of turbulent motion in the lower thermosphere.

7.5 Solar Heating and Radiational Cooling Rates

As discussed below only solar heating and infrared cooling by atomic oxygen are the major heating and cooling sources in the thermosphere. These heating rates are externally specified in the numerical model calculations discussed in the next chapter. They are obtained from a detailed one-dimensional study carried out by Mahoney (1966). The magnitude of Q^* reported by Mahoney has

been multiplied by 1.41, given a net ionization heating efficiency of 85% (see section 7.2) and dissociation heating efficiency of 14%. The heating rate Q has been assumed to be of the form

$$Q(\lambda, \phi, z, t) = \mathrm{Re} \sum_{m,n=0}^{\infty} Q^*(z, t)\, Y_n^m(\lambda, \phi) = \mathrm{Re} \sum_{mn=0}^{\infty} Q_n^m(z)\, Y_n^m(\lambda, \phi)\, e^{i\sigma t}$$

where $Y(\lambda, \phi) = \frac{1}{4\pi} - \left(\frac{3}{8\pi} \cos\phi + \frac{1}{4} \frac{21}{4\pi} \cos\phi \left(5 \sin^2\phi - 1 \right) \right) e^{i\lambda}$.

This representation gives only three terms in the spherical harmonics expansion. We think that this is the smallest subset in the expansion still capable of representing the general feature of the thermospheric diurnal bulge. From these three components, the first one is responsible for the determination of the mean thermospheric structure. The rest, $Y_1^1\ Q_1^1$ and $Y_3^1\ Q_3^1$, are used for the determination of the perturbation quantities. Figs. 7.7 and 7.8 show the amplitude dependence on altitude and latitude respectively. Fig. 7.7 depicts the magnitude of $Y_0^0\ Q_0^0$, $Y_1^1\ Q_1^1$, and $Y_3^1\ Q_3^1$ versus latitude. The last two components are for 15 degrees latitude. Note that Q_0^0 (mean solar heating) and Q_1^1 have almost the same magnitude. Also note that the broken lines in Q_0^0 from 90 to about 130 km represents cooling, that is, the values are negative. In Fig.

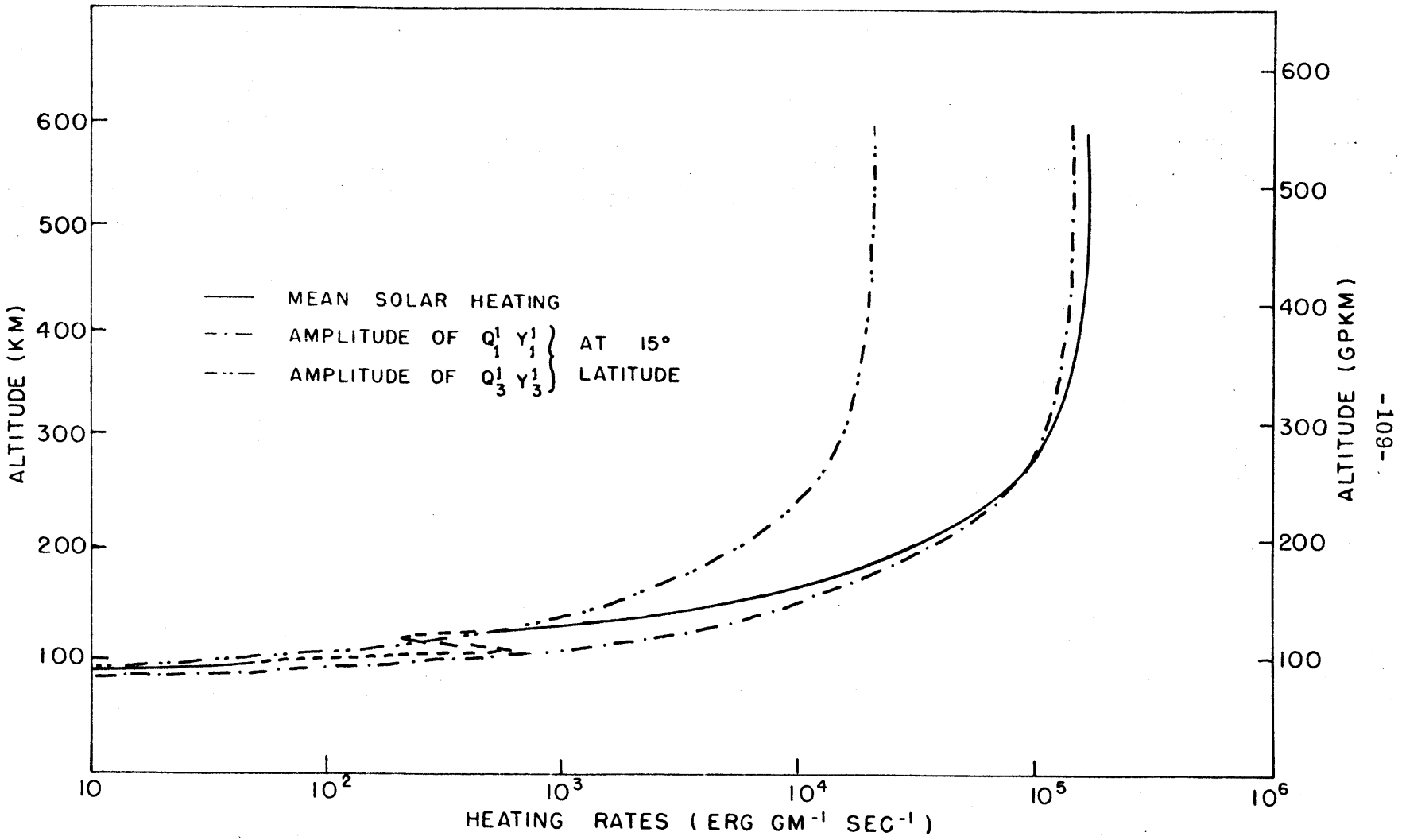

Fig. 7.7. Vertical variability of the first three components in the spherical harmonics expansion of the solar heating rates.

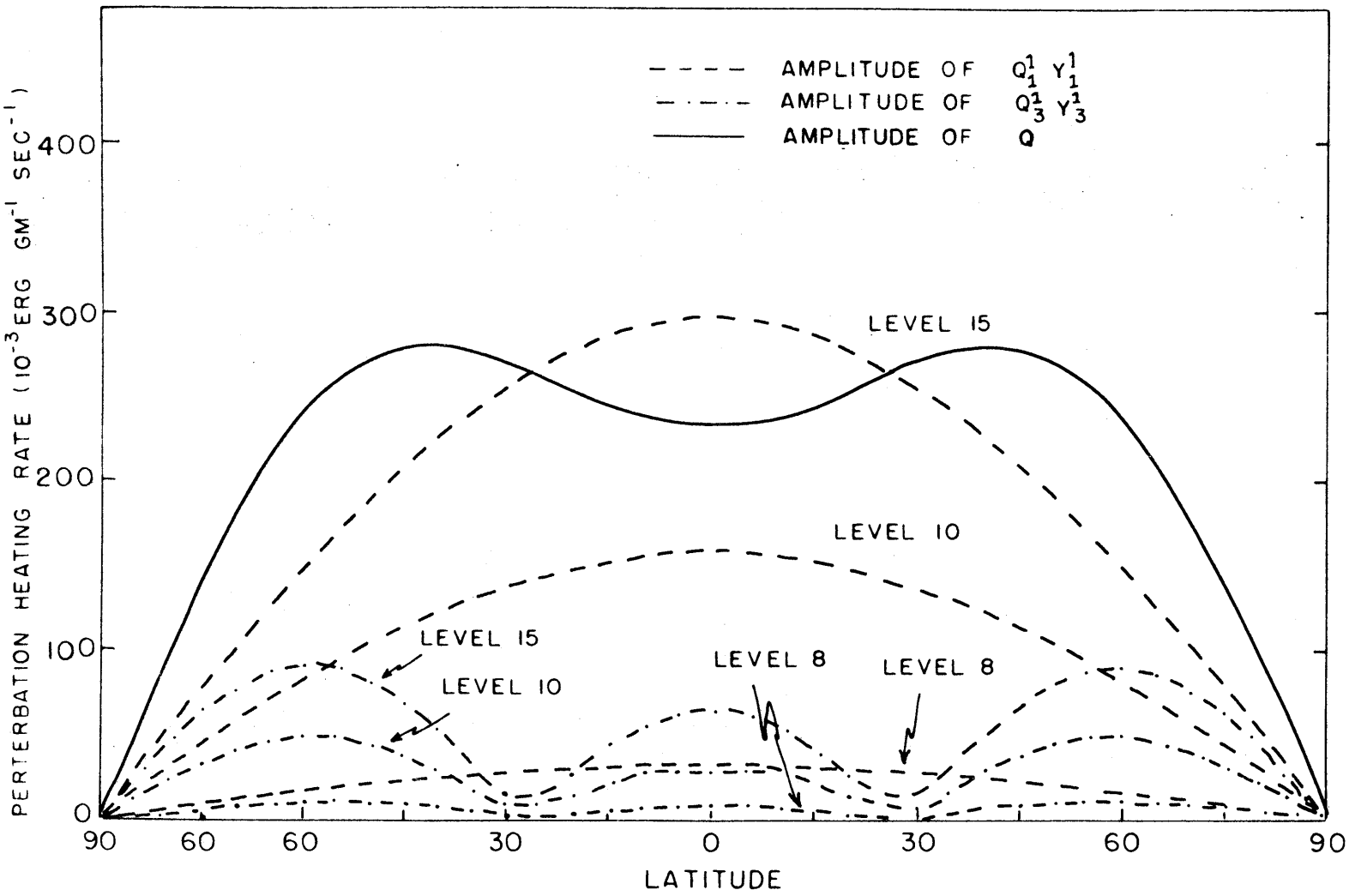

Fig. 7.8. Latitudinal dependence of the perturbation heating rates amplitude. The amplitude of Q is obtained as the sum of $Q_1^1 Y_1^1$ and $Q_3^1 Y_3^1$.

7. 8 we present the perturbation heating rates at three of the model levels. Here the amplitude of Q which is the sum of the amplitudes of $Q_1^1\ Y_1^1$ and $Q_3^1\ Y_3^1$ is shown for level 15 only. Note here that $Q = \dot{q}_{SR} + \dot{q}_{IR}$.

Other modes of diabatic heating mentioned above include corpuscular and chemical heating. The particle precipitation is observed directly from artificial satellites (cf. O'Brien et al, 1964; Sharp et al, 1964;; Sharp et al, 1967), by rockets, by monitoring secondary X-rays with high level balloons (cf. the review by Brown, 1966), and by surface observations of auroral arcs (cf. Chamberlain, 1961).

Two questions on heating by particles and accompanying radiations in the auroral region have been discussed by Chamberlain (1961). The first is concerned with the temperature increase during a bright aurora. The second is concerned with whether particle bombardment affects the average temperature and structure of the thermosphere in the polar regions. Regarding the first one, he estimates that a bright aurora caused by particle bombardment may consume as much energy as 400 ergs/cm^2 sec. From this about 350 ergs/cm sec is reradiated and about 50 ergs / cm^2 sec is dissipated as heat primarily between the 1μb to .1 μb levels. This gives roughly 12% of the energy of the energetic electron converted to heat

A mean quiet day particle precipitation along the auroral oval of roughly .1 erg/cm^2 sec is consistent with available observations (Sharp et al., 1964, Sharp et al., 1966), given an upper limit of about .01 ergs/cm^2 sec for the energy converted into heat. Regarding the second question, Chamberlain finds plausible that bombardment during a great aurora, especially a high-altitude one, might produce temporary but large changes in the polar thermospheric temperature. Dalgarno et al. (1965) have presented a table which summarises some quantitative information about typical auroras. The energy flux of a beam of fast electrons absorbed by the atmosphere has been derived from the intensity of the first negative system of molecular nitrogen, which arises from the electron impact with N_2. The energy fluxes given by Dalgarno et al. (1965) and the conversion into heat by assuming a 12% efficiency is given below,

Parameter	Intensity of Visual Auroras			
	I	II	III	IV
Energy flux (erg/cm^2 sec)	.6	6	60	600
Auroral heating (erg/cm^2 sec)	.07	.7	7	70

We can, therefore, conclude that corpuscular fluxes are a negligible source of thermospheric heating except possibly during geo-

magnetic storms. Even then, considering the small portion of the sky that auroral forms cover, a hemispheric mean heat absorption in the middle thermosphere much exceeding .01 ergs/cm^2 sec seems unlikely. Cole (1966) tentatively concludes that even in the auroral atmosphere the integrated heat input by Joule dissipation will be significantly greater than that by corpuscular bombardment.

A detailed computation of the corpuscular heating for the incoming particles and all the relevant cross sections, would be based on the principles outlined in 7.2 and 7.3. This mode of heating will not be included in the numerical computation.

As discussed in 7.2, a significant fraction of the extreme ultraviolet absorbed in the thermosphere (a daily average of 6 ergs/cm^2 sec) goes into the production of atomic from molecular oxygen. Another major source of O comes from direct dissociation of O_2 by the Schumann-Range continuum. The atomic oxygen so produced is transported downward to the turbopause primarily by diffusion, and then further downward until at some level, around 1μ b where the number densities of atmospheric constituents are sufficiently great that three body recombination can rapidly occur, and the energy be released. This energy as released at this level is probably insignificant in the energy budget of the thermosphere and

therefore will not be included in the numerical model.

In addition to diabatic heating, other modes of heating which strongly depend on the motion and on the electromagnetic fields include Joule heating and heating by viscous dissipation. The rate of Joule heating is given by

$$\dot{q}_{JE} = \underset{\sim}{J} \cdot (\underset{\sim}{E} + \underset{\sim}{V} \times \underset{\sim}{B}) \tag{7.16}$$

which can be written as

$$\dot{q}_{JE} = [\sigma \cdot \underset{\sim}{V} - \underset{\sim}{V}_d] \cdot [(\underset{\sim}{V} - \underset{\sim}{V}_d) \times \underset{\sim}{B}] \tag{7.17}$$

where again σ is the anisotropic electric conductivity tensor and $\underset{\sim}{V}_d$ is the drift velocity vector. Using the expression for (see Appendix II) and assuming that horizontal velocity is much larger than vertical velocity, we find the rate of Joule heating per unit mass is given by

$$\dot{q}_{JE} = \frac{n_i \nu_i}{n_n (1 + \rho_i^2)} [(u - u_d)^2 + (v - v_d)^2 \sin^2 I] \tag{7.18}$$

This formulation is very useful for direct computation of $\dot{q}_{JE}$ and is valid provided that the ion-electron collision frequency is negligible compared to the collision frequency of ions or electrons with neutrals. Eq. (7.18) will describe the total Joule heating that is associated with motions whose time scales are greater than 10^3 sec. Motions with shorter time scale, such as nonhydrostatic gravity-waves, high frequency hydromagnetic waves, and

plasma waves, will also give a contribution to $\dot{q}_{JE}$, which is not described by (7.18). According to the discussion of Karplus et al. (1962) and Campbell (1967), the Joule heating provided by the hydromagnetic waves is of the order of 10^{-8} ergs/cm^2, which is, of course, negligible. The Joule heating associated with small scale turbulence or acoustic-gravity waves with time scale smaller than 10^3 sec is not known. The magnitude probably is negligible compared to the heating provided by (7.18). The Joule heating associated with plasma waves is apparently of no significance.

To estimate the Joule heating expected from dissipation of gravity-tidal waves and meteorological motions, consider a typical value for $n_i \gamma_i / n_n \sim 10^{-4}$ sec^{-1} ($N_i \sim 1$), assume $\rho_+ \sim e^{-z}$, take $\rho_+ = 1$ at the .01 μb level, assume also that sin I $\sim$ 1 and that the wind velocities $(u - u_d)$ and $(v - v_d)$ are typically 70 m/sec. Then from (7.18) we find the rate of Joule heating to be of the order .1 erg/cm^2 sec which will heat the atmosphere at the rate of 100°K/day above .01 μb level. At maximum solar activity this value should be about five times as large, since the ion concentration will increase by about this amount. Likewise, if the amplitude of the winds exceeds the value quoted above, the Joule heating will accordingly increase.

The importance of Joule heating as a heat source at the ionospheric levels has been found to be significant especially during geomagnetic storms over the polar cap (Cole, 1962, 1963, 1966; Kato, 1962; Cummens and Dessler, 1967). The Pederson conductivities may be expected to increase in the auroral regions by at least a factor of ten. Thus an increase in Joule heating by at least a factor of a hundred may locally be expected. In the mean, however, Joule heating will probably be in an order of magnitude less than solar heating. This mode of heating will not be included in the numerical calculations.

The implication of Joule heating as a source for driving the semi-annual variation in density in the thermosphere has been recently discussed by Newell (1968). Internal gravity wave generation by Joule heating in the region of the auroral electrojet has been discussed by Blumen and Hendl (1969).

In order to calculate the heating by viscous dissipation, we need to know the dissipative function Φ which can be derived from equation (2.8), and which, in an invariant vector form is

$$\Phi = \mu \{\nabla \cdot \nabla \underset{\sim}{V}^2 + 2\nabla \cdot [(\nabla \times \underset{\sim}{V}) \times \underset{\sim}{V}] - 2 (\underset{\sim}{V} \cdot \nabla)\nabla \cdot \underset{\sim}{V} + (\nabla \times \underset{\sim}{V})^2 - \frac{2}{3} (\nabla \cdot \underset{\sim}{V})^2\} \qquad (7.19)$$

The rate of dissipation of energy in any finite volume is

$$\int \Phi d v = \int \frac{\mu}{\rho} \nabla \cdot [\nabla \underset{\sim}{V}^2 + 2(\nabla \times \underset{\sim}{V})] dm$$
$$- 2 \int \frac{\mu}{\rho} (\underset{\sim}{V} \cdot \nabla) \nabla \cdot \underset{\sim}{V} dm + \int \frac{\mu}{\rho} \nabla \times \underset{\sim}{V})^2 dm$$
$$- \frac{2}{3} \int \frac{\mu}{\rho} (\nabla \cdot \underset{\sim}{V})^2 dm \qquad (7.20)$$

where dm is an element of mass.

This, to a first approximation (using (3. 3) and definition of $\tilde{\mu}$) is

$$\int \Phi dv = \int 2 \Omega \mu E e^z \left(\left| \frac{\partial u}{\partial z} \right|^2 + \left| \frac{\partial v}{\partial z} \right|^2 \right) dm \qquad (7.21)$$

As an estimate of the magnitude of conversion of kinetic energy to heat energy by viscous dissipation that might occur, consider a typical value of $\frac{\partial u}{\partial z}$ and $\frac{\partial v}{\partial z}$ in the thermosphere to be 15 m/sec, assume $\tilde{\mu} \sim 1$ and $E \sim 1$. Then from (7. 21) we find an energy conversion of the order .05 erg/cm^2 sec and will heat the atmosphere 50 degrees per day above the .01 μ b level. This mode of heating also will not be included in the numerical calculations.

PART II. ANALYTICAL AND NUMERICAL STUDIES

8. THE CIRCULATION IN THE MIDDLE THERMOSPHERE: PROCEDURE

8.1 General Remarks and Description of the Simple Case Study

In the previous chapters we have derived a set of approximate systems of equations for the analysis of thermospheric dynamics and discussed the relevant boundary conditions and diabatic processes. We have classified the thermospheric motions according to the driven force, the time scale, and the importance of viscosity, heat conduction, and ion drag. The system of equations describing various types of motions in the thermosphere show that only vertical motion can give adiabatic heating and cooling in the thermodynamic equation.

We have indicated the convenience of using (3.14) as the only system valid at all heights for actual application to the thermosphere. In general, to get actual solution representing the dynamical structure of the thermospheric diurnal bulge using (3.14) is not a trivial problem. As discussed below, several practical difficulties arise when all the terms of (3.14) are kept. This leaves us with no other choice but to consider other equivalent systems to (3.14) which may

be simpler, but still give some new insights, or reduce some uncertainties, as to the nature of the thermospheric processes. These "alternative models" must be considered in a systematic fashion, starting with the simplest to the most complex ones.

We have learned a great deal about the thermal structure of the thermosphere considering the one-dimensional quasistatic models, and still more about the two dimensional dynamical model. The shortcoming of the latter, as mentioned in the introduction, was the uncertainty as to whether the divergence of the north-south component of the motion field would cancel the divergence of the east-west component, and consequently lead to a negligible adiabatic heating or cooling. Therefore, we need to consider the three-dimensional picture if more meaningful, or less uncertain, results are required.

We have one such alternative model to consider, the thermal geoplasma regime, which describes the balance of the thermal forcing and the ion drag in the momentum equation and uses the complete linearized thermodynamic equation. As we have discussed in section 4.5, this motion regime is appropriate for describing the coupling between the dynamics and thermodynamics at altitudes of the F region peak.

The main purpose of this and the next chapters is, therefore,

to obtain solutions of the system of equations given by (4.4) and use them to substantiate our earlier discovery that only adiabatic heating and cooling by vertical motion can shift the phase of maximum temperature to a time two hours earlier than that obtained in the absence of motions, and thus, to establish adiabatic heating as the explanation of the Harris and Priester's second heat source.

8.2 Representation of the System of Equations in Terms of Spherical Harmonics

Having established (4.4), we revert to the dimensional variables of chapter 2. Since we are only concerned with thermally driven motion, the drift velocity is omitted from here on. Dropping the subscript 1 on all variables, (4.4) becomes

$$\left.\begin{aligned}
\frac{1}{a\cos\varphi}\frac{\partial \Phi}{\partial \lambda} &= -2\Omega N_i U \\
\frac{1}{a}\frac{\partial \Phi}{\partial \varphi} &= -2\Omega N_i V \\
\frac{1}{a\cos\varphi}\frac{\partial u}{\partial \lambda} + \frac{1}{a\cos\varphi}\frac{\partial}{\partial \varphi}(V\cos\varphi) + \frac{\partial w}{\partial z} - w &= 0 \\
\frac{\partial \Phi}{\partial z} &= RT \\
\frac{\partial T}{\partial t} - \frac{g}{P_0 c_p} e^{z}\frac{\partial}{\partial z}\left(\frac{K}{H}\frac{\partial T}{\partial z}\right) + wS &= Q/c_p
\end{aligned}\right\} \quad (8.1)$$

where here

$$N_i = \frac{n_i}{n_n} \quad \frac{\nu_i}{2\Omega} \quad , \qquad S = \left(\frac{\partial T_o}{\partial z} + \frac{R}{c_P} T_o \right)$$

Next, we assume that all perturbation variables and the heating source Q are proportional to $\exp (im\lambda + i\nu t)$ and that the latitudinal variable φ is changed to μ (= sin φ).

Upon substitution, (8.1) becomes

$$\left.\begin{aligned}
\frac{im}{a(1-\mu^2)^{1/2}} \phi &= -2\Omega N_i U \\
\frac{(1-\mu^2)^{1/2}}{a} \frac{\partial \phi}{\partial \mu} &= -2\Omega N_i V \\
\frac{im}{a(1-\mu^2)^{1/2}} u + \frac{1}{a} \frac{\partial}{\partial \mu} [v(1-\mu^2)^{1/2}] + \frac{\partial w}{\partial z} - w &= 0 \\
\frac{\partial \phi}{\partial z} &= RT \\
i\nu T - \frac{S}{\rho_o c_p} e^z \frac{\partial}{\partial z} \left(\frac{K}{H} \frac{\partial T}{\partial z}\right) + wS &= Q/c_P
\end{aligned}\right\} \quad (8.2)$$

The first two equations can be used to solve for u and v. The resulting expression can be substituted in the third equation, given the following equation

$$F(\phi) - 2\Omega a^2 N_i \left(\frac{\partial w}{\partial z} - w \right) = 0 \qquad (8.3)$$

Where the operator F is defined by

$$F = \frac{\partial}{\partial \mu}(1-\mu^2)\frac{\partial}{\partial \mu} - \frac{m^2}{(1-\mu^2)} \tag{8.4}$$

Equation (8.3) can be solved by the method of separation of variables. Noting that the generalized Legendre equation is

$$F\,(P_n^m) + \gamma_n^m P_n^m = 0, \tag{8.5}$$

where $\gamma_n^m = n(n+1)$.

It is convenient to expand each dependent variable in Legendre Polynomials $P_n^m(\mu)$, so that

$$\begin{bmatrix} \phi \\ u \\ v \\ w \\ T \\ Q \end{bmatrix} = \mathrm{Re}\, e^{i\nu t} \sum_n \sum_m \begin{bmatrix} \phi_n^m(z) \\ u_n^m(z) \\ v_n^m(z) \\ w_n^m(z) \\ T_n^m(z) \\ Q_n^m(z) \end{bmatrix} P_n^m(\mu)\, e^{im\lambda} \tag{8.6}$$

Hence (8.3) and the fourth and fifth equations of (8.2) can be rewritten as

$$\gamma_n^m \phi_n^m + 2\Omega a^2 N_i \left(\frac{\partial W_n^m}{\partial z} - W_n^m\right) = 0 \tag{8.7}$$

$$\frac{\partial \phi_n^m}{\partial z} = RT_n^m \tag{8.8}$$

$$i\nu T_n^m - \frac{g}{\rho_0 c_p} e^2 \frac{\partial}{\partial z}\left(\frac{K}{H}\frac{\partial T_n^m}{\partial z}\right) + S W_n^m = Q_n^m / c_P \tag{8.9}$$

Eliminating ϕ_n^m from (8.7) and (8.8) gives

$$\gamma_n^m RT_n^m + 2\Omega a^2 \left[N_i \frac{\partial^2 W_n^m}{\partial z^2} + \left(\frac{\partial N_i}{\partial z} - N_i\right)\frac{\partial W_n^m}{\partial z} - \frac{\partial N_i}{\partial z} W_n^m\right] = 0 \tag{8.10}$$

which together with (8.9) form a system of two second-order ordinary differential equations.

9.3 Formulation of Variables

Taking

$$W_n^m = e^{\frac{1}{2}\int (1 - N_i'/N_i)\,dz} X_n^m$$

$$T_n^m = e^{-\frac{1}{2}\int \left(\frac{K}{H}\right)' \frac{H}{K}\,dz} Y_n^m \tag{8.11}$$

$$' = \frac{d}{dz}$$

the vertical structure of the system of equations takes its simple form

$$\frac{d^2 X_n^m}{dz^2} + f_x(z)\, X_n^m + h_x(z)\, Y_n^m = 0 \qquad (8.12)$$

$$\frac{d^2 Y_n^m}{dz^2} + f_y(z)\, Y_n^m + h_y(z)\, X_n^m = G_n^m(z) \qquad (8.13)$$

where

$$f_x = \tfrac{1}{4}\left[-4(N_i'/N_i) + 2(1 - N_i'/N_i)' - (1 - N_i'/N_i)^2\right]$$

$$f_y = -\tfrac{1}{4}\left\{4 c_p E_h^{-1} \nu e^{-z} i + 2\left[\left(\tfrac{\kappa}{\mu}\right)' \tfrac{\mu}{\kappa}\right]' + \left[\left(\tfrac{\kappa}{\mu}\right)' \tfrac{\mu}{\kappa}\right]^2\right\}$$

$$h_x = \left(\gamma_n^m R / 2\Omega a^2 N_i\right) \exp -\tfrac{1}{2}\int\left[(1 - N_i'/N_i) + \left(\tfrac{\kappa}{\mu}\right)' \tfrac{\mu}{\kappa}\right] dz$$

$$h_y = -c_p E_h^{-1} S \exp\left\{-z + \tfrac{1}{2}\int\left[\left(\tfrac{\kappa}{\mu}\right)' \tfrac{\mu}{\kappa} + (1 - N_i'/N_i)\right] dz\right.$$

$$G_n^m = -E_h^{-1} \exp\left\{-z + \tfrac{1}{2}\int\left(\tfrac{\kappa}{\mu}\right)' \tfrac{\mu}{\kappa} dz\right\} Q_n^m(z)$$

$$E_h = 9\kappa / p_0 H$$

Once X_n^m and Y_n^m are obtained from (8.12) and (8.13), the other dependent variables are calculated from these solutions. The final dependent variables computed in this study are:

(1) h = geopotential height perturbation

(2) u = eastward wind velocity perturbation

(3) v = northward wind velocity perturbation

(4) $\dot{h}$ = upward wind velocity perturbation

(5) T = temperature perturbation

Each of these variables is next expressed in terms of W_n^m and T_n^m.

Geopotential height perturbation (h)

The starting point for this variable is (8.7), which gives for ϕ_n^m

$$\phi_n^m = 2\Omega a^2 N_i (w_n^m - d w_n^m/dz)/\gamma_n^m \tag{8.14}$$

since $\phi_n^m = g h_n^m$, (8.14) can be solved for h

$$h = Re\left\{\sum_n \sum_m 2\Omega a^2 N_i P_n^m(\mu)\left[(w_n^m - d w_n^m/dz)/g\gamma_n^m\right] \exp(im\lambda + i\nu t)\right\} \tag{8.15}$$

Likewise, u, v, $\dot{h}$, and T are given by

$$u = -Re\left\{\sum_n \sum_m 2\Omega a^2 N_i P_n^m(\mu)\left[(w_n^m - d w_n^m/dz)/(1-\mu^2)^{1/2}\gamma_n^m\right] \times \exp(im\lambda + i\nu t)\right\} \tag{8.16}$$

$$v = -Re\left\{\sum_n \sum_m (1-\mu^2)^{1/2} a (d P_n^m(\mu)/d\mu)\left[(w_n^m - d w_n^m/dz)/\gamma_n^m\right] \times \exp(im\lambda + i\nu t)\right\} \tag{8.17}$$

$$\dot{h} = \frac{1}{g}\frac{\partial \phi}{\partial t} + wH \quad , \quad \dot{h}_n^m = i\nu \phi_n^m/g + H w_n^m \tag{8.18}$$

$$\dot{h} = Re\left\{\sum_n \sum_m \left(2\Omega a^2 N_i \nu i P_n^m(\mu)\left[(w_n^m - d w_n^m/dz)/g\gamma_n^m\right] + H w_n^m\right) \exp(im\lambda + i\nu t)\right\} \tag{8.19}$$

$$T = Re\left\{\sum_n \sum_m P_n^m(\mu)\, T_n^m \exp(im\lambda + i\nu t)\right\} \qquad (8.20)$$

Let

$$T_n^m(z) = T_r^{(m,n)}(z) + i\, T_i^{(m,n)}(z)$$

$$W_n^m(z) = W_r^{(m,n)}(z) + i\, W_i^{(m,n)}(z)$$

where $T_r^{(m,n)}$, $T_i^{(m,n)}$, $w_r^{(m,n)}$, and $w_i^{(m,n)}$ are real functions of z.

The final formulae for h, u, v, $\dot{h}$, and T are found from (8.15), (8.16), (8.17), (8.19), and (8.20) to be

$$h = \sum_n \sum_m 2\Omega a^2 N_i P_n^m(\mu) \left\{\left[\left(W_r^{(m,n)} - d W_r/dz\right)/g\gamma_n^m\right]\cos(m\lambda + \nu t) - \left[\left(W_i^{(m,n)} - d W_i^{(m,n)}/dz\right)/g\gamma_n^m\right]\sin(m\lambda+\nu t)\right\} \qquad (8.21)$$

$$u = \sum_n \sum_m a m P_n^m(\mu) \left\{\left[\left(W_i^{(m,n)} - d W_i^{(m,n)}/dz\right)/\gamma_n^m(1-\mu^2)^{1/2}\right]\cos(m\lambda + \nu t) + \left[\left(W_r^{(m,n)} - d W_r^{(m,n)}/dz\right)/\gamma_n^m(1-\mu^2)^{1/2}\right]\sin(m\lambda+\nu t)\right\} \qquad (8.22)$$

$$v = -\sum_n \sum_m a(1-\mu^2)^{1/2}(dP_n^m/d\mu) \left\{\left[\left(W_r^{(m,n)} - d W_r^{(m,n)}/dz\right)/\gamma_n^m\right]\cos(m\lambda + \nu t) - \left[\left(W_i^{(m,n)} - d W_i^{(m,n)}/dz\right)/\gamma_n^m\right]\sin(m\lambda+\nu t)\right\} \qquad (8.23)$$

$$\dot{h} = \sum_n \sum_m P_n^m(\mu) \Big\{ \Big(-2\Omega a^2 N_i \nu \big[\big(W_i^{(m,n)} - dW_i^{(m,n)}/dz \big) / g\gamma_n^m \big] + H W_r^{(m,n)} \Big) \cos(m\lambda + \nu t) - \big(2\Omega a^2 N_i \nu \big[\big(W_r^{(m,n)} - dW_r^{(m,n)}/dz \big) / g\gamma_n^m \big] + H W_i^{(m,n)} \Big) \sin(m\lambda + \nu t) \Big\} \tag{8.24}$$

$$T = \sum_n \sum_m P_n^m(\mu) \Big\{ T_r^{(m,n)} \cos(m\lambda + \nu t) - T_i^{(m,n)} \sin(m\lambda + \nu t) \Big\} \tag{8.25}$$

8.4 Analytical Solution and Discussion of Vertical Boundary Conditions

8.4.1 Discussion of the problem

The system of ordinary differential equations (8.12) - (8.13) is seen to be fourth order in z, so that we require four boundary conditions in order to uniquely define the solutions. These conditions are obtained and constructed by matching the analytical solutions of the system of equations for large and small z to the numerical solutions for intermediate values of z, at the upper and lower boundaries of the numerical model.

Analytical solutions to the system of Eqs. (8.12) - (8.13) can only be obtained if N_i, $\frac{K}{H}$, S, R, and c_p are all independent of alti-

tude. With these assumptions and away from the heat source, (8.12)-(8.13) becomes

$$\frac{d^2 X}{dz^2} - \frac{1}{4} X + \alpha_n r Y = 0 \tag{8.26}$$

$$\frac{d^2 Y}{dz^2} - i\beta r^2 Y - \delta r X = 0 \tag{8.27}$$

where

$$\alpha_n = \frac{\gamma_n^m R}{2\pi a^2 N_i} \quad , \quad \delta = \frac{s c_p}{}$$

$$\beta = \frac{\rho c_p}{E_h} \quad , \quad E_h = \frac{g}{P_o} \frac{K}{H}$$

$$r = e^{-z/2}$$

elimination of X gives

$$\frac{d^4 Y}{dz^4} + \frac{d^3 Y}{dz^3} - i\beta e^{-z} \frac{d^2 Y}{dz^2} + i\beta e^{-z} \frac{dY}{dz} - \alpha_n \delta e^{-z} Y = 0 \tag{8.28}$$

As $z \to \infty$ it is expected that solutions of (8.28) will behave like solutions of

$$\frac{d^4 Y}{dz^4} + \frac{d^3 Y}{dz^3} = 0 \tag{8.29}$$

i.e. like linear combination of a constant, z, z^2, and e^{-z}. This is the heat conduction mode solution since $z \to \infty$ is formally the same as $K \to \infty$ (e^{-z} occur only in combination with E_h^{-1}).

Likewise as $z \to -\infty$, the solution of (8.28) is expected to behave like solutions of

$$\frac{d^2 Y}{dz^2} - \frac{dY}{dz} + \frac{\alpha_n \delta i}{\beta} Y = 0 \qquad (8.30)$$

i.e. like

$$Y_{\pm} \sim e^{z/2} \exp\left[\pm \left(\frac{1}{4} - K_n i\right)^{1/2} z\right] \qquad (8.31)$$

where $K_n = \alpha_n \delta / \beta$.

Eq. (8.30) is the differential equation for the inviscid regime.

On the other hand, elimination of Y from (8.26) - (8.27) gives

$$\frac{d^4 X}{dz^4} + \frac{d^3 X}{dz^3} - i\beta e^{-z} \frac{d^2 X}{dz^2} - \frac{1}{4}\frac{dX}{dz} + \left[e^{-z}\left(\frac{i\beta}{4} + \alpha_n \delta\right) - \frac{1}{16}\right] X = 0 \qquad (8.32)$$

As $z \to \infty$ the solution behaves like the solution of

$$\frac{d^4 X}{dz^4} + \frac{d^3 X}{dz^3} - \frac{1}{4}\frac{dX}{dz} - \frac{1}{16} X = 0 \qquad (8.33)$$

i.e. the corresponding heat conduction modes are

$$X \sim e^{z/2}, \quad e^{-z/2}, \quad z e^{-z/2}, \quad z^2 e^{-z/2}$$

Likewise as $z \to -\infty$, the solution to (8.32) behaves like solutions of

$$\frac{d^2 X}{dz^2} - (\frac{1}{4} - K_n i) X = 0 \qquad (8.34)$$

i. e.

$$X \sim \exp [\pm (\frac{1}{4} - K_n i)^{1/2} z] + O (e^{-z/2}) \qquad (8.35)$$

8.4.2 Change of variables and asymptotic behaviour

It is convenient to introduce a new variable $P = p / p_o = e^{-z}$, where p is pressure, mapping $z \to \infty$ to $P \to 0$ and $z \to -\infty$ to $P \to \infty$. Thus d/dz goes over into $- P d/d P = D$, the differential equation (8.28) tranforms into

$$D^4 Y - D^3 Y - i \beta P D^2 Y - i \beta D Y + \alpha_n \delta P Y = 0 \qquad (8.36)$$

The differential equation for the inviscid regime in the new variable is

$$D^2 Y + D Y + K_n i Y = 0 \qquad (8.37)$$

with solutions

$$Y_{\pm}^{i} (P) \sim P^{-1/2} \exp [\pm (\tfrac{1}{4} - K_n i)^{1/2} \log P]. \qquad (8.38)$$

the substitution of $Y \sim P^s [1 + 0 (P)]$ into (8.36) yields the indicial equation

$$s^3 (s - 1) = 0 \qquad (8.39)$$

which according to the Frobenius technique indicated that (8.36) has four independent solutions with leading terms for small P of the form

$$\left.\begin{aligned} Y_1(P) &\sim 1 + O(P) \\ Y_2(P) &\sim [1 + O(P)]\log P + O(P) + O(1) \\ Y_3(P) &\sim [1 + O(P)]\log^2 P + [1 + O(P)]\log P + O(P) + O(1) \\ Y_4(P) &\sim P + O(P^2) \end{aligned}\right\} \qquad (8.40)$$

the leading terms corresponding to W ($W = e^{z/2} X$) are

$$\left.\begin{aligned} W_1(P) &\sim O(1) + O(P) \\ W_2(P) &\sim O(1) + O(P) + \log P \\ W_3(P) &\sim O(1) + O(P) + \log P + P^{-1} \\ W_4(P) &\sim 1 + O(P) \end{aligned}\right\} \qquad (8.41)$$

Finite heat flux $\sim T_z \cong PY_P$ is given by Y_2 and Y_3 and finite mass flux $\sim e^{-z}W$, is given by W_3. Thus only Y_1 and Y_4 satisfy the upper boundary condition of no heat flux at $P \to 0$, which in terms of z they are

$$\left.\begin{aligned} Y_1(z) &\sim 1 + O(e^{-z}) \\ Y_4(z) &\sim e^{-z} + O(e^{-2z}) \end{aligned}\right\} \qquad (8.42)$$

The asymptotic solution as $P \to \infty$ is obtained by replacing $1/P$ by a new independent variable ζ, and considering the solutions of the new equation for small values of ζ, since $\zeta \to 0$ as $P \to \infty$. The new equation is

$$\zeta^5 \frac{d^4Y}{d\zeta^4} + 7\zeta^4 \frac{d^3Y}{d\zeta^3} + (10\zeta - i\beta)\zeta^2 \frac{d^2Y}{d\zeta^2} + 2\zeta^2 \frac{dY}{d\zeta} + \alpha_n \delta Y = 0 \qquad (8.43)$$

The substitution of $Y \sim \zeta^s [1 + o(\zeta)]$ yields the indicial equation

$$s^2 - s - K_n i = 0 \qquad (8.44)$$

which gives two independent solutions for large P with leading terms proportional to

$$Y_{\pm}^*(P) \sim [1 + O(P^{-1})] P^{-\frac{1}{2} \pm (\frac{1}{4} - K_n i)^{1/2}} \qquad (8.45)$$

and which are identical with $Y_{\pm}^i$, the solution to the inviscid regime.

In order to obtain the constant coefficients in (8.42), we need a more exact solution to (8.36).

8.4.3 Series solution

The solution to (8.36) can be found by taking linear combination

of series solution constructed about the regular singular point P = 0.

$$Y_j(P,s) = \sum_{n=0}^{\infty} a_n(s) P^{n+s} \tag{8.46}$$

where $s \geq 0$, the subscript j corresponds to the four values of s, and the coefficients are evaluated by substituting (8.46) in (8.36), and are given by the recursion formula

$$\begin{aligned} a_n(s) &= \frac{i\beta\left[(n+s)^2 - (n+s) + \kappa_n i\right]}{(n+s)^3(n+s-1)} a_{n-1} \\ &= \frac{i\beta\left(n+s-\frac{1}{2}+\gamma\right)\left(n+s-\frac{1}{2}-\gamma\right)}{(n+s)^3(n+s-1)} a_{n-1}. \end{aligned} \tag{8.47}$$

We can write

$$a_n(s) = \frac{\psi(s,\gamma)\,\Gamma\left(n+s+\frac{1}{2}+\gamma\right)\Gamma\left(n+s+\frac{1}{2}-\gamma\right)}{\Gamma^3(n+s+1)\,\Gamma(n+s)} \tag{8.48}$$

where

$$\psi(s,\gamma) = \frac{i\beta\,\Gamma^3(s+1)\,\Gamma(s)}{\Gamma\left(s+\frac{1}{2}+\gamma\right)\Gamma\left(s+\frac{1}{2}-\gamma\right)}, \qquad \gamma = \left(\frac{1}{4} - \kappa_n i\right)^{1/2}$$

and we have set $a_o(s) = 1$. Since the recurrence formula (8.47) or (8.48) cannot be solved for any value of a_n when $s = 0$, equation (8.36) does not possess a solution of the type (8.46) beginning with a term of the form $a_o P^o$. Therefore, the third order $s = 0$ root of Eq. (8.39) establishes three logarithmic solutions of the form

$$Y_1(P,0) = \sum_{n=0}^{\infty} \left[s\, a_n(s) \log P \right]_{s=0} P^n + \sum_{n=0}^{\infty} b_n'(0)\, P^n \tag{8.49}$$

$$Y_2(P,0) = \sum_{n=0}^{\infty} \left[a_n'(s) \log P + s\, a_n(s) \log^2 P \right]_{s=0} P^n + \sum_{n=0}^{\infty} \left[b_n''(0) + b_n'(0) \log P \right] P^n \tag{8.50}$$

$$Y_3(P,0) = \sum_{n=0}^{\infty} \left[a_n''(s) \log P + 2\, a_n'(s) \log^2 P + s\, a_n(s) \log^3 P \right]_{s=0} P^n + \sum_{n=0}^{\infty} \left[b_n'''(0) + 2\, b_n''(0) \log P + b_n'(0) \log^2 P \right] P^n \tag{8.51}$$

Likewise the single $s = 1$ root of Eq. (8.39) establishes the power series solution

$$Y_4(P,1) = \sum_{n=0}^{\infty} a_n(1)\, P^{n+1} \tag{8.52}$$

where

$$a_n^{i}(s) = \left[\frac{\partial^i}{\partial s^i}\, s\, a_n(s) \right]_{s=0}, \quad i = 1,2$$

$$b_n^{i}(0) = \left[\frac{\partial^i}{\partial s^i}\, s\, a_n(s) \right]_{s=0}, \quad i = 1,2,3$$

From (8.49) - (8.52) we have to select the solution which satisfies the requirement of no fluxes of heat at $P \to 0$ ($z \to \infty$). Only the $Y_1(P, 0)$ and $Y_4(P, 1)$ solutions satisfy this condition.

8.4.4 Integral representation and asymptotic behaviour

We shall now transform the series representation of $Y_j(P, s)$ into an integral, evaluate this integral by contour integration, and investigate the asymptotic behaviour for large P.

Let $a(\xi)$ be an analytic function of the complex variable ξ which coincides with a_n when $\xi = n$. The series (8.52) is summed by

$$Y_4(P,1) = \frac{1}{2\pi i} \int_C F(\xi, P)\, d\xi \qquad (8.53)$$

where

$$F(\xi, P) = a(\xi)\, e^{(\xi+1)\log P}$$

and the path of integration is presented in Fig. 8.1

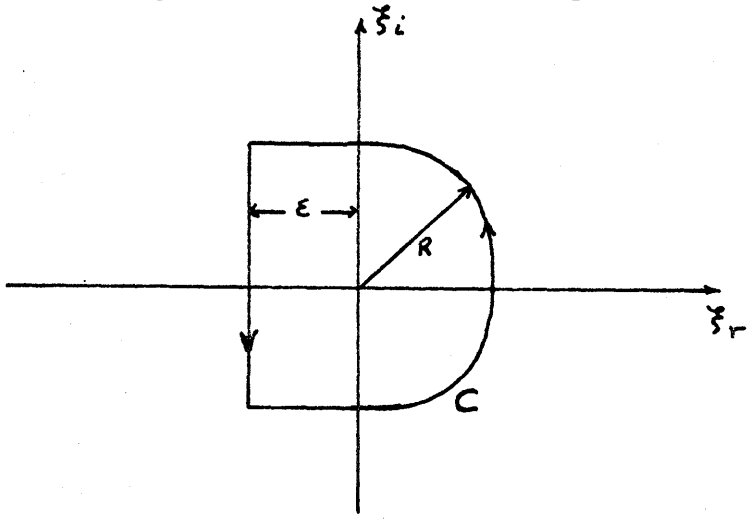

Fig. 8.1 Contour of Integration

Since $\gamma - 1 - 1/2 \neq$ integer, the function $F(\xi, P)$ is analytic except for a finite number of poles, all of which are to the right of some line $\xi_r = \varepsilon$. It can be shown that $F(\xi, P)$ tends uniformly to zero along the contour C as $R \to \infty$ and for large P.

Then

$$Y_4(P,1) \cong \sum_{\kappa} \text{Res} \left\{ F(\xi, P); \hat{\xi}_\kappa \right\}, \tag{8.54}$$

where the points $\hat{\xi}_\kappa$ are the poles of $F(\xi, P)$.

The function $F(\xi, P)$ has simple poles at

$$\xi = \hat{\xi} = [-(\tfrac{1}{2}+1) \pm \gamma] \quad \text{if} \quad \kappa_n i \neq 1/4,$$

All of these poles are nonintegers. The residue of $F(\xi, P)$ at $\hat{\xi}_+$ is given by

$$\text{Res}(\hat{\xi}_+) = \frac{\psi(1,\gamma)\,\Gamma(2\gamma)}{\Gamma(\gamma-\frac{1}{2})\,\Gamma^3(\gamma+\frac{1}{2})}\, P^{-\frac{1}{2}+\gamma} \tag{8.55}$$

Likewise the residue of $F(\xi, P)$ at $\hat{\xi}_-$ is given by

$$\text{Res}(\hat{\xi}_-) = \frac{\psi(1,\gamma)\,\Gamma(-2\gamma)}{\Gamma(-\gamma-\frac{1}{2})\,\Gamma^3(-\gamma+\frac{1}{2})}\, P^{-\frac{1}{2}-\gamma} \tag{8.56}$$

thus

$$Y_4(P,1) \tilde{=} P^{-1/2}(A P^{\gamma} + B P^{-\gamma}) \qquad (8.57)$$

where

$$A = \frac{\psi(1,\gamma)\Gamma(2\gamma)}{\Gamma(\gamma-\frac{1}{2})\Gamma^3(\gamma+\frac{1}{2})}$$

$$B = \frac{\psi(1,\gamma)\Gamma(-2\gamma)}{\Gamma(-\gamma-\frac{1}{2})\Gamma^3(-\gamma+\frac{1}{2})}$$

for large P. Hence, the series solution $Y_4(P,1)$ is asymptotically proportional to $Y_{\pm}^*$. The solution (8.57) will be used as solution for large P (or small z). Three other solutions for large P can be obtained from the corresponding integral representations of (8.49)-(8.51), with asymptotic approximation different to $Y_{\pm}^*$, and hence will not be necessary to obtain here. The large P solutions cannot be connected to the small P solution through the transition region because Y (or X) does not satisfy (8.28) or (8.32) in this region.

8.4.5 Matching solutions and determination of the model vertical boundary conditions

In this section, the two flux-free solutions for small P is matched to the numerical solution at the top boundary and the bounded solution for large P is matched to the numerical solution at the

lower boundary.

We shall take the solution for small P a linear combination of $Y_1(P,0)$ and $Y_4(P,1)$ solutions, thus

$$Y(P) = C_1 Y_1(P,0) + C_2 Y_4(P,1) \qquad (8.58)$$

where $Y_1(P,0)$ and $Y_4(P,1)$ are given by (8.49) and (8.52) respectively. We shall take the three leading terms of $Y_1(P,0)$ and the first leading term of $Y_4(P,1)$. To insure that the remaining terms in the power series are small compared to the leading terms, we select the reference level for the power series solution in such a way that the coefficients are 0 (1). Having established this, we may write (8.58) as

$$Y(P) = C_1 (r_0 + r_1 P + r_2 P \log P) + C_2 a_0 P \qquad (8.59)$$

$$\text{since} \quad a_0(s) = 1, \quad r_0 = \left[\frac{\partial}{\partial s} s a_0(s)\right]_{s=0} = 1$$

and

$$r_1 = 3\beta K_n + i\beta \quad ; \quad r_2 = -\beta K_n$$

We want r_1 and r_2 to be 0 (1). Since $K_n = 0(1)$ when evaluated at the upper boundary of the numerical model, we take $\beta = 1$ by choosing $P_0 = g \frac{K}{H} \frac{1}{\rho c_p}$. In terms of z, (8.59) is

$$Y(z) = C_1 (1 + r_1 e^{-z} - r_2 z e^{-z}) + C_2 e^{-z} \qquad (8.60)$$

the corresponding expression for X(z) is obtained from (8.27) and is given by

$$X(z) = c_1 \left[(r_1 + 2r_2 - i\beta) e^{-z/2} - r_2 z e^{-z/2} - i\beta r_1 e^{-\frac{3}{2}z} + i\beta r_2 z e^{-3/2 z} \right] \delta^{-1} + c_2 \left(e^{-z/2} - i\beta e^{-\frac{3}{2}z} \right) \delta^{-1} \qquad (8.61)$$

The matching procedure is accomplished by taking X, Y, dX/dz, and dY/dz to be continuous across the boundary. Eqs. (8.60) and (8.61) can be written as

$$\left.\begin{aligned} X(z) &= C_1 F_1(z) + C_2 F_2(z) \\ Y(z) &= C_1 F_3(z) + C_2 F_4(z) \end{aligned}\right\} \qquad (8.62)$$

where

$$F_1(z) = \delta^{-1} \left[(r_1 + 2r_2 - i\beta) e^{-z/2} - r_2 z e^{-z/2} - i\beta r_1 e^{-\frac{3}{2}z} + i\beta r_2 z e^{-\frac{3}{2}z} \right]$$

$$F_2(z) = \delta^{-1} \left(e^{-z/2} - i\beta e^{-\frac{3}{2}z} \right)$$

$$F_3(z) = 1 + r_1 e^{-z} - r_2 z e^{-z}$$

$$F_4(z) = e^{-z}$$

From (8.62) we can obtain the constants C_1 and C_2, which are

given by

$$C_1 = \frac{F_4 X - F_2 Y}{F_1 F_4 - F_2 F_3} \quad , \quad C_2 = \frac{F_1 Y - F_3 X}{F_1 F_4 - F_2 F_3}$$

Now we can write the expression for X_z and Y_z

$$\frac{dX}{dz} = \delta^{-1} \frac{[r_2 - (i\beta)^2 e^{-z} + (i\beta)^2 r_2 e^{-2z}] e^{-z/2}}{(2 r_2 e^{-z} - 1)} Y + \frac{[\frac{1}{2} - i\beta(1 + r_2 e^{-z}) e^{-z}}{(2 r_2 e^{-z} - 1)} X \tag{8.63}$$

$$\frac{dY}{dz} = \frac{[-r_2 + i\beta(1 - r_2 e^{-z})] e^{-z}}{(2 r_2 e^{-z} - 1)} Y + \delta \frac{(1 - r_1 e^{-z}) e^{-z/2}}{(2 r_2 e^{-z} - 1)} X . \tag{8.64}$$

Likewise, for large P (or $z \ll 0$), we shall take the bounded Y solution, i.e. Y - (P) in (8.57).

Hence

$$Y(P) = B P^{-1/2} P^{-\gamma} \tag{8.65}$$

or in terms of z

$$Y(z) = B e^{z/2} e^{(\gamma_r + i\gamma_i) z} \tag{8.66}$$

where

$$B = \left[\frac{i\beta \Gamma(s) \Gamma^3(s+1) \Gamma(-2\gamma)}{\Gamma(s + \frac{1}{2} + \gamma) \Gamma(s + \frac{1}{2} - \gamma) \Gamma(-\gamma - \frac{1}{2}) \Gamma^3(-\gamma + \frac{1}{2})} \right]_{s=1}$$

$$\gamma_r = \sqrt{(\tfrac{1}{4})^2 + K_n^2}\ \cos\theta_n > 0$$

$$\gamma_i = \sqrt{(\tfrac{1}{4})^2 + K_n^2}\ \sin\theta_n < 0$$

$$\theta_n = \mathrm{Tan}^{-1}(-4K_n)$$

The term (8.66) represents a wave, which has upward traveling phase and downward energy flow, with exponentially decaying amplitude for $z << 0$.

The corresponding expression for X(z) is obtained again from (8.27) and is given to order e^z by

$$X(z) = -i\beta\ \delta^{-1}\ e^{\gamma z}\ . \tag{8.67}$$

To insure that solutions at the lower boundary contain no gravity wave component that propagates energy upward, we see from (8.66) and (8.67) that we need to apply the condition

$$\frac{dY}{dz} = (\frac{1}{2} + \gamma_r + i\gamma_i)\,Y \tag{8.68}$$

and

$$\frac{dX}{dz} = (\gamma_r + i\gamma_i)\,X. \tag{8.69}$$

The system of equations (8.12) - (8.13), (8.63) - (8.64), and (8.68) - (8.69) will be the starting point for the numerical model which we discuss below. We shall also consider the set of boundary

conditions, $dY/dz = 0$ and $dX/dz = 0$ at the upper boundary.

8.5 Numerical Procedure

In this chapter we shall describe the numerical procedure used to obtain the solutions of the system of equations (8.12) - (8.13) together with boundary conditions (8.63), (8.64), (8.68), and (8.69).

Eqs. (8.12) - (8.13) should more precisely be written as the four equations

$$\frac{d^2 X_r^{(m,n)}}{dz^2} + f_x(z) X_r^{(m,n)} + h_x(z) Y_r^{(m,n)} = 0 \tag{8.70}$$

$$\frac{d^2 X_i^{(m,n)}}{dz^2} + f_x(z) X_i^{(m,n)} + h_x(z) Y_i^{(m,n)} = 0 \tag{8.71}$$

$$\frac{d^2 Y_r^{(m,n)}}{dz^2} + f_y^*(z) Y_r^{(m,n)} - g_y(z) Y_i^{(m,n)} + h_y(z) X_r^{(m,n)} = G_r^{(m,n)}(z) \tag{8.72}$$

$$\frac{d^2 Y_i^{(m,n)}}{dz^2} + f_y^*(z) Y_i^{(m,n)} + g_y(z) Y_r^{(m,n)} + h_y(z) X_i^{(m,n)} = G_i^{(m,n)}(z) \tag{8.73}$$

where here

$$f_x = \tfrac{1}{4}\left[-4(N_i'/N_i) + 2(1 - N_i'/N_i)' - (1 - N_i'/N_i)^2\right]$$

$$h_x = \left(\gamma_n^m R/2\pi a^2 N_i\right) \exp -\tfrac{1}{2}\int\left[(1 - N_i'/N_i) + (K/H)'\tfrac{H}{K}\right]dz$$

$$f_y^* = -\tfrac{1}{4}\left\{2\left[(K/H)'\tfrac{H}{K}\right]' + \left[(K/H)'\tfrac{H}{K}\right]^2\right\}$$

$$g_y = - C_p E_h^{-1} \nu e^{-z}$$

$$h_y = - c_p E_h^{-1} s \exp\left\{-z + \tfrac{1}{2}\int \left[(K/H)' \frac{H}{K} + (1 - N_i'/N_i) \right] dz \right.$$

$$G_r^{(m,n)} = - E_h^{-1} \exp\left\{-z + \tfrac{1}{2}\int (K/H)' H/K \, dz \right\} \varphi_r^{(m,n)}$$

$$G_i^{(m,n)} = - E_h^{-1} \exp\left\{-z + \tfrac{1}{2}\int (K/H)' H/K \, dz \right\} \varphi_i^{(m,n)}$$

Likewise, the boundary conditions (8.63) - (8.64) and (8.68) - (8.69) are also separated in real and imaginary parts.

In order to simplify the notation, the following variables are defined

$$X_r(z) = X_r^{(m,n)}(z)$$

$$X_i(z) = X_i^{(m,n)}(z)$$

$$Y_r(z) = Y_r^{(m,n)}$$

$$Y_i(z) = Y_i^{(m,n)}$$

$$G_r(z) = G_r^{(m,n)}$$

$$G_i(z) = G_i^{(m,n)}$$

$$f_y(z) = f_y^*(z)$$

Eqs. (8.70) - (8.73) become

$$\frac{d^2 X_r}{dz^2} + f_x(z) X_r + h_x(z) Y_r = 0 \tag{8.74}$$

$$\frac{d^2 X_i}{dz^2} + f_x(z) X_i + h_x(z) Y_i = 0 \tag{8.75}$$

$$\frac{d^2 Y_r}{dz^2} + f_y(z) Y_r - g_y(z) Y_i + h_y(z) X_r = G_r(z) \tag{8.76}$$

$$\frac{d^2 Y_i}{dz^2} + f_y(z) Y_i + g_y(z) Y_r + h_y(z) X_i = G_i(z) \tag{8.77}$$

Eqs. (8.74) - (8.77) will now be put into finite-difference form. The following finite-difference notation will be needed:

$$h = z = z_{Top}/N$$

$$z_n = n \Delta z$$

$$(\quad)_n = (\quad) \text{ evaluated at } z_n$$

$$\delta^2(\quad)_K = (\quad)_{K+1} - 2(\quad)_K + (\quad)_{K-1}$$

We use the discussion given by Hildebrand (1956) to write

$$X_{n+1} - 2X_n + X_{n-1} = h^2 \left(1 + \frac{1}{12} \delta^2\right) X_n'' + T_n \tag{8.78}$$

where the truncation error T_n is expressible in the form

$$T_n = -\frac{h^6}{240} X^{vi}(\xi) \qquad (z_{n-1} < \xi < z_{n+1}) \tag{8.79}$$

Thus, if we use (8.74) to replace X_n'' by $(-f_x X_r - h_x Y_r)$, the equivalent form for (8.78) is

$$X^r_{n+1} - 2X^r_n + X^r_{n-1} = h^2\left(1 + \frac{1}{12}\delta^2\right)(-f_x X^r - h_x Y^r) \tag{8.80}$$

where we have neglected T_n. Similar procedure is applied to (8.75) - (8.77). By expanding δ^2, in (8.80) and in those corresponding to X^i, Y^r, and Y^i, the following equations are derived:

$$\left(1 + \frac{h}{12} f^x_{n+1}\right) X^r_{n+1} - 2\left(1 - \frac{5h^2}{12} f^x_n\right) X^r_n + \left(1 + \frac{h^2}{12} f^x_{n-1}\right) X^r_{n-1} \tag{8.81}$$
$$+ \frac{h^2}{12} h^x_{n+1} Y^r_{n+1} + \frac{5}{6} h^2 h^x_n Y^r_n + \frac{h^2}{12} h^x_{n-1} Y^r_{n-1} = 0$$

$$\left(1 + \frac{h^2}{12} f^x_{n+1}\right) X^i_{n+1} - 2\left(1 - \frac{5h^2}{12} f^x_n\right) X^i_n + \left(1 + \frac{h^2}{12} f^x_{n-1}\right) X^i_{n-1} \tag{8.82}$$
$$+ \frac{h^2}{12} h^x_{n+1} Y^i_{n+1} + \frac{5}{6} h^2 h^x_n Y^i_n + \frac{h^2}{12} h^x_{n-1} Y^i_{n-1} = 0$$

$$\left(1 + \frac{h^2}{12} f^y_{n+1}\right) Y^r_{n+1} - 2\left(1 - \frac{5}{12} h^2 f^y_n\right) Y^r_n + \left(1 + \frac{h^2}{12} f^r_{n-1}\right) Y^r_{n-1} \tag{8.83}$$
$$- \frac{h^2}{12} g^y_{n+1} Y^i_{n+1} - \frac{5}{6} h^2 g^y_n Y^i_n - \frac{h^2}{12} g^y_{n-1} Y^i_{n-1} + \frac{h^2}{12} h^y_{n+1} X^r_{n+1}$$
$$+ \frac{5h^2}{6} h^y_n X^r_n + \frac{h^2}{12} h^y_{n-1} X^r_{n-1} = \frac{h^2}{12}\left(G^r_{n+1} + 10 G^r_n + G^r_{n-1}\right)$$

$$\left(1+\frac{h^2}{12}f^{Y}_{n+1}\right)Y^{i}_{n+1}-2\left(1-\frac{5}{12}h^2 f^{Y}_{n}\right)Y^{i}_{n}+\left(1+\frac{h^2}{12}f^{Y}_{n-1}\right)Y^{i}_{n-1}$$

$$+\frac{h^2}{12}g^{Y}_{n+1}Y^{r}_{n+1}+\frac{5}{6}h^2 g^{Y}_{n}Y^{r}_{n}+\frac{h^2}{12}g^{Y}_{n-1}Y^{r}_{n-1}+\frac{h^2}{12}h^{Y}_{n+1}X^{i}_{n+1} \qquad (8.84)$$

$$+\frac{5}{6}h^2 h^{Y}_{n}X^{i}_{n}+\frac{h^2}{12}h^{Y}_{n-1}X^{i}_{n}+\frac{h^2}{12}h^{Y}_{n-1}X^{i}_{n-1}=\frac{h^2}{12}\left(G^{i}_{n+1}+10\,G^{i}_{n}+G^{i}_{n-1}\right)$$

In virtue of (8.79), this procedure is of fifth order, in the sense that it would afford exact results if X^r , X^i , Y^r , and Y^i were polynomials of degree five or less.

This system of equations must be supplemented by the boundary conditions. The real and imaginary parts of the boundary conditions (8.63) - (8.64) and (8.68) - (8.69) must now be put into finite-difference form to complete the formulation of the numerical problem. It will, for this purpose, be necessary to expand d/dz numerically at both the upper and lower boundaries.

The formula for forward and backward differences in terms of derivatives are (see Hildebrand, 1956, p. 138) ,

$$\Delta = \frac{hD}{1!} + \frac{h^2 D^2}{2!} + \frac{h^3 D^3}{3!} + \cdots\cdots \qquad (8.85)$$

$$\nabla = -\frac{hD}{1!} + \frac{h^2 D^2}{2!} - \frac{h^3 D^3}{3!} + \cdots\cdots \qquad (8.86)$$

where

$$\Delta(\ )_n = (\ )_{n+1} - (\ )_n$$

$$\nabla (\quad)_n = (\quad)_n - (\quad)_{n-1}$$

$$\mathcal{D} (\quad)_n = d(\quad)n/dz$$

Using eq. (8.85) at z = 0 (n=0) and eq. (8.86) at $z = z_{top}$ (n=N), the following expressions are obtained

$$\chi_1 - \chi_0 = h\,\chi_0' + \frac{h^2}{2}\chi_0'' + O(h^3) \tag{8.87}$$

$$\chi_N - \chi_{N-1} = h\,\chi_N' + \frac{h^2}{2}\chi_N'' + O(h^3) \tag{8.88}$$

Hence to second order

$$\left.\begin{aligned}
X_0^{r\prime} &= \frac{1}{h}(X_1^r - X_0^r) - \frac{h}{2}(-f_0^x X_0^r - h_0^x Y_0^r) \\
X_0^{i\prime} &= \frac{1}{h}(X_1^i - X_0^i) - \frac{h}{2}(-f_0^x X_0^i - h_0^x Y_0^i) \\
Y_0^{r\prime} &= \frac{1}{h}(Y_1^r - Y_0^r) - \frac{h}{2}(-f_0^y Y_0^r + g_0^y Y_0^i - h_0^y X_0^r + G_0^r) \\
Y_0^{i\prime} &= \frac{1}{h}(Y_1^i - Y_0^r) - \frac{h}{2}(-f_0^y Y_0^i - g_0^y Y_0^r - h_0^y X_0^i + G_0^i)
\end{aligned}\right\} \tag{8.89}$$

and

$$
\left.
\begin{aligned}
X_N^{r\prime} &= \frac{1}{h}\left(X_N^r - X_{N-1}^r\right) - \frac{h}{2}\left(-f_N^X X_N^r - h_N^X Y_N^r\right) \\
X_N^{i\prime} &= \frac{1}{h}\left(X_N^i - X_{N-1}^i\right) - \frac{h}{2}\left(-f_N^X X_N^i - h_N^X Y_N^i\right) \\
Y_N^{r\prime} &= \frac{1}{h}\left(Y_N^r - Y_{N-1}^r\right) - \frac{h}{2}\left(-f_N^Y Y_N^r + g_N^Y Y_N^i - h_N^Y X_N^r + G_N^r\right) \\
Y_N^{i\prime} &= \frac{1}{h}\left(Y_N^i - Y_{N-1}^i\right) - \frac{h}{2}\left(-f_N^Y Y_N^i - g_N^Y Y_N^r - h^Y X_N^i + G_N^i\right)
\end{aligned}
\right\} \quad (8.90)
$$

The lower boundary conditions (8.68) and (8.69) can be written as

$$
\left.
\begin{aligned}
\frac{dX_r}{dz} &= a_B X_r - b_B X_i \\
\frac{dX_i}{dz} &= a_B X_i + b_B X_r \\
\frac{dY_r}{dz} &= c_B Y_r - d_B Y_i \\
\frac{dY_i}{dz} &= c_B Y_i + d_B Y_r
\end{aligned}
\right\} \quad \begin{array}{l} at \\ z = 0 \end{array} \qquad (8.91)
$$

where

$$a_B = \gamma_r \quad , \qquad b_B = \gamma_i$$

$$c_B = \frac{1}{2} + \gamma_r$$

$$d_B = \gamma_i$$

a_B, b_B and d_B are all evaluated at $z=0$

Eq. (8.91) can now be written in finite difference form by use of (8.89) giving

$$\left.\begin{aligned}
&\frac{1}{h}\left(X_1^r - X_0^r\right) - \frac{h}{2}\left(-f_0^X X_0^r - h^X Y_0^r\right) = a_B X_0^r - b_B X_0^i \\
&\frac{1}{h}\left(X_1^i - X_0^i\right) - \frac{h}{2}\left(-f_0^X X_0^i - h_0^X Y_0^i\right) = a_B X_0^i + b_B X_0^r \\
&\frac{1}{h}\left(Y_1^r - Y_0^r\right) - \frac{h}{2}\left(-f_0^Y Y_0^r + g_0^Y Y_0^i - h_0^Y X_0^r + G_0^r\right) = c_B Y_0^r - d_B Y_0^i \\
&\frac{1}{h}\left(Y_1^i - Y_0^r\right) - \frac{h}{2}\left(-f_0^Y Y_0^i - g_0^Y Y_0^r - h_0^Y X_0^i + G_0^i\right) = c_B Y_0^i + d_B Y_0^r
\end{aligned}\right\} \quad (8.92)$$

The upper boundary conditions (8.63) and (8.64) can similarly be written as

$$\left.\begin{aligned}
\frac{dX_r}{dz} &= a_T^x Y_r + b_T^x X_r + c_T^x X_i \\
\frac{dX_i}{dz} &= a_T^x Y_i - c_T^x X_r + b_T^x X_i \\
\frac{dY_r}{dz} &= a_T^Y Y_r - b_T^Y Y_i + c_T^Y X_r \\
\frac{dY_i}{dz} &= -b_T^Y Y_r + a_T^Y Y_i + c_T^Y X_i
\end{aligned}\right\} \quad \text{at } z = z_{TOP} \qquad (8.93)$$

where

$$a_T^x = \delta^{-1}\left(r_2 + \beta^2 e^{-2} - \beta^2 r_2 e^{-2z}\right) e^{-z/2}/D$$

$$b_T^x = 1/2D$$

$$c_T^x = \beta\left(1 - r_2 e^{-2}\right) e^{-z}/D$$

$$a_T^Y = -r_2 e^{-z}/D$$

$$b_T^Y = -\beta\left(1 - r_2 e^{-2}\right) e^{-z}/D$$

$$c_T^Y = \delta\left(1 - r_2 e^{-2}\right) e^{-z/2}/D$$

$$D = \left(2r_2 e^{-2} - 1\right)$$

a_T^x, b_T^x, c_T^x, a_T^Y, b_T^Y, and c_T^Y are all evaluated at $z = z_{TOP}$.

Thus, the upper boundary condition can be written in finite difference form using (8.90) and (8.93), giving

$$\frac{1}{h}\left(X_N^r - X_{N-1}^r\right) - \frac{h}{2}\left(-f_N^x X_N^r - h_N^x Y_N^r\right) = a_T^x Y_r + b_T^x X_r + c_T^x X_i$$

$$\frac{1}{h}\left(X_N^i - X_{N-1}^i\right) - \frac{h}{2}\left(-f_N^x X_N^i - h_N^x Y_N^i\right) = a_T^x Y_i - c_T^x X_r + b_T^x X_i \qquad (8.94)$$

$$\frac{1}{h}\left(Y_N^r - Y_{N-1}^r\right) - \frac{h}{2}\left(-f_N^y Y_N^r + g_N^y Y_N^i - h_N^y X_N^r + G_N^r\right) = a_T^y Y_r + b_T^y Y_i + c_T^y X_r$$

$$\frac{1}{h}\left(Y_N^i - Y_{N-1}^i\right) - \frac{h}{2}\left(-f_N^y Y_N^i - g_N^y Y_N^r - h_N^y X_N^i + G_N^i\right) = -b_T^y Y_r + a_T^y Y_i + c_T^y X_i$$

The total finite-difference system can be written in matrix form as

$$A * Y = B \qquad (8.95)$$

where

$$Y = \begin{Bmatrix} X_0^r \\ X_0^i \\ Y_0^r \\ Y_0^i \\ \vdots \\ X_N^r \\ X_N^i \\ Y_N^r \\ Y_N^i \end{Bmatrix} \quad , \quad B = \begin{Bmatrix} 0 \\ 0 \\ G_0^r \\ G_0^i \\ \vdots \\ 0 \\ 0 \\ G_N^r \\ G_N^i \end{Bmatrix}$$

and A is a (4N+8) x (4N+8) band-structured matrix, whose elements are coefficients of X_n^r, X_n^i, Y_n^r, and Y_n^i.

The set of simultaneous linear equations given by the matrix eq. (8.95) is then solved numerically by GELB, an IBM subroutine.

8.6 A Justification of the Simple Case Study

There are several technical and practical reasons that makes difficult to solve completely the system of Egs. (3.14). First, we have to justify that diffusive transfer of heat and momentum, to a first order, depends only on the vertical gradient of the temperature and motion fields. This amounts to show that all terms in the express-

ion of the viscous force for example, are very small compared to that term retained in (3.14). This turns out to be the case as long as the parameter $\delta = D/a$ is much smaller than one. From the present and our previous studies we find that $\delta \sim \dot{h}/u \ll 1$ at least to the base of the exosphere (500 km). As , however, the motion can choose its own vertical scale such that and horizontal diffusion must be kept. This would lead to a difficult 4th order equation in latitude for separation. On the other hand, viscosity, compared to ion drag, is only important above 350 to 400 km. Inclusion of viscosity greatly complicates the calculations and for reasons stated in earlier sections we have omitted viscosity in the model calculations.

Secondly, inclusion of coriolis force and time derivative in the momentum equations does not amount to simple replacing spherical harmonics by Hough functions. The operator F (8.4) has complex parameters in it because of the ion drag term.

Thirdly, the ion drag parameter N_i actually undergoes a significant diurnal change and hence, the zonal component of the ion drag term should properly be written as $-2\Omega\,(N_i'\bar{U} + \bar{N}_i U')$, where $\bar{N}_i$ and $\bar{U}$ are average values and N_i' and U' are the perturbation quantities. Inclusion of $N_i'\bar{U}$ in the equations, however, would

interfere with the separability condition (8. 3) thus only the $\overline{N}_i U'$ term is retained in the model calculations.

Finally, correct inclusion of drift velocity is not possible at present mainly because of insufficient knowledge of electric fields in the dynamic region and magnetosphere.

9. RESULTS

9.1 General Description of the Model Calculation

In the previous chapter, we have described a simple model that can be used to attempt simulation of several features of the diurnal circulation of the thermosphere. We have also presented the numerical method used to compute the circulation and the temperature fields. Having done all of this, the results of these calculations are given in this chapter. Particular attention is paid to the field of motion and temperature.

The model preassumes the knowledge of heating rates and a distribution of ion concentration. The continuously varying ion distribution is replaced by a time independent profile as discussed in section 8.6. We approximate the height dependence by the Chapman formula

$$n_i = n_m \exp\{1 - (z-z_m)/D - \exp-(z-z_m)/D\} \tag{9.1}$$

where n_m, z_m, and D are variable parameters in the model and represent the maximum ion concentration, the height of the maximum

ion concentration, and the thickness of the distribution, respectively. Note that $z = \int^h dh/H$, where h and H are the altitude and scale height respectively.

The elements in the spectral expansion for the heating rates inputs has been truncated so that only Y_1^1 Q_1^1 and Y_3^1 Q_3^1 have been retained. Consequently, our perturbation variables will be restricted to be the response to this forcing alone.

Figures 9.1 - 9.22 show these results. The final variables are presented as being proportional to $\cos[\ \lambda + \gamma t - \phi(z)\ ]$. Here ϕ (z) is the variable part of the total phase which we shall call here phase lag. For $\lambda = 0$ the amplitude reaches a maximum at $\gamma = \phi(z)/15^\circ$ hours of local time. Each of the variables is represented by a curve in which the amplitude and phase is plotted as a function of z. Each of the variables is now discussed separately.

9.2 Derivation of the Standard Data

For the purpose of comparing the results by changing different parameters in the model calculation, we find it convenient to define arbitrarily a standard result or a standard data, meaning our guess as to the most typical behavior. This standard data is based on a typical ion density profile, which we take here to be the

day-night time averaged ion density profile for middle latitudes and for maximum solar activity. We recall that the motion regime we are concerned with is most likely to occur at high solar activity and during daytime at mean solar activity, when the ion drag term is the dominant term in the momentum equation. Note, however, that the perturbation heating rates used in the calculation are for average solar activity. We take for this average condition n_m, z_m, and D, to be $10^6 cm^{-3}$, .01234μb $\sim$ 243km, and 2, respectively. Heating efficiency for $\lambda \leq$ 1027 is 85% and for the Shamann-Range region is 14 %.

The basic defining variables for the model calculation are h, u, v, $\dot{h}$, and T, which are obtained at every 15^o latitude. The result at 30^olatitude will be used as a reference for comparison involving the systematic changes of the parameter in the model. Only one parameter is changed at a time. When the latitude is not indicated explicitly in the discussion below, it must be regarded as representing 30^olatitude.

Geopotential height (h)

The height of the standard pressure surfaces used in the model is described by this variable. Only the perturbation height

associated with the diurnal bulge is obtained from the model. The hemispheric averages of h and T are assumed to be known. This mean state is determined by the mean solar heating. It can be derived by solving the zeroth order approximation discussed in section 3.2 (see Eq. 3.13). However, we have used here the average values of h and T obtained from the two-dimensional study (Lagos, 1967; Dickinson, Lagos, and Newell, 1968). Table 3 gives the mean heights and height range of the pressure levels used in the numerical study. These mean heights are used here to present our data results. The actual heights will depend, of course, on longitude, latitude and time.

The vertical structure of the perturbation geopotential height is given in Figs. 9.1 - 9.6. Figs. 9.1 and 9.2 show the hour of maximum and the amplitude of h at 0^{o} latitude, Figs 9.3 - 9.4 for 30^{o} latitude, and Figs 9.5 - 9.6 for 60^{o} latitude. Amplitude is maximum at 0200 local time at about 100km altitude and shifts to earlier time as altitude increases. Above about 200km the hour of maximum height occurs at 1600 L.T. to 14:30 L.T..

The amplitude of h is about 1.5km at 160km altitude and increases to 20km at 400km altitude. At about 243km altitude, the hour of maximum height changes from about 15:30 hrs L.T. at 0^{o} latitude to about 15:00 hrs.

TABLE 3

Pressure, Mean Heights and Height Range for the Levels Used in the Model Calculations

Level	Pressure (μb)	Mean Height (Km)	Pressure (μb)	Height Range (Km)
1	10.0	80.0	10	80
2	3.68	85.6		
3	1.35	91.6	10^{0}	92
4	0.498	98.4		
5	0.183	107.4	10^{-1}	108
6	0.0674	117.0		
7	0.0248	130.7		
8	0.0091	160.0	10^{-2}	140
9	0.0033	200.6		
10	0.00123	243.1	10^{-3}	203-260
11	0.000454	293.4		
12	0.000167	349.5	10^{-4}	320-380
13	0.0000614	409.5		
14	0.0000236	471.8		
15	0.0000083	535.5	10^{-5}	400-600

L. T. at 75° latitude. The corresponding change in amplitude is from 8 km at 0° latitude to 3 km at 75° latitude.

Horizontal Velocity (u, v)

The height dependence of the eastward wind u and the northward wind v due to the diurnal bulge are shown in Figs. 9.1 - 9.6. These figures show the phase and amplitude at 0°, 30°, and 60° latitude. Above 200km, this maximum occurs at night around 21:00 hrs. L. T.. Maximum westward velocity is 12 hours apart from maximum eastward velocity. The phase of the meridional component is always ahead of the u. Thus maximum northward velocity above 200km altitude occurs at about 1600 hrs. L. T.

The amplitude of u ranges from 5 m/sec at 150km to 115 m/sec at about 400km. The corresponding amplitude of v is from 3 m/sec to 35 m/sec, at 150km and 400km altitudes respectively.

The latitudinal dependence of the hours of maximum eastward and northward, at about 243km altitude, is presented in Fig. 9.7. This time of maximum has little change for u, but large for v. We find maximum northward at 1900 hrs. L. T. at 15° latitude and shifts to earlier time as the latitude increases. At 75° latitude, the

maximum northward occurs at 15:20 hrs. L.T.. The latitudinal dependence of the amplitude at the 243km level is presented in Fig. 9.8. Note that the amplitude of v is identically zero at the equator. A detailed discussion of the field of motion and its comparison with current values available in the literature will be presented in the next chapter.

Vertical Velocity ($\dot{h}$)

The phase and amplitude of the vertical component of motion as a function of altitude is also presented in Figs. 9.1 - 9.6. There is a maximum upward motion above 200km altitude at about 14:30 hrs. L.T., and maximum downward motion above 200km altitude at about 02:30 hrs. L.T. The amplitude of this wind component ranges from 10cm/sec at 150km to about 4 m/sec at 400km. Both the phase and amplitude depend strongly on latitude. At the equator there is a maximum upward velocity at 1600 hrs. L.T., and at 75^{o} latitude the maximum upward velocity occurs around 1400 hrs. L.T., as can be seen from Fig. 9.7. The amplitude of $\dot{h}$ at 45^{o} latitude is 1.6 times larger than the value at the equator at the 243km level. This space and time variation of $\dot{h}$ and its implication in determining the temperature structure of the thermosphere will also be dis-

cussed in the next chapter.

Temperature (T)

The vertical structure of temperature is presented in Figs. 9.1 - 9.6. The hour of maximum temperature variation has an altitude dependence, as we can see from all of these figures. At 150km altitude, for example, the maximum temperature occurs around 1600 hrs. L.T., at 250km around 14:30 hrs. L.T., and at 400km around 14:20 hrs. L.T. Likewise, the amplitude varies from 150km, 106^{o}K at 250km, to 108^{o}K at 400km. These values change with latitude as we can see from Figs. 9.7 - 9.8. The latitudinal dependence of the perturbation temperature varies essentially as P_1^1 (φ).

We shall compare our results with observed data and attempt to explain the phase and amplitude variability with altitude and latitude in the next chapter. It will also be illustrative to compare our results when adiabatic heating is and is not included in the thermodynamic equation. This will be discussed in the next chapter. The temperature distribution when heating efficiency, boundary conditions, and ionization profiles are changed, will be discussed next.

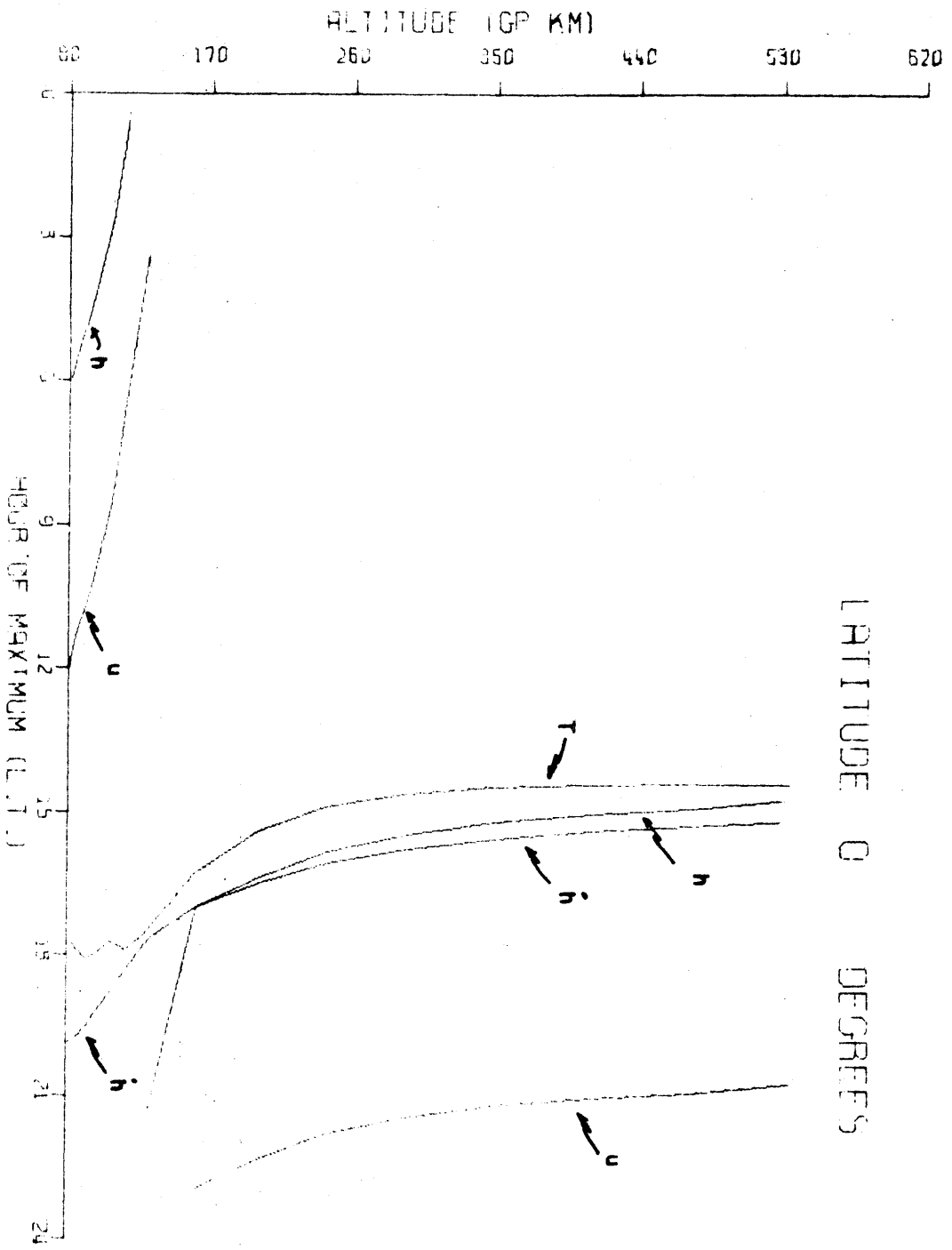

Fig. 8.1. The hour of maximum magnitude of the perturbation variables h, u, $\dot{h}$, and T, as a function of altitude for 0° latitude. $h(km), u(msec^{-1}), \dot{h}(cmsec^{-1}), T(^{\circ}K)$.

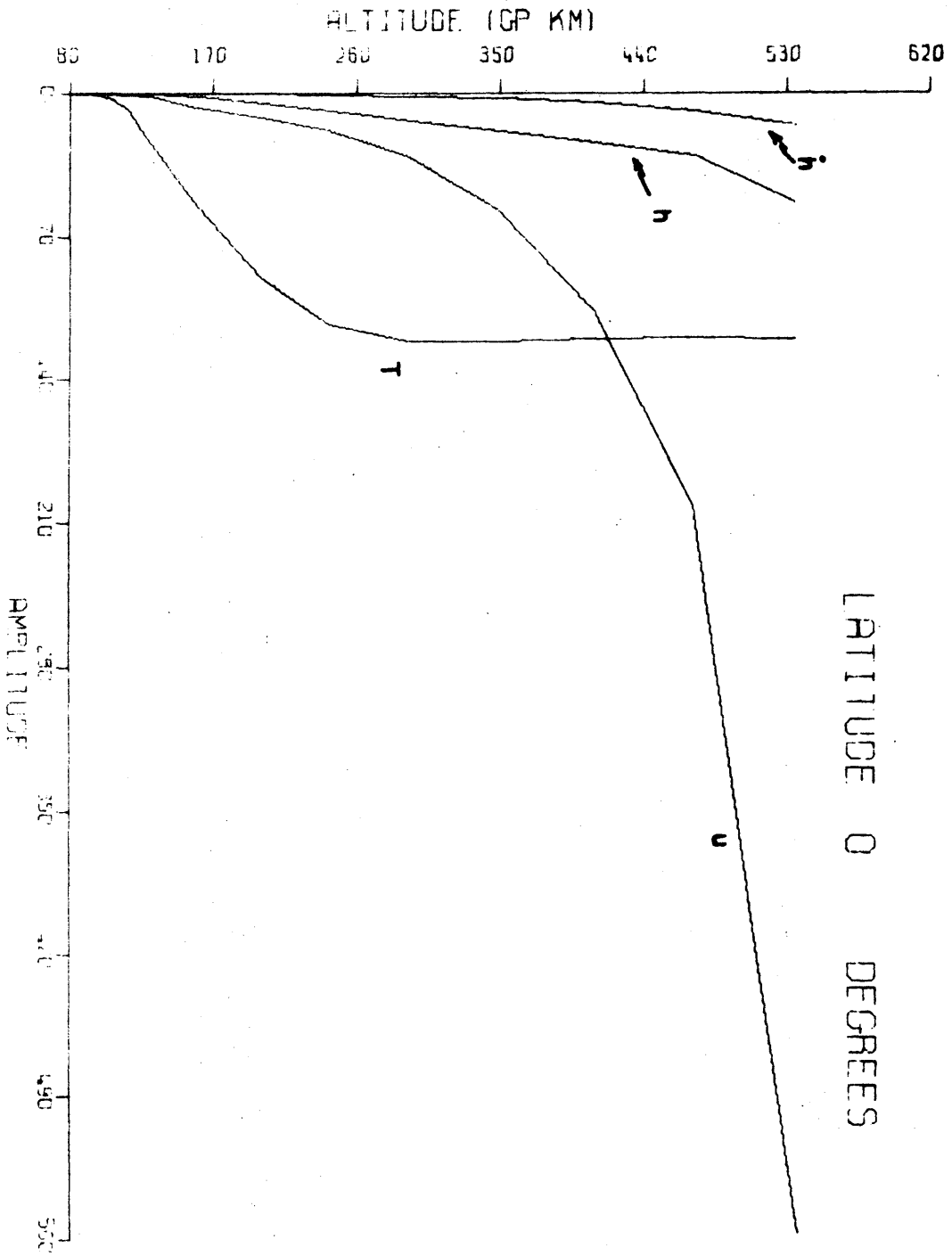

Fig. 9.2. Amplitude of the perturbation variables h, u, $\dot{h}$, and T, as a function of altitude for 0^{o} latitude.

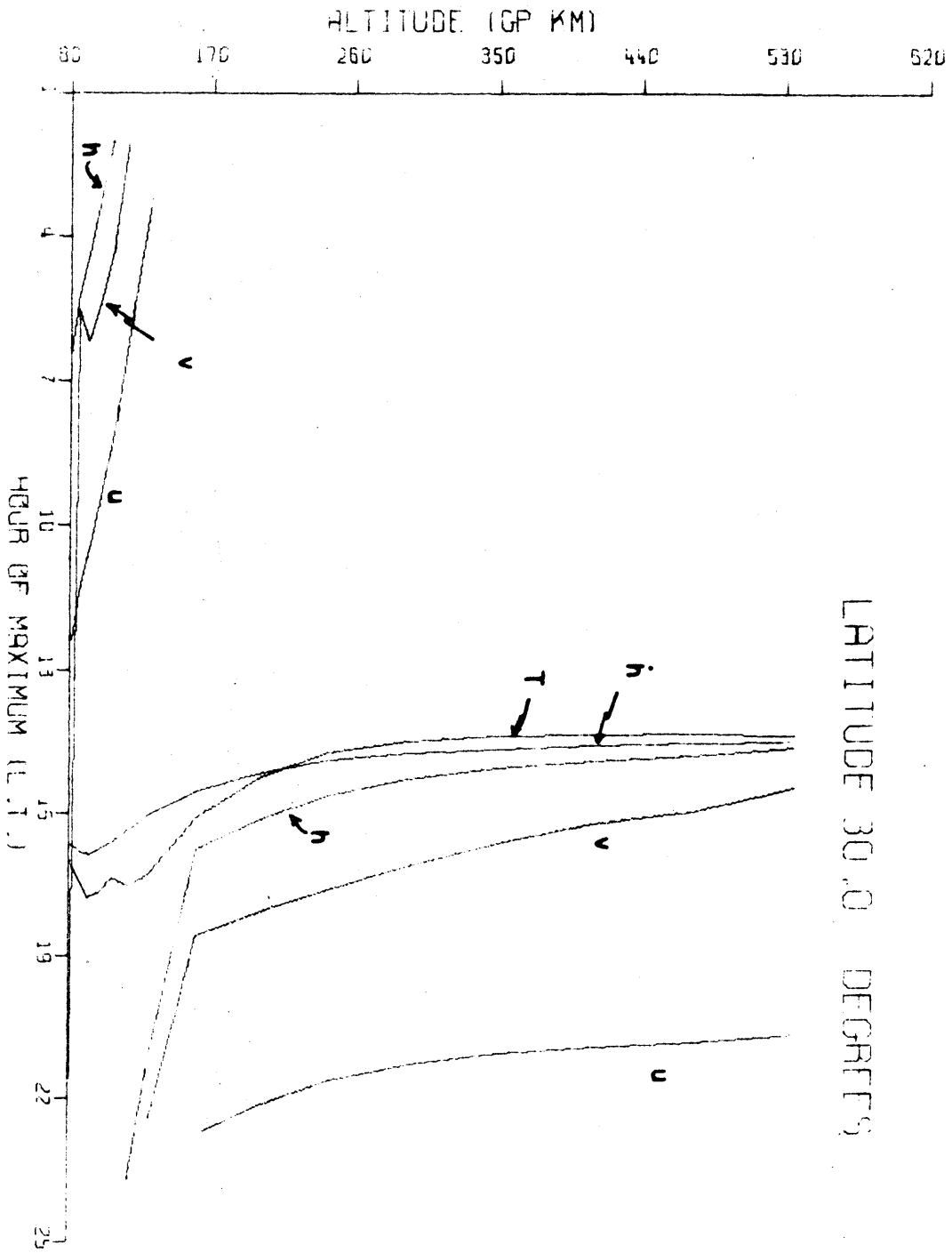

Fig. 9.3. The hour of maximum magnitude of the perturbation variables h, u, v, $\dot{h}$, and T, as a function of altitude for 30^{o} latitude.

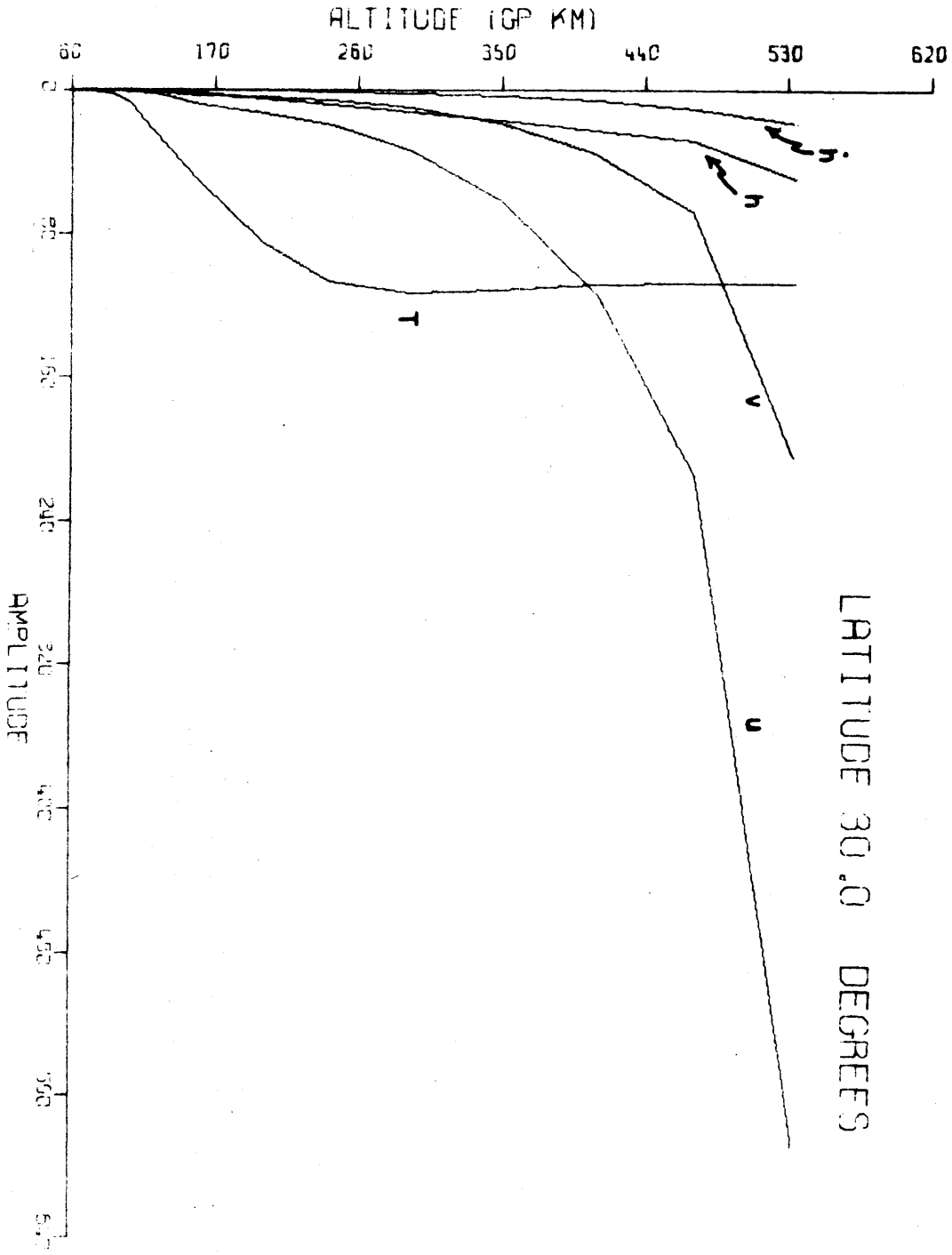

Fig. 9.4. Amplitude of the perturbation variables h, u, v, $\dot{h}$, and T as a function of altitude for 30° latitude.

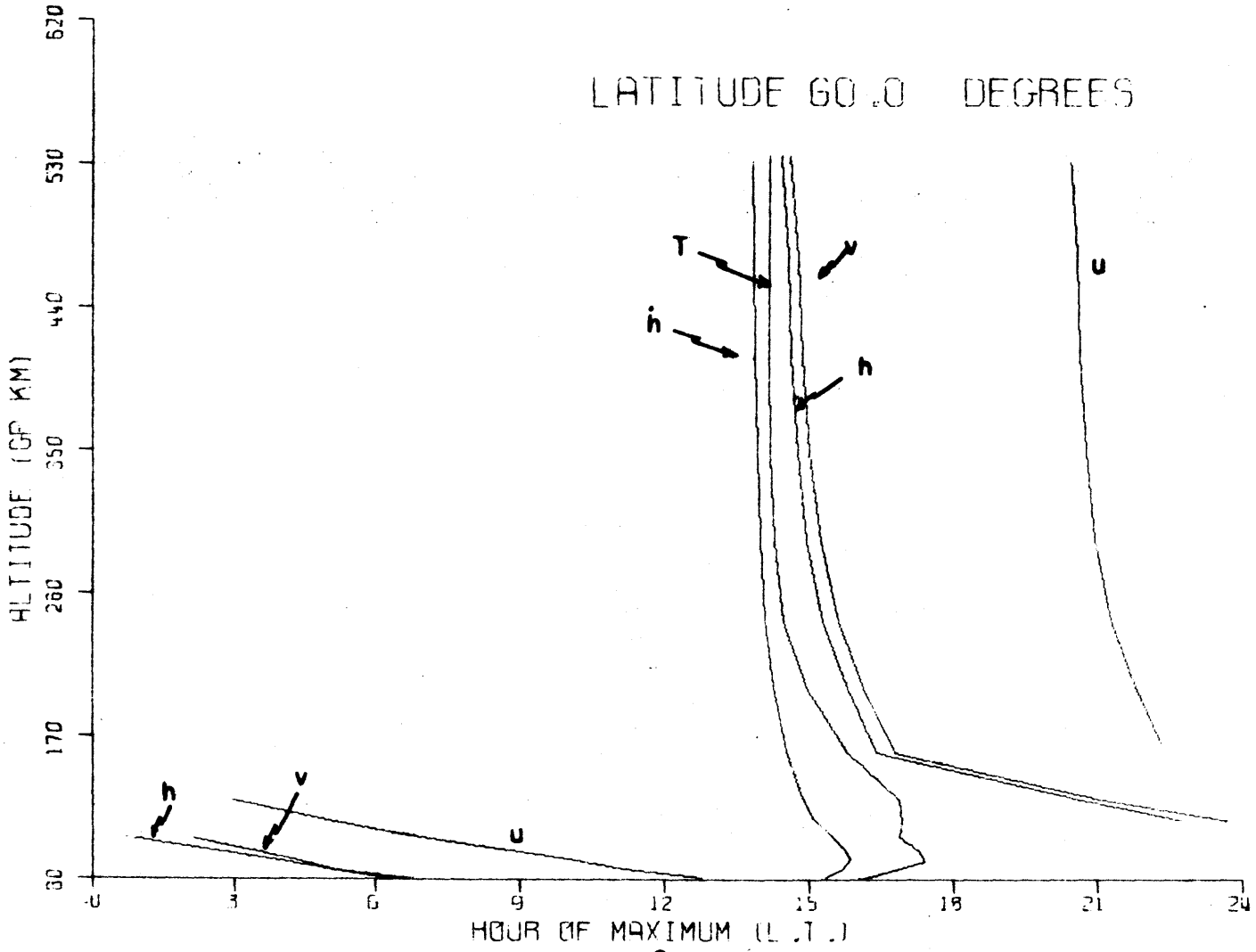

Fig. 9.5. Same as Fig. 9.3 but for 60° latitude.

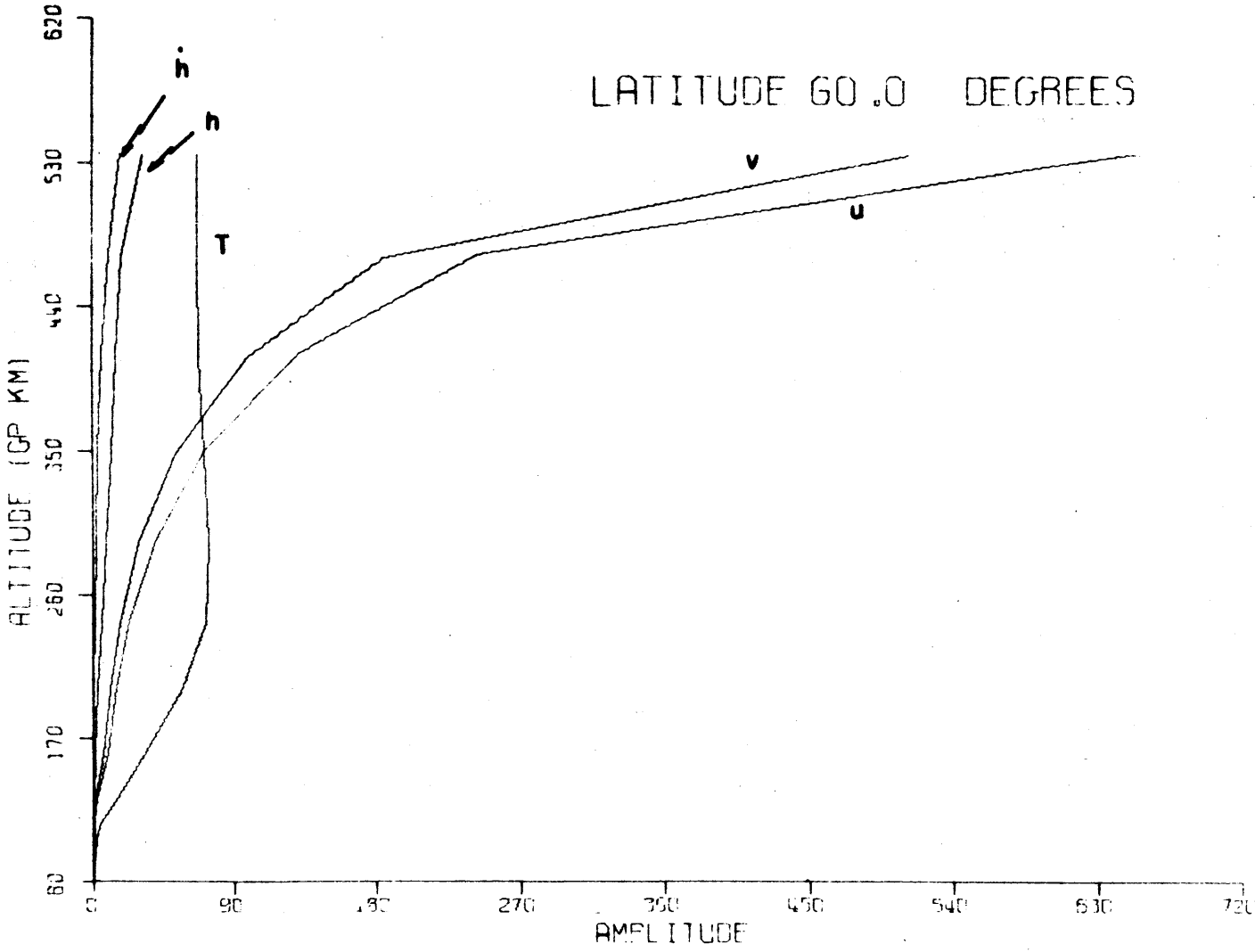

Fig. 9.6. Same as Fig. 9.4 but for 60^{o} latitude.

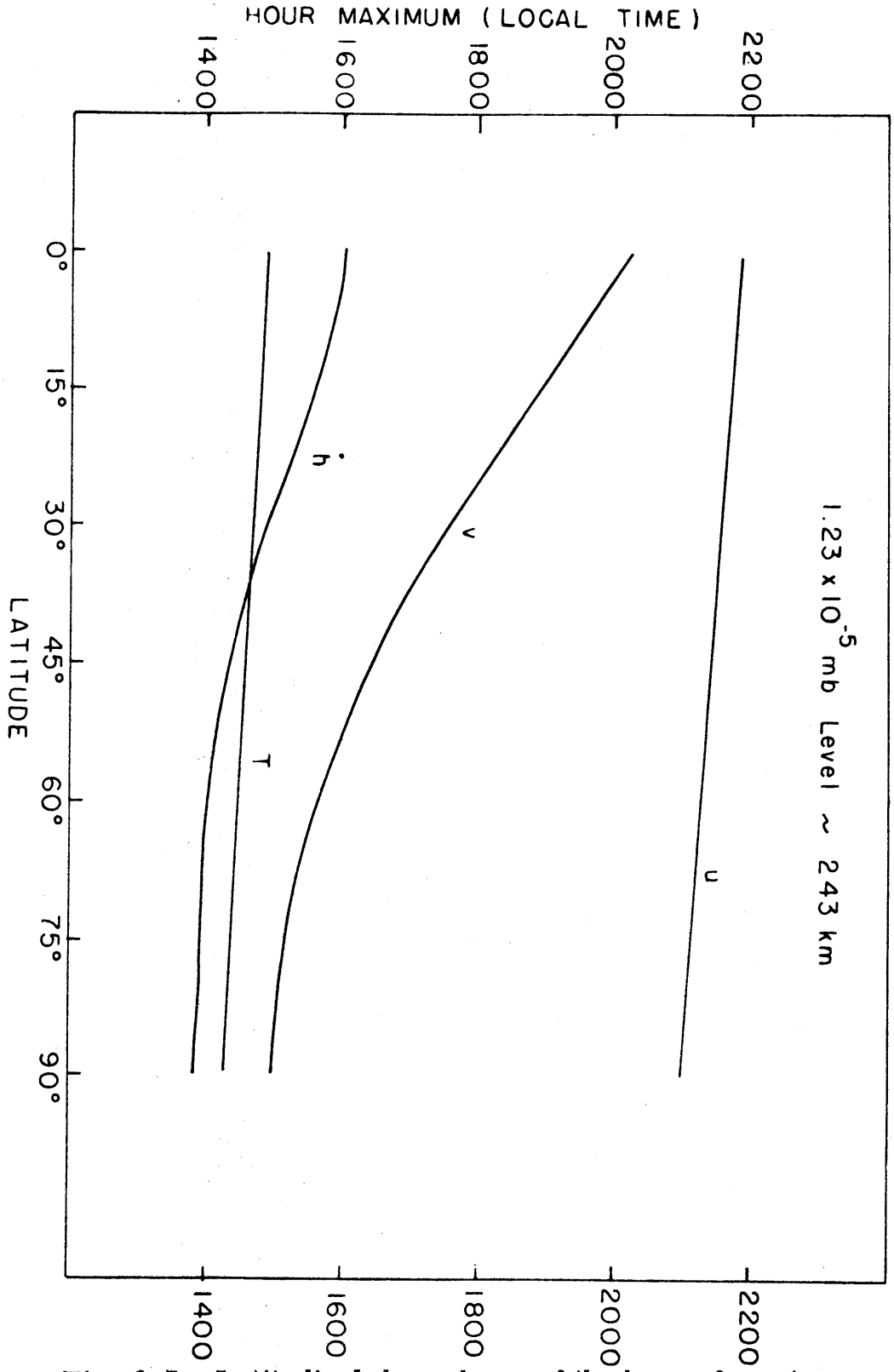

Fig. 9.7. Latitudinal dependence of the hour of maximum magnitude of u, v, $\dot{h}$, and T at about 243 km.

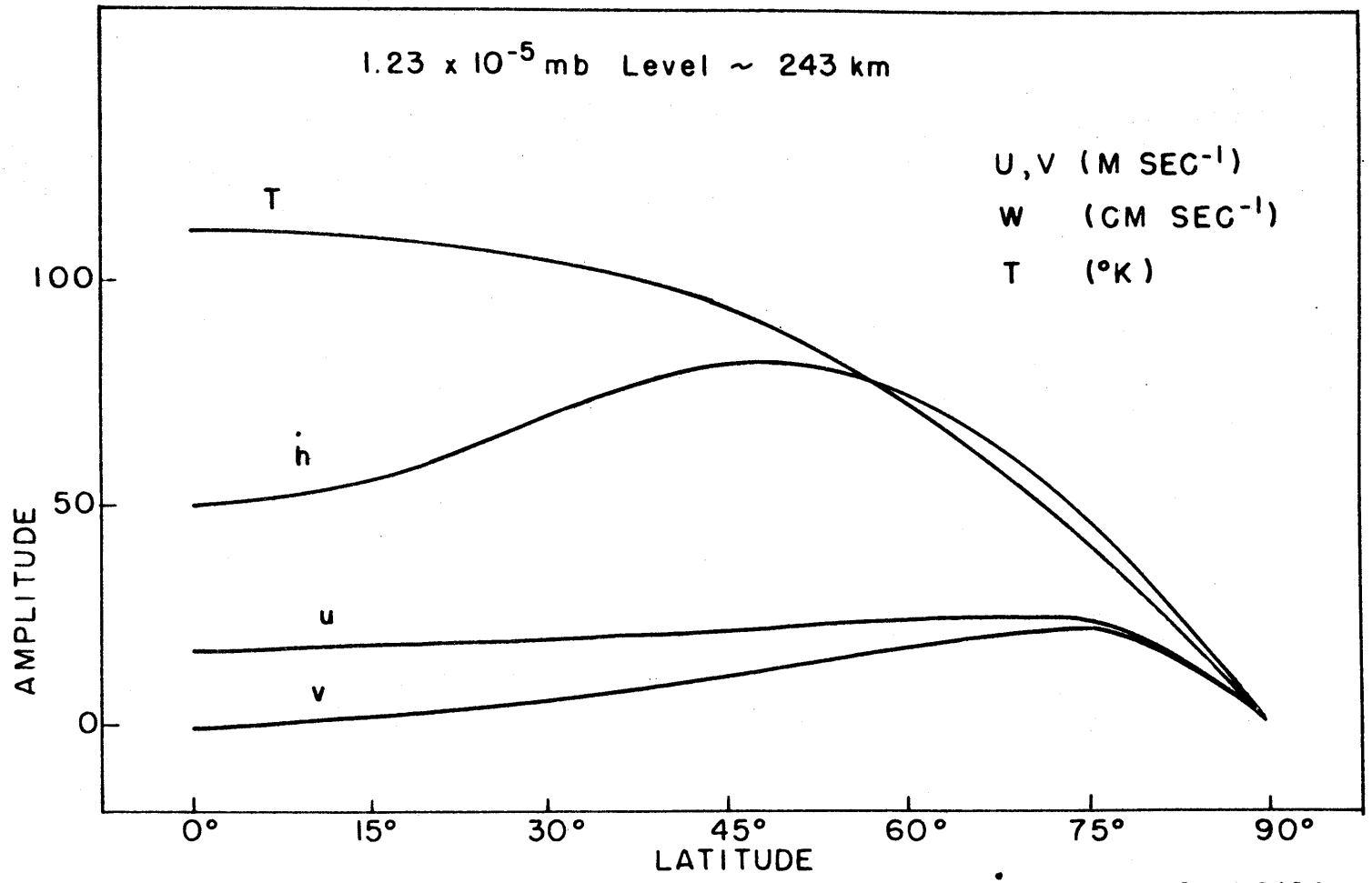

Fig. 9.8. Latitudinal dependence of the amplitude of u, v, $\dot{h}$, and T at about 243 km.

9.3 Results for Different Heating Efficiencies

Having established the standard data, we proceed now to alter each of the free parameters in the model, and examine to what extent the results are changed.

A set of model calculations have been obtained by changing the value of heating efficiency. ϵ_n^I and ϵ_n^d were set as low as 60% and 10% respectively. These values were used by Mahoney (1966). The result of this calculation is shown in Figs. 9.9 - 9.10. The amplitude of perturbation temperature and other variables resulted to be small, as indicated in Fig. 9.10 (cp. Fig. 9.4). The hour of maximum h, u, v, $\dot{h}$ and T shown in Fig. 9.9 has practically no change with reference to the standard result shown in Fig. 9.3. From this calculation it was evident that more solar heating was required, and consequently, ϵ_n^I and ϵ_n^d were increased. A constant average value of 85% for ϵ_n^I (ϵ_n^d was set equal to 14%), as predicted from theory, gives amplitudes of temperature perturbation that are in better agreement with observations. These values were selected for the standard and subsequent model calculations.

9.4 Results for Different Boundary Conditions

Let us now consider the problem of solving the system

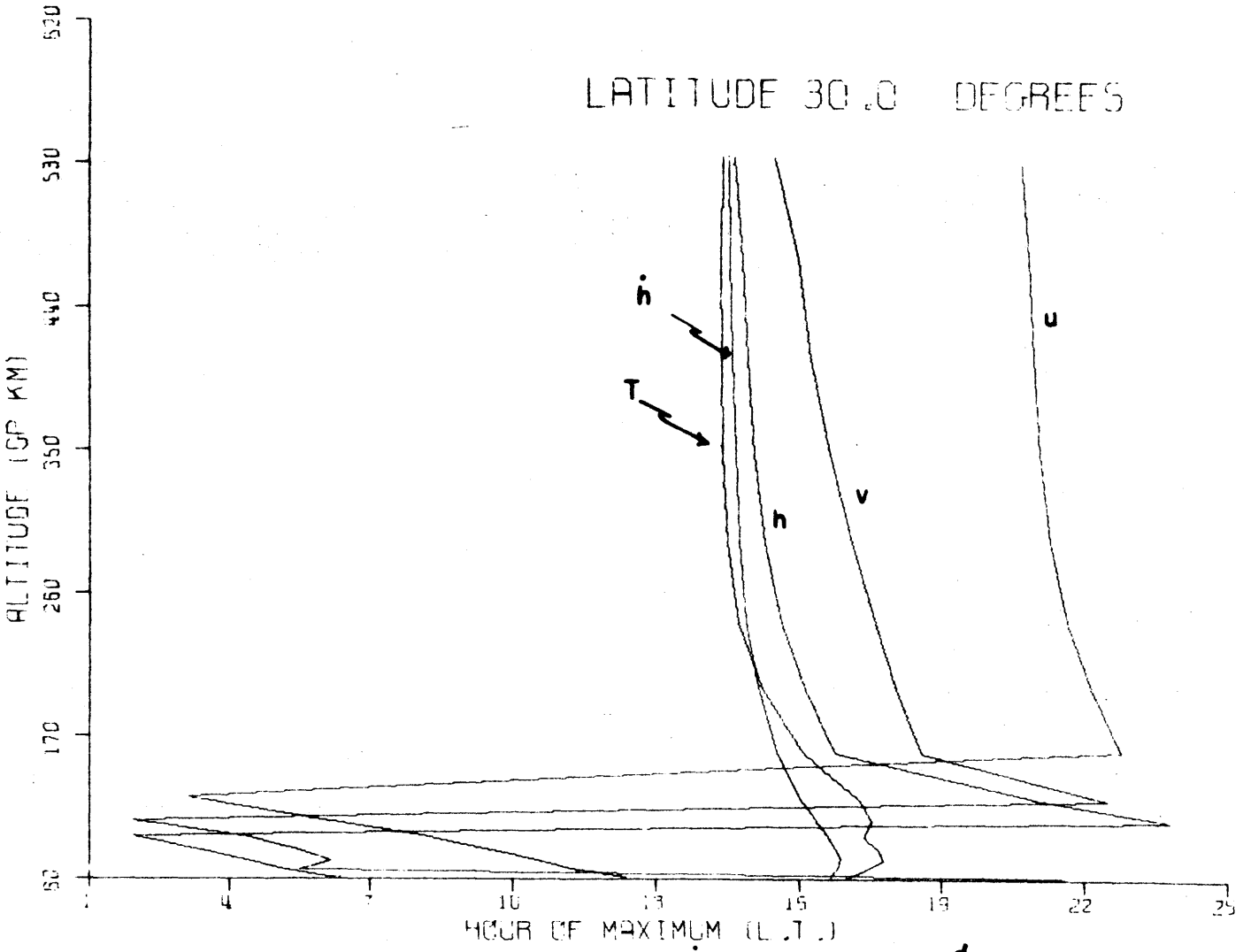

Fig. 9.9. Same as Fig. 9.3. but with ϵ_N^i = 60% and ϵ_N^d = 10%.

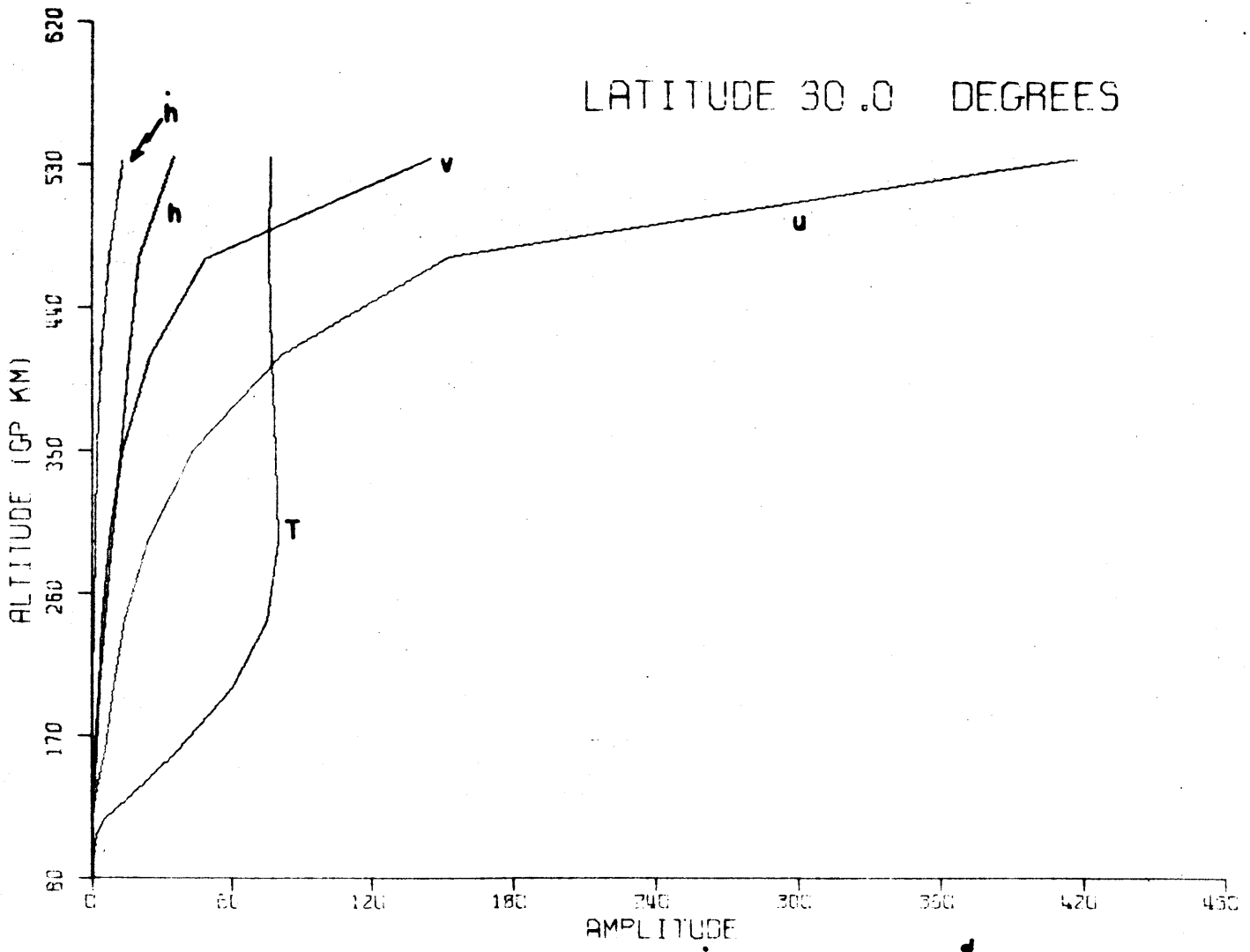

Fig. 9.10. Same as Fig. 9.4 but with ϵ_N^i = 60% and ϵ_N^d = 10%.

of equations (8.74) - (8.77) with boundary conditions which specify that heat flux and the gradient of $e^{-z/2}w$ vanish at the top boundary, and compare the results with the standard data. The solutions of (8.74) - (8.77) together with the finite difference analog of $(e^{-z/2}w)_z = T_z = 0$, are summarized in Figs. 9.11 - 9.12. There are two points worth mentioning.

First, there is practically no change of the phase of the temperature perturbation with reference to the standard data. The hour of maximum temperature occurs at 14:30 hrs. L.T. at 250 km and 14:06 hrs. L.T. at 400 km. Secondly, the amplitude is somewhat smaller than the standard results. It is 5% smaller at 250 km and 10% smaller at 400 km.

The phase of the three components of the velocity and h have also negligible change with reference to the standard data. The amplitude of the horizontal velocity field and h are smaller than the standard value by about 5% at 250 km and 18% at 400 km. The amplitude of h , however, is larger than the standard value by about 5% at 250 km and 18% at 400 km.

9.5 Results for Various Ion Density Profiles

We next examine the effects on the model when the ion

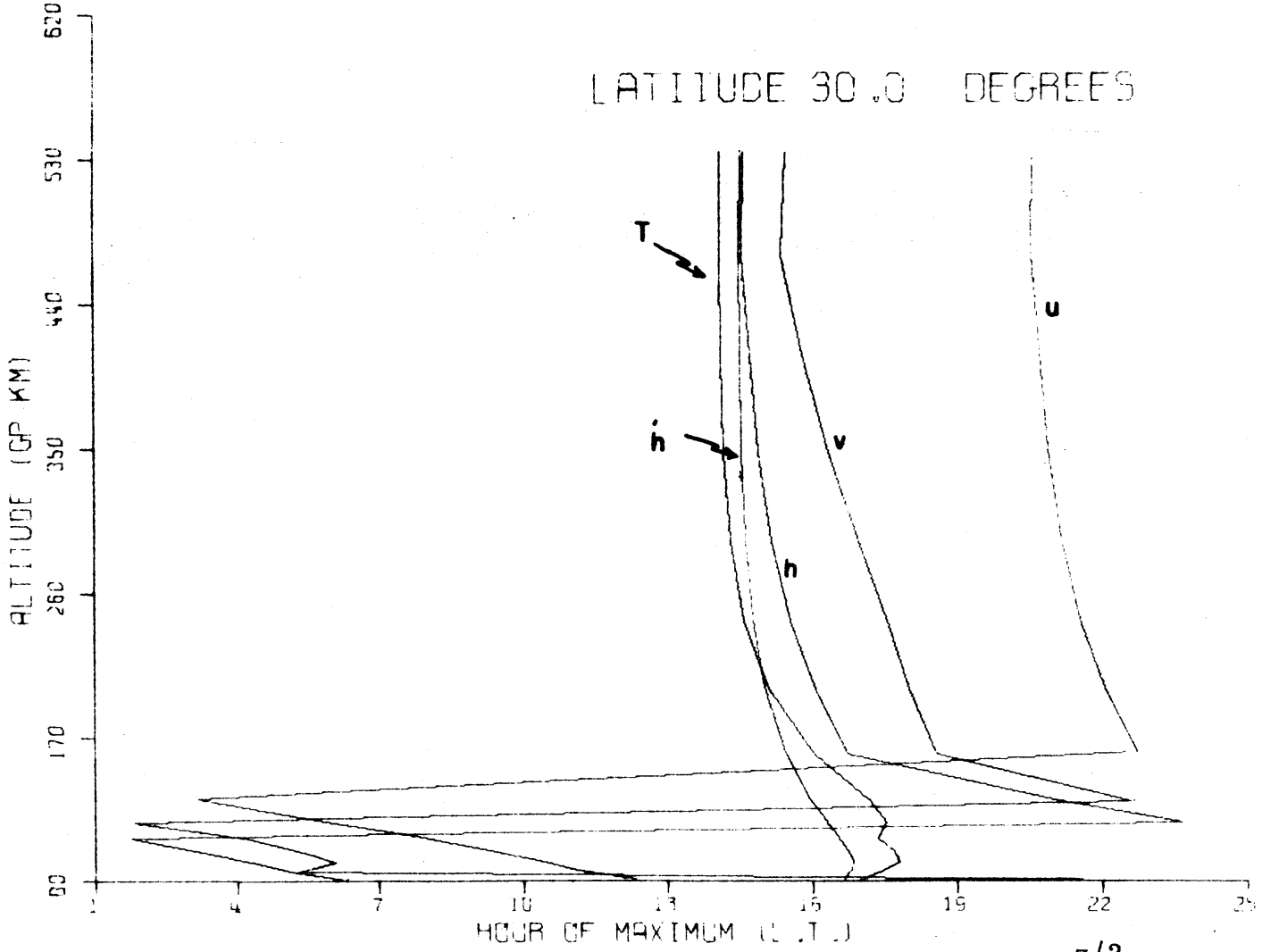

Fig. 9.11. Same as Fig. 9.3 but with upper boundary condition $(e^{-z/2}w)_z = T_z = 0$.

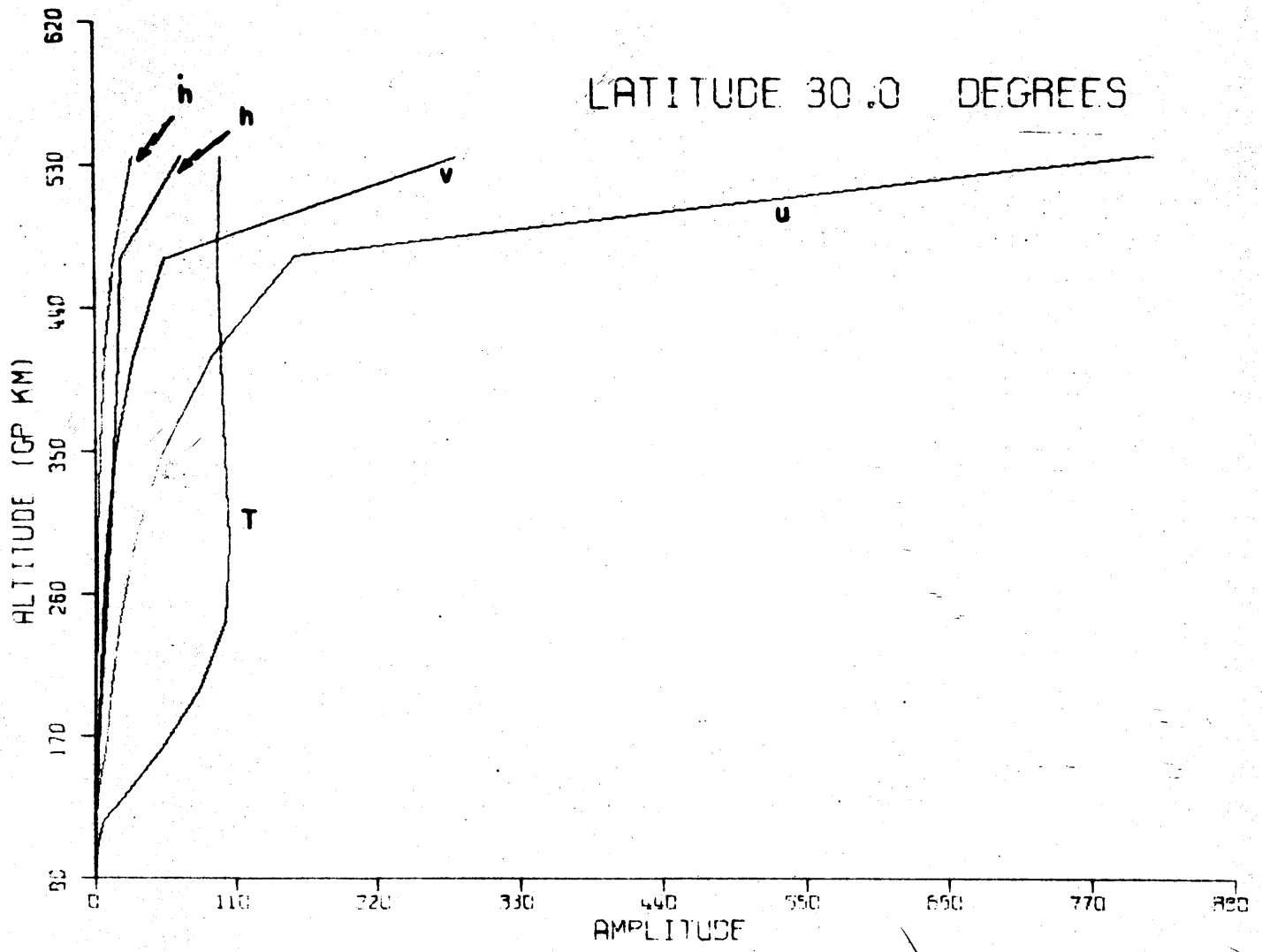

Fig. 9.12. Same as Fig. 9.4 but with upper boundary condition $(e^{-z/2}w)_z = T_z = 0$.

drag parameter is changed. There are three free parameters to play with, n_m , z_m , and D. Six sets of these parameters were selected as shown in Table 4.

TABLE 4. Numerical Values of Ion Drag Parameters Used in the Model Calculations

Model	1*	2	3**	4	5	6
n_m	$1 \cdot 10^6$	$1 \cdot 10^6$	$1 \cdot 10^6$	$1 \cdot 10^6$	$5 \cdot 10^5$	$5 \cdot 10^6$
z_m	10	10	10	11	10	10
D	2	3	2	2	2	2

* Reference model (standard)
**Expression (9.1) + .5(z - 6.5). Second term added from Level 7 up.

Fig. 9.13 shows the set of ion density profiles. Figs. 9.14 - 9.15 summarize the results of the temperature calculations when the parameters of ion drag take the values of the first four columns given in Table 4. Likewise, Figs. 9.16 - 9.17 show the results when the parameters of ion drag take the values of the last two columns of Table 4, i.e. n_n is decreased by a factor of two and increased by a factor of five.

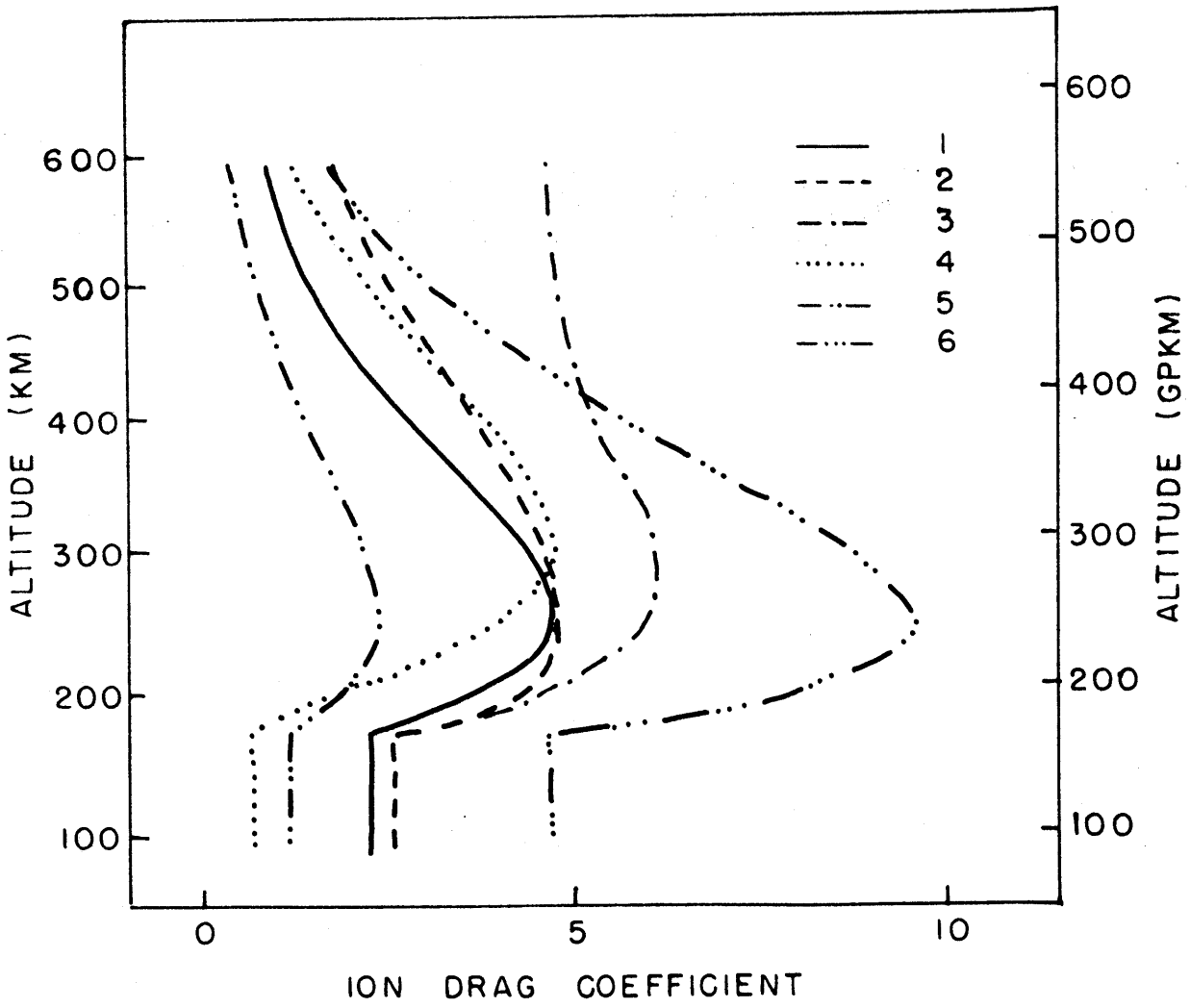

Fig. 9.13. Profiles of ion drag coefficient N_i used in the model calculations.

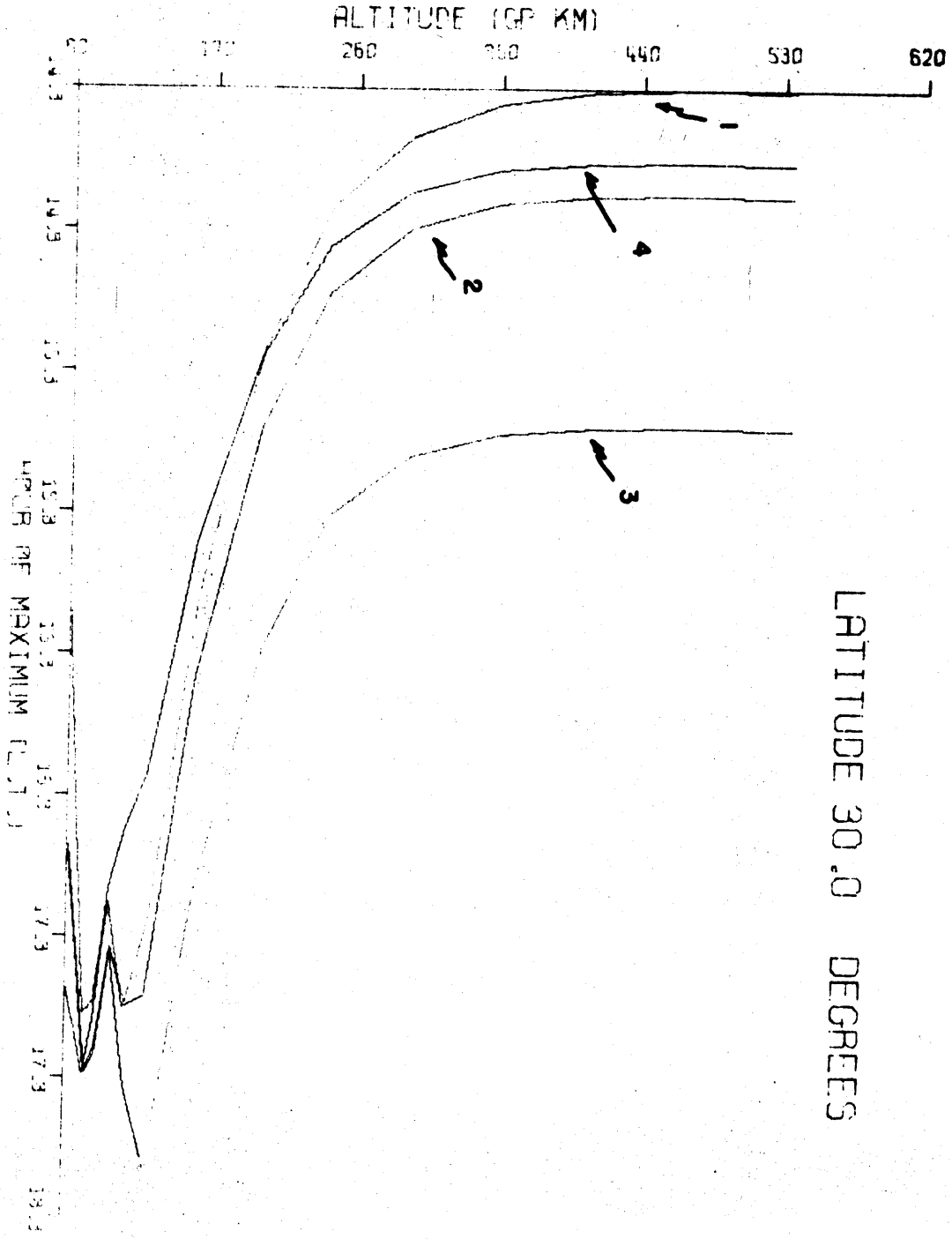

Fig. 9.14. Altitude dependence of the hour of maximum temperature for different N_i profiles as shown in Fig. 9.13.

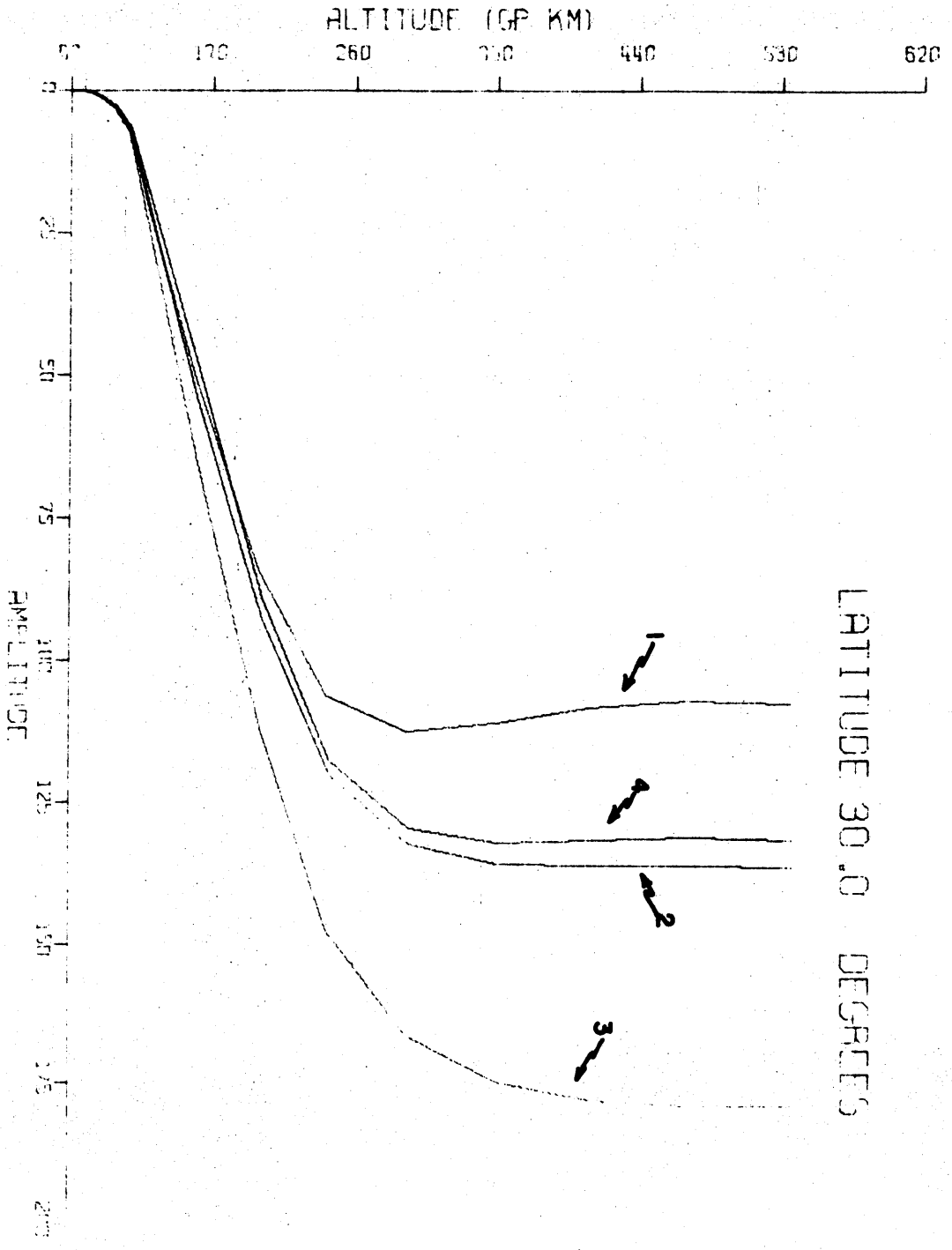

Fig. 9.15. Altitude dependence of the temperature amplitude for different N_i profiles as shown in Fig. 9.13.

Let us consider the model results individually. The thickness of the ion drag coefficient distribution of Model 2 is wider. The hour of maximum of the vertical temperature structure shifts to later time by about .5 hrs. The amplitude increases at all levels, 8^{o}K at 200km altitude, 20^{o}K at 300 km, and 28^{o}K at about 400 km altitude. In model 3 a term, .5(z-6.5), has been added above level 7 to N_i corresponding to model 1, in order to keep the magnitude of N_i almost constant above F2 peak. The hour of maximum shifts to later time by about 1:10 hrs. The amplitude increases by about 40^{o}K at 250 km and about 70^{o}K at 400 km. In model 4, the height of n_m has been raised to level 11 (about 300 km), the other parameters are kept the same as in model 1. The changes in phase and amplitude of the temperature are not large. The hour of maximum shifts only 0.2 hrs. to later time, and the amplitude increases by about 10^{o}K at 250 km and about 23^{o}K at 400 km. In model 5, n_m has been decreased by 50%. The hour of maximum shifts by about one hour to earlier time, the amplitude decreases by about 30^{o}K at 250 km and 45^{o}K at 400 km. Finally in model 6, we have increased the n_m by 500%, (an upper limit, although never observed)the resulting phase change is that maximum temperature variation occurs 1:20 hrs. later, and the amplitude increases by about 36^{o}K at 250 km and 65^{o}K

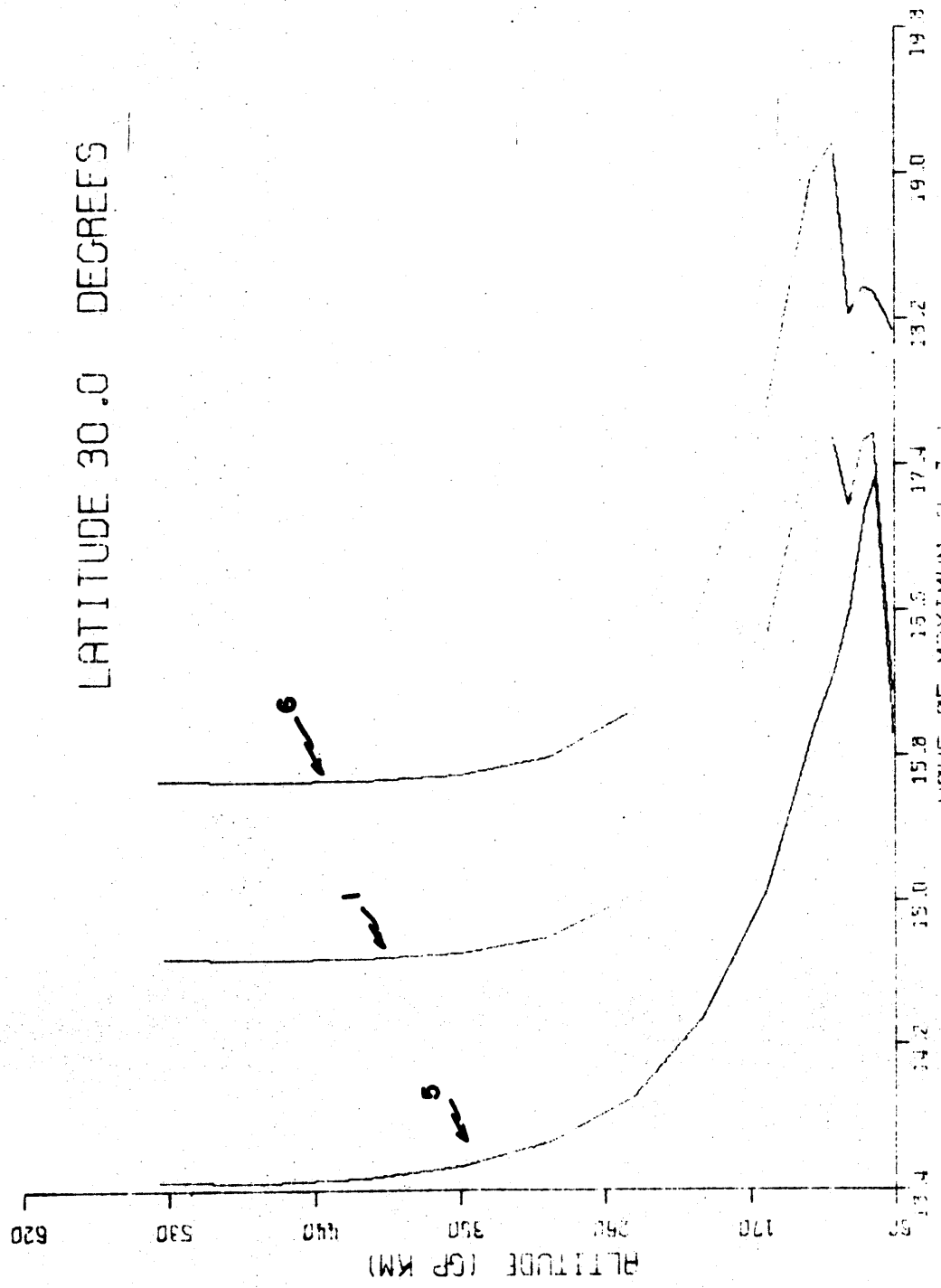

Fig. 9.16. Same as Fig. 9.14.

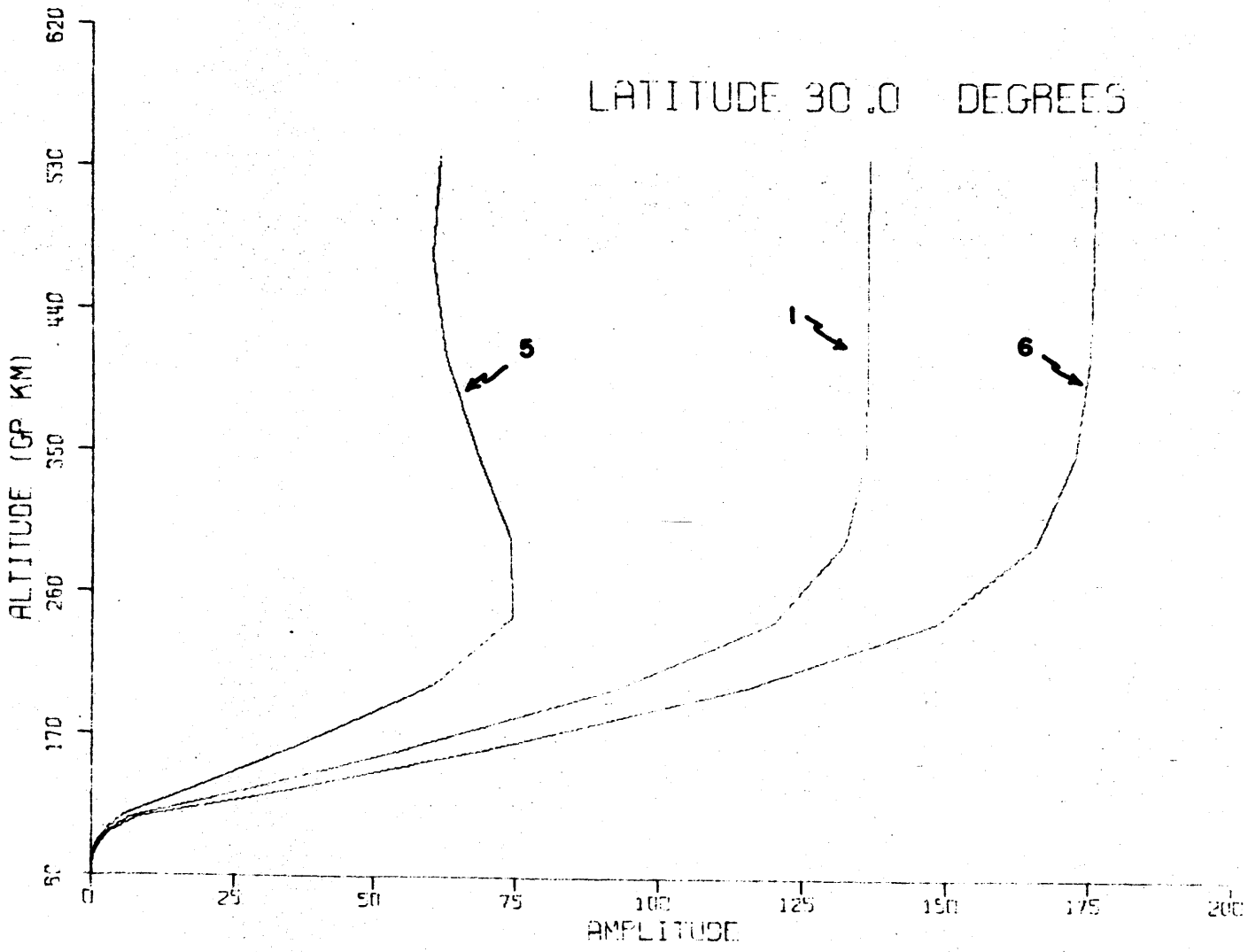

Fig. 9.17. Same as Fig. 9.15.

at 400 km. These results encompass the actual range of observed electron density profile.

9.6 Results for Changes in the Mean Temperature Field

Let us consider next the changes that may result in the vertical structure of temperature when the mean state is altered. The effect of the basic state condition (e.g. the hemispheric average temperature) in the model calculation comes in through the thermodynamic heating or adiabatic heating, which depend on the static stability S.

Fig. 9.18 shows the vertical distribution of mean temperature for average and high solar activity, and the corresponding distribution of S.

Fig. 9.19 illustrates the results for the high solar activity case for the hour of maximum h, u, v, $\dot{h}$, and T. There is a phase shift of about 0:30 hrs. toward earlier time on h, u, $\dot{h}$, and T, and about 0:50 hrs. on v. The amplitude of h, u, and v decreases by about 10%,the amplitude of T decreases by about 10% at 250 km and 18% at 400 km, whereas the amplitude of $\dot{h}$ increases by about 15% as we can see from Fig. 9.20.

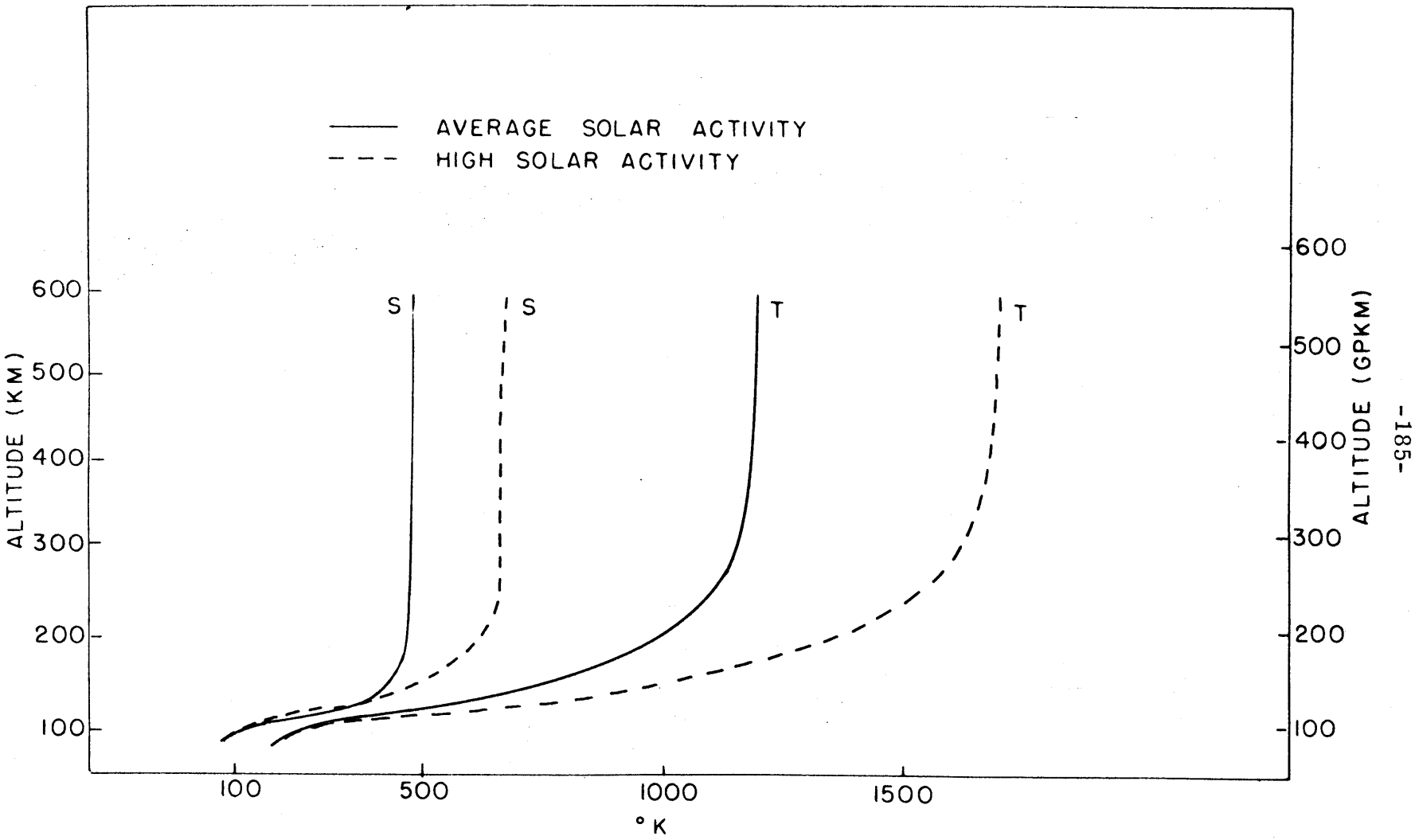

Fig. 9.18. Vertical distribution of mean temperature and static stability for average and high solar activity.

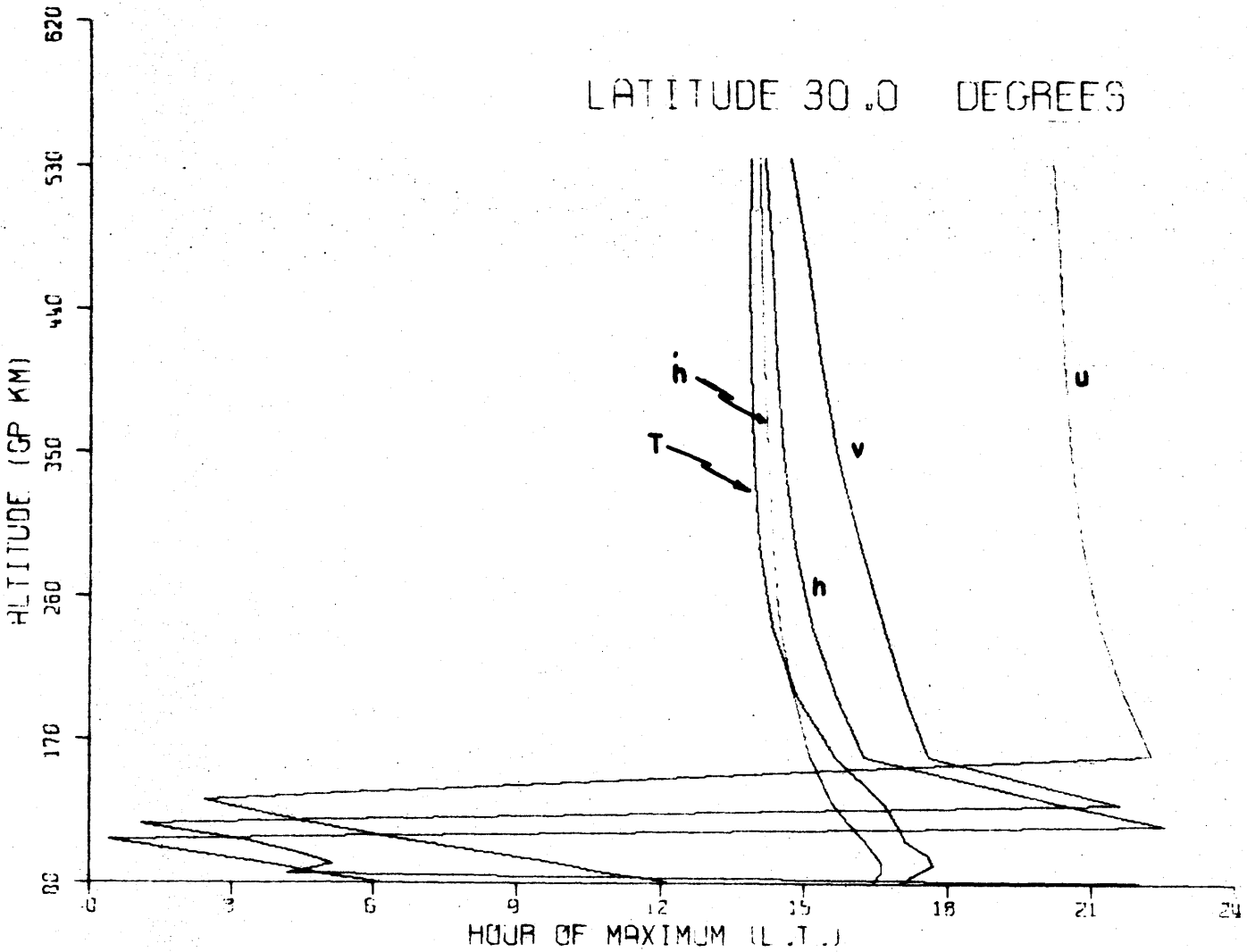

Fig. 9.19. Same as Fig. 9.3 but with T_o and s corresponding to high solar activity.

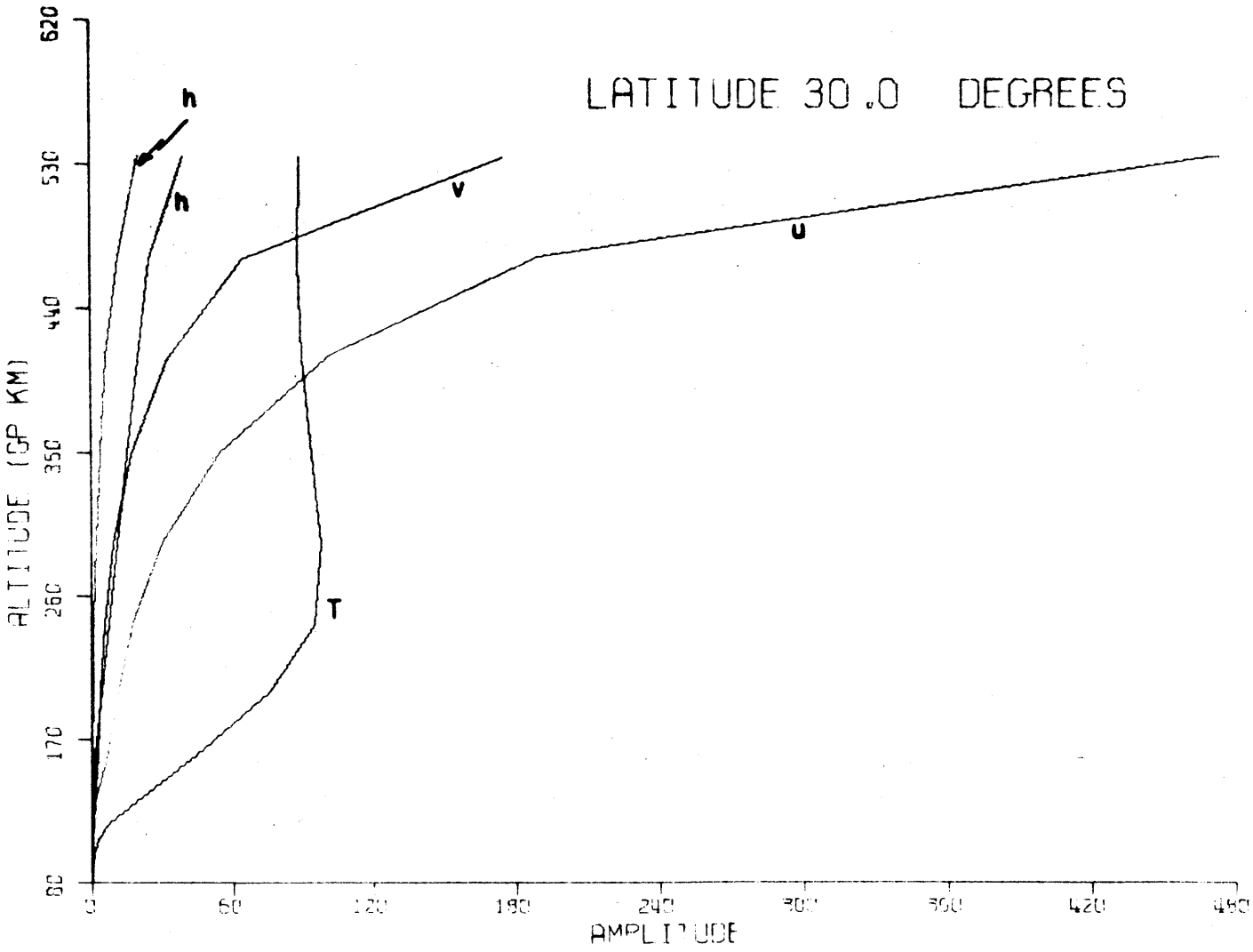

Fig. 9.20. Same as Fig. 9.4 but with T_o and s corresponding to high solar activity.

9.7 Results for Subsidence Heating

It is of interest to calculate the magnitude of subsidence heating (or adiabatic heating, or thermodynamic heating, or heating by compression) and compare with heating by solar radiation. The subsidence heating is given by

$$\mathcal{H} = w\left[c_p \frac{dT_o}{dz} + R T_o\right] \qquad (9.2)$$

Fig. 9.21 shows the vertical distribution of $\mathcal{H}$ for 30^o latitude. Fig. 9.22 shows the latitudinal distribution of $\mathcal{H}$ at 245 km level. The magnitudes of $\mathcal{H}$ are of the same order of magnitude as of the solar heating (cp Figs. 7.7 - 7.8). The hour of maximum heating by $\mathcal{H}$ is the same as the hour of maximum downward motion. In general, maximum cooling by $\mathcal{H}$ is associated with maximum heating by Q.

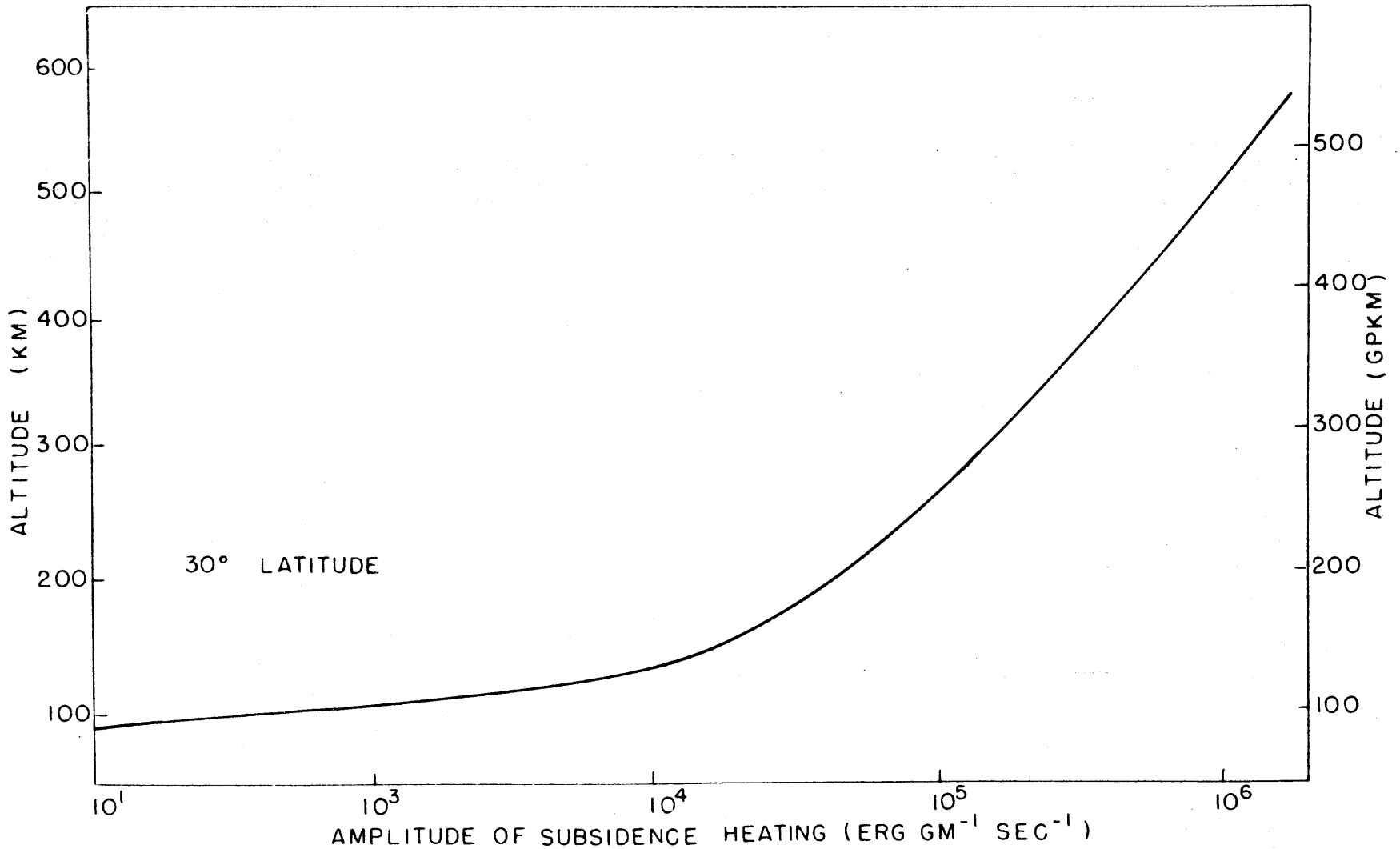

Fig. 9.21. Vertical distribution of the amplitude of adiabatic heating by vertical motion corresponding to the standard results.

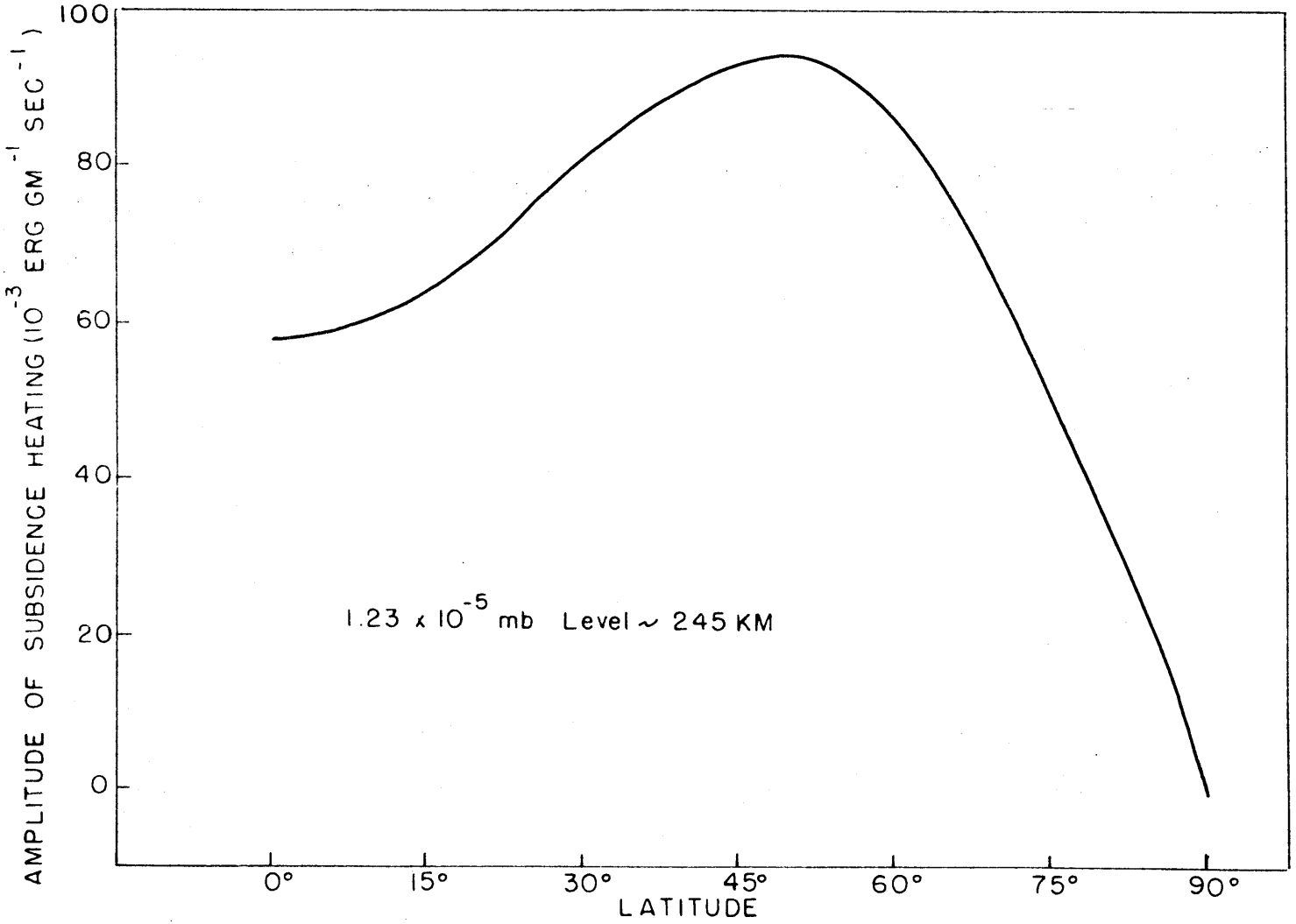

Fig. 9.22. Latitudinal distribution of the amplitude of adiabatic heating by vertical motion corresponding to the standard results.

10. GENERAL DISCUSSION AND CONCLUSION

A system of equations describing the global circulation of the thermosphere has been formulated in the previous chapters. A simpler model describing the diurnal circulation in the middle thermosphere has been derived with the additional approximation that the thermal forcing in the momentum equation is balanced by the ion drag term alone. This model has been integrated numerically and the results were presented in the last chapter. It is now our task to discuss the results of the model and derive the consequences in so far as they concern current ideas about the circulation of the thermosphere.

10.1 Discussion of the Motion Field

The horizontal component of the motion field has been computed from the momentum equation after neglecting inertial forces, coriolis force, viscous drag, and electromagnetic drifts. This is a very crude approximation, but appears to be satisfactory if the ion drag parameter is large. This will be the case, as discussed in section 4.5, during maximum solar activity, or at summer solstice near higher solar activity, and at daytime during average solar activity. This motion regime, which has been given the name cross isobaric (Geisler, 1966), will be limited to the region where $N_i > 1$. This condition will be

satisfied around the F region peak, say between 165km and 400km altitude. Outside this region our results are not applicable. The values of the ion drag parameter adopted for the calculation have been selected such that they will cover the actual range of the average electron (ion) density profile observed at sunspot maximum (see Fig. 9.13). We have also assumed that N_i is independent of time (and latitude). In general the calculated amplitudes of zonal and meridional components of horizontal velocity are small whenever N_i is large, and vice versa. The amplitudes of u and v at the hour of maximum at about 350km are 70 m/sec and 35 m/sec respectively for the reference model at 45^o latitude. The amplitudes of u and v at the hour of maximum for model 5 at about 300km are 60 m/sec and 30 m/sec respectively at 45^o latitude.

The pressure gradients associated with the diurnal bulge of atmospheric density as deduced from satellite drag measurements have been used to derive horizontal winds in the thermosphere (Geisler, 1966, 1967; Kohl and King, 1967; Lindzen, 1967a). Geisler (1966) has calculated the horizontal components of the geostrophic and cross-isobaric winds for sunspot maximum and minimum, at 45^o latitude. He finds that during the day, the peak ion concentration is sufficiently high for the cross-isobaric component to be dominant. The maximum amplitudes of the zonal and meridional components that he obtains at the F2

peak (about 340 km) around 2000 hrs. L.T. (for u) and 1600 hrs. L.T. (for v), for summer and high solar activity are 60 m/sec and 20 m/sec, respectively. The corresponding values for winter at the F2 peak (about 260 km) are 120 m/sec and 40 m/sec respectively. Although these results and those reported here can not be compared directly due to the difference in n_m used to compute them (see Table 4 and Fig. 9.13, and Table 1 in Geisler (1966)), the amplitudes are in agreement within a factor of two.

The orientation and time of maximum eastward and northward velocity are also in agreement with Geisler's calculation. From Fig. 9.7 we can see that the zonal component is eastward from 1500 hrs. to 0300 hrs. local time, with maxima at 2200 hrs., and the meridional component is poleward from 1000 hrs. to 2200 hrs. L.T., with maxima at 1600 hrs. L.T.. Geisler's calculations also indicate a maximum eastward velocity at 2200 hrs. and maximum northward at 1500-1600 hrs.L.T.

It is also interesting to note that the inclusion of inertial, coriolis force, and viscouse drag (Geisler, 1967) does not substantially change the phase of the north-south wind component. From Fig. 9.7 we note that the time of maximum northward velocity change with latitude, shifting to earlier time as latitude increases. Similar results have also been obtained by Geisler (1967).

The amplitudes of u, v, and h obtained in the present study increase unrealistically with altitude above about 400 km. This

is because we have neglected viscosity, which becomes important above about 400 km. Our results, therefore, are not applicable above 400 km.

The field of vertical velocity is also in agreement in phase and amplitude with the vertical velocity calculated from the horizontal wind system of Geisler (1967) (Dickinson and Geisler, 1968), below 400 km.

The average rotational speed of the upper atmosphere at heights of 200 to 300 km has been evaluated by analysing the changes in the orbital inclination of several satellites (King-Hele and Allan, 1966, and King-Hele and Scott, 1966). These studies suggest that the atmosphere rotates at a rate of about 1.3 (1.1 to 1.5) faster than the earth, given a diurnal average westerly wind between 100 to 200 m/sec. The results of the linear model presented here provide no average zonal wind.

10.2 Discussion of Temperature Field

Let us now examine the question of the phase and amplitude of the perturbation temperature associated with the diurnal bulge. The results presented in the previous chapter show that the phase and amplitude depend to some extent on what boundary conditions (for amplitude only) and ion drag coefficient are adopted in the model calculations. In general the results indicate that the phase is height dependent. The time of maximum temperature lags behind the hour of maximum heating by more than 4 hours below 150 km, but 2.3 hours above 250 km.

Temperature data inferred from density observations indicate that maximum temperature lags maximum heating by 2 hours and remains independent of height above about 200 km.

We have mentioned above that the horizontal component of wind and consequently the vertical component, are unrealistically large above 400 km. Larger vertical velocity leads to larger adiabatic heating. Adiabatic heating by vertical motion is about 140^{o} out of phase with solar heating. That is, there is a maximum cooling at 14:30 hrs. L.T. As a net result, the amplitude of the temperature perturbation decreases slowly above 400 km.

The amplitude of the temperature perturbation can be increased by increasing the ion drag, so that the velocity field is small and consequently the adiabatic heating by vertical motion will be small, however, the hour of maximum shifts to later time. The contrary holds true if we decrease the ion drag. From Figs. 9.11-9.12 we can also see that changes in the upper boundary conditions could lead to some changes in the amplitude of T.

Jacchia (1965) has investigated the amplitude of diurnal exospheric temperature variability and found that the ratio of daily maximum to minimum temperature remains very near to 1.3, independent of latitude and season. The maximum and minimum exospheric temperatures change with solar cycle. For mean solar activity (10.7 - cm solar flux = 150), $T_{max} \cong 1230^{o}K$ and $T_{min} \cong 960^{o}K$; for periods

between mean and high solar activity (10.7 - cm solar flux = 175), $T_{max} \cong 1345^{\circ}K$ and $T_{min} \cong 1050^{\circ}K$. Similar data from the present standard model calculations gives at 0° latitude Tmax $\cong 1300^{\circ}K$ and Tmin $\cong 1056^{\circ}K$, given a Tmax to Tmin ratio of 1.23; at 30° latitude Tmax $\cong 1290^{\circ}K$ and Tmin $\cong 1066^{\circ}K$ with Tmax to Tmin ratio of 1.21; and at 60° latitude Tmax $\cong 1252^{\circ}K$ and Tmin $\cong 1104^{\circ}K$, with Tmax to Tmin ratio of 1.14.

We have neglected the coupling between the lower atmosphere and the thermosphere, and between the thermosphere and the exosphere. Probably, the diurnal tide originated in the lower atmosphere will be dissipated below 150km but the semidiurnal tide might reach up to the 200km level. The momentum and heat fluxes associated with these tides should be incorporated in the model if we seek a more complete description of the circulation in the lower thermosphere. It seems that on account of the lack of experimental evidence for a vertical heat flux coming in from the magnetosphere, we can safely neglect it. On this basis one can justify the simpler boundary conditions used in our previous study so long as we choose the top boundary at altitudes higher than 500km.

Perhaps the most important shortcoming of the present model is to have neglected viscosity. Its omission cannot be justified above 400km, since $E = O(R_o^{-1})$ in this region. If $N_i = O(1)$, it cannot be

even justified above 300km. Its omission in the present model has lead us to obtain results for the motion field increasing with altitude. If we had included viscosity in the model, the solution for the motion field would have been independent of altitudes for large z, as we found in our two dimensional model.

10.3 The Significance of Adiabatic Heating by Vertical Motion

We want to end by summarizing the positive qualities and consequences that can be derived from the present study.

It has been established by a scale analysis of the dynamic equations in chapter 4 (see also Lagos, 1967; Dickinson, Lagos, and Newell, 1968) that only vertical motion can give adiabatic heating and cooling in the thermosphere that is of the same magnitude as the heating by EUV solar radiation. These studies have been supplemented with two-dimensional numerical models to support the above conclusion (see references above). Because of the approximations inherent in these models, the uncertainty, regarding the exact description of the "second heat source" as due mainly to adiabatic heating and cooling by vertical motion, has remained. We have then sought a more correct description of the "second heat source" using a more elaborate dynamical model which is described in the present study. Yet, even here

we were forced to make some approximations. Our results indicate, however, that these approximations are not serious. We may regard, therefore, the present and our earlier studies as complementary and consider as satisfactory our explanation of the "second heat source".

From our theoretical formulation and the numerical solutions presented in the previous chapters, we can safely claim, that the model reproduces the main features of the diurnal bulge in the region from about 160km to about 400km. The error in describing properly the lower boundary condition and the interaction with the lower atmosphere is certainly no larger than the error in neglecting inertial and coriolis force. Likewise, the error that may be introduced by specifying properly the upper boundary condition is certainly no larger than the error introduced by neglecting viscosity and electromagnetic drifts.

Noting again that only vertical motions couple the equations of motion to the thermodynamic equations, the numerical solutions presented in chapter 9, all showing that maximum temperature occurs near 1400 hrs. L. T., must therefore, be regarded as due to adiabatic heating and cooling by vertical motion, which shifts the phase to earlier time by almost exactly two hours. To prove that indeed adiabatic heating and cooling by vertical motion can shift the phase of the maximum temperature, solutions of the thermodynamic equation with and without the subsidence heating term have been obtained. Figs. 10.1 - 10.3 summarize the re-

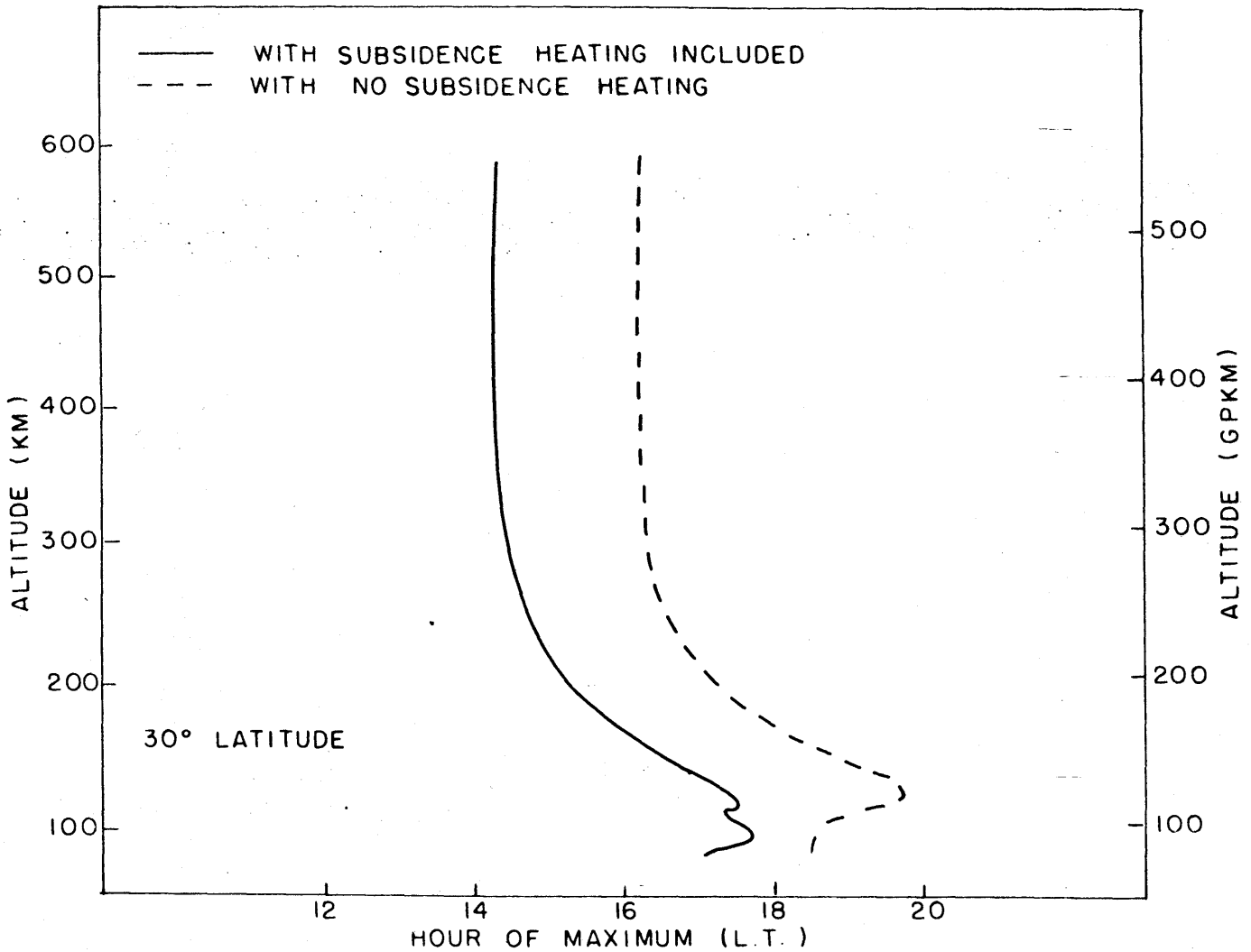

Fig. 10.1. Vertical distribution of the hour of maximum temperature when the subsidence heating is and is not included in the standard model calculations.

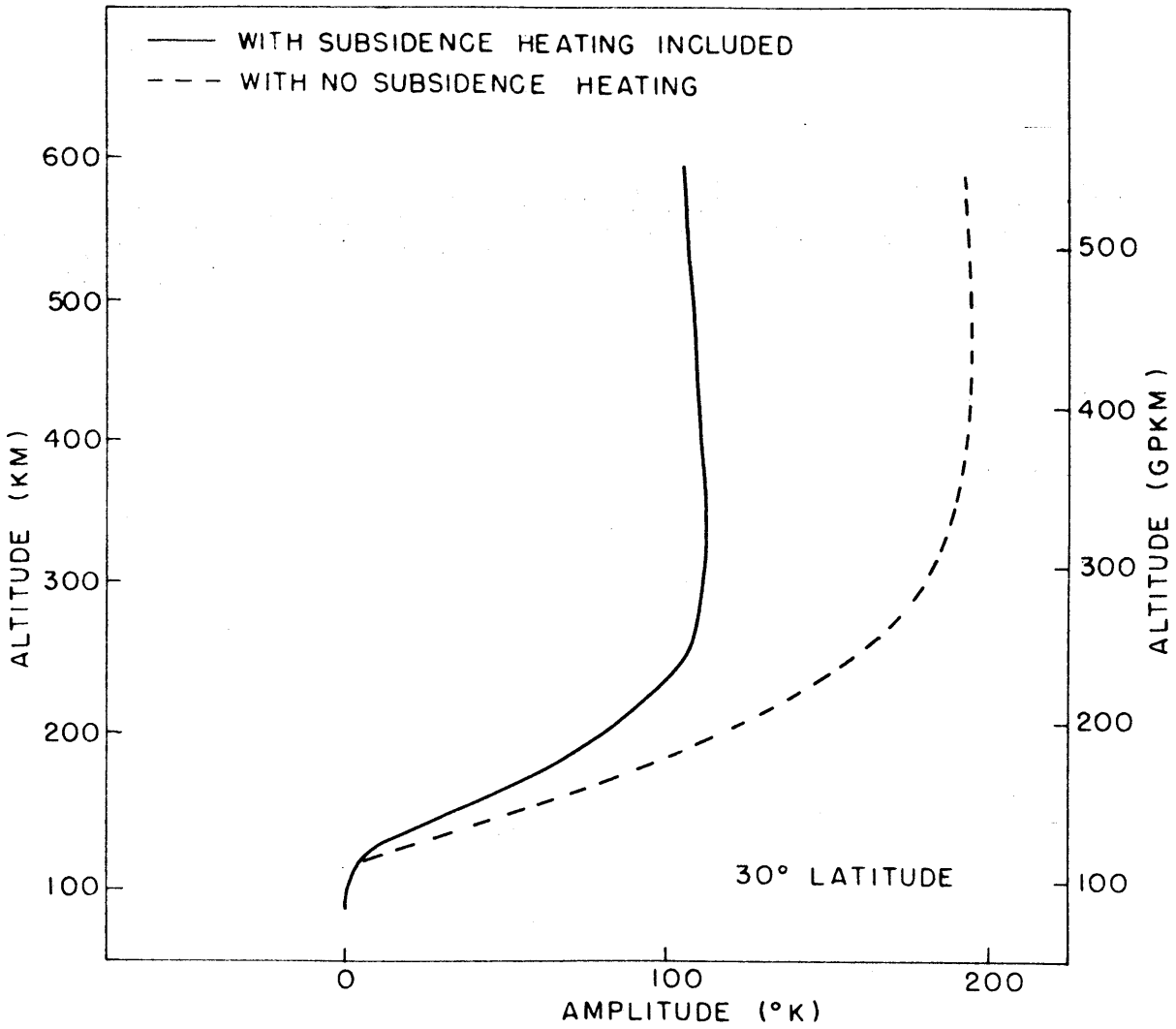

Fig. 10.2. Vertical distribution of the temperature amplitude when subsidence heating is and is not included in the standard model calculations.

sults. Figs. 10.1 - 10.2 show the solution with the boundary conditions used in the present model, whereas Fig. 10.3 shows the solution using the boundary conditions that allow no flux of heat at the top boundary. Figs. 10.1 and 10.3 show the hour of maximum temperature and Fig. 10.2 shows the corresponding amplitude of Fig. 10.1. Note that the amplitude in absence of adiabatic heating has increased by about 80% above 200 km. In view of these results, there can be little doubt that the "second heat source" is due to adiabatic heating, or to heating by compression, or to thermodynamic heating. These names have been used to describe the pressure-work term.

The role and consequences of vertical motion in other thermospheric processes is evident of course, but we do not want to discuss them here. There is no question about the work that remains to be done before we can understand fully the circulation of the thermosphere.

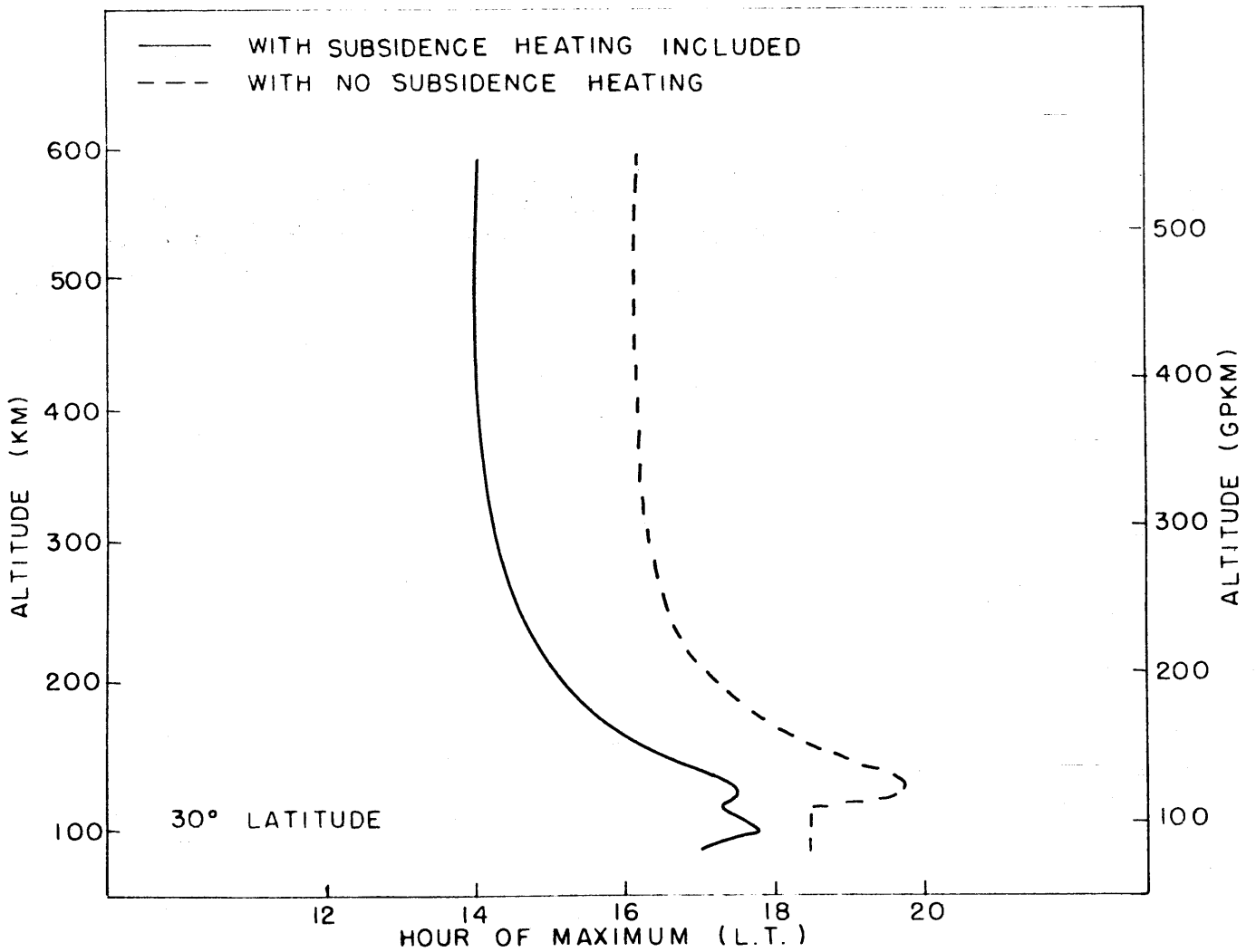

Fig. 10.3. Same as Fig. 10.1 but for model calculation with upper boundary conditions $(e^{-z/2w})_z = T_z = 0$.

ACKNOWLEDGEMENTS

I am deeply grateful to Prof. Reginal E. Newell for his advice and useful comments during the course of this study and to Prof. Norman A. Phillips for suggesting improvements and for his contribution to my understanding of atmospheric dynamics.

I wish to thank Dr. Robert E. Dickinson for his valuable contribution during the basic formulation of this research. I have also benefited from useful discussions with Dr. John Evans. The computational work was performed at the M.I.T. Information Processing Center. The manuscript was typed by Mrs. Cynthia Webster, Miss Susana Vargas, and Miss Cora Gordon. The figures were drafted by Miss Isabel Kole.

Financial support during my tenure as a graduate student at M.I.T. came from the Instituto Geofísico del Perú, International NASA Fellowship, Organization of American States Fellowship, and from Atomic Energy Commission.

Finally I wish to express my appreciation to all my colleagues and friends who have made pleasant my stay at M.I.T.

References

Allen, C.W., 1965: Interpretation of the XUV solar spectrum. Space Sci. Rev. 4, 91.

Anderson, A.D., 1965: Long-term (solar cycle) variation of the extreme ultraviolet radiation and 10.7-centimeter flux from the sun. J. Geophys. Res. 70, 3231.

Anderson, A.D. and Francis, W.E., 1966: The variation of the neutral atmospheric properties with local time and solar activity from 100 to 10,000 km. J. Atmos. Sci. 23, 110.

Axford, W.I., and Hines, C., 1961: A unifying theory of high-latitude geophysical phenomena and geomagnetic storms. Can. J. Phys. 39, 1433.

Banks, P.M., 1966: Collision frequencies and energy transfer: electrons. Planet. Space Sci. 14, 1085.

Bates, D.R., 1951: The temperature of the upper atmosphere. Proc. Phys. Soc., 64B, 805.

Bjerknes, V. and Coll., 1910: Dynamic meteorology and hydrography. Washington.

Bjerknes, V., Bjerknes, J., Solberg, H., and Bergeron, T., 1933: Physikalische hydrodynamik. J. Springer, Berlin, 1933.

Blumen, W. and Hendl, R.G., 1969: On the role of Joule heating as a source of gravity-wave energy above 100 km. J. Atmos. Sci. 26, 210.

Bourdeau, R.E., Chandra, S., and Neupert, W.M., 1964: Time correlation of extreme ultraviolet radiation and thermospheric temperature. J. Geophys. Res. 69, 4531.

Bramley, E.N., 1967: The effects of ion drag and of plasma forces on neutral air winds in the F-region. J. Atmos. Terr. Phys. 29, 1317.

Brown, R.R., 1966: Electron precipitation in the auroral zone. Space Sci. Rev. 5, 311.

Burger, A., 1958: Scale considerations of planetary motions of the atmosphere. Tellus, 10, 195.

Campbell, W.H., 1967: Low attenuation of hydromagnetic waves in the iono-

sphere and implied characteristics in the magnetosphere for Pc 1 events. J. Geophys. Res. 72, 3429.

Chamberlain, J.W., 1961: Physics of the Aurora and Airglow. Academic Press, New York.

Chapman, S., 1956: The electrical conductivity of the ionosphere; a review. Nuovo Cim. Suppl. 4, 1385.

Chapman, S. and Bartles, J., 1940: Geomagnetism. Oxford University Press, London, 542 pp.

Chapman, S. and Cowling, T.G., 1952: The mathematical theory of non-uniform gases, Cambridge University Press, Cambridge.

Charney, J.G., 1947: On the scale of atmospheric motions. Geofys. Publikasjoner, Norske Videnskaps, Akad, Oslo, 17 (2).

Chu, B., 1959: Thermodynamics of electrically conducting fluids. Physics of Fluids 2, 473.

Cole, K.D., 1962: Joule heating of the upper atmosphere. Aust. J. Phys. 15, 223.

_____, 1963: Damping of a magnetospheric motion by the ionosphere. J. Geophys. Res. 68, 3231.

_____, 1966: Magnetic storms and associated phenomena. Space Sci. Rev. 5, 699.

COSPAR International Reference Atmosphere, 1965, North-Holland Pub. Co., Amsterdam.

Craig, R.A. and Gille, J.C., 1969: Cooling of the thermosphere by atomic oxygen. J. Atmos. Sci. 26, 205.

Cummings, W.D. and Dessler, A.J., 1967: Ionospheric heating associated with the main-phase ring current. J. Geophys. Res. 72, 257.

Dalgarno, A. and Degges, T.C., 1968: Electron cooling in the upper atmosphere. Planet. Space Sci. 16, 125.

Dalgarno, A. and Smith, F.J., 1962: The thermal conductivity and viscosity of atomic oxygen. Planet. Space Sci. 9, 1.

Dalgarno, A. and Walker, J.C.G., 1964: Red line of atomic oxygen in the day airglow. J. Atmos. Sci. 21, 463.

Dalgarno, A., Latimer, I.D., and McConkey, J.W., 1965: Corpuscular bombardment and N_2^+ radiation. Planet. Space Sci. 13, 1008.

Dalgarno, A., McElroy, M.B. and Moffett, R.J., 1963: Electron temperature in the ionosphere. Planet. Space Sci. 11, 463.

Dalgarno, A., McElroy, M.B. and Stewart, A.I., 1969: Electron impact excitation of the dayglow. To be published.

Dalgarno, A., McElroy, M.B., and Walker, J.C.G., 1967: The diurnal variation of ionospheric temperatures. Planet. Space Sci. 15, 331.

Davies, Kenneth, 1965: Ionospheric radio propagation. National Bureau of Standards, Monograph 80, 470 pp.

DeWitt, R.N. and Akasofu, S., 1964: Dynamo action in the ionosphere and motions of the magnetospheric plasma. I: Symmetric dynamo action. Planet. Space Sci. 12, 1147.

Dickson, R.E., 1966: Propagators of atmospheric motions. Rept. No. 18, Department of Meteor., M.I.T., 243 pp.

Dickinson, R.E., 1968: On the formulation of a nonlinear atmospheric tidal theory from the meteorological primitive equations. Pure Appl. Geophys. 72, 198.

Dickinson, R.E. and Gersler, J.E., 1968: On the vertical motion field in the middle thermosphere from satellite drag densities. Private Communication.

Dickinson, R.E. and Geller, M.A., 1968: A generalization of "Tidal theory with Newtonian cooling", J. Atmos. Sci. 25, 932.

Dickinson, R.E., Lagos, C.P. and Newell, R.E., 1968: On the dynamics of the neutral gas in the thermosphere for small Rossby number motions. Submitted to J. Geophys. Res.

Donahue, T.M., 1966: Ionospheric reaction rates in the light of recent measurements in the ionosphere and the laboratory. Planet. Space Sci. 14, 33.

Dougherty, J.P., 1963: Some comments on dynamo theory. J. Geophys. Res. 68, 2383.

Eliassen, A., 1949: The quasi-static equations of motion with pressure as independent variable. Geofisiske publikasjoner, Norske Videnskaps-Akademi, Oslo, 17, No. 3.

Flattery, T.W., 1967: Hough functions. Technical Rept. No. 21, Dept. of Geophys. Sci., University of Chicago, 175 pp.

Geisler, J.E., 1966: Atmospheric winds in the middle latitude F-region.

J. Atmos. Terr. Phys. 28, 703.

_____, 1967: A numerical study of the wind system in the middle thermosphere. J. Atmos. Terr. Phys. 19. In press.

Goldstein, S., 1960: Lectures on fluid mechanics. Interscience Publishers, London. New York.

Greenspan, H.P., 1964: On the transient motion of a contained rotating fluid. J. Fluid Mech. 20, part 4, 673.

Hanson, W.B., 1963: Electron temperature in the upper atmosphere. Space Res. III, 282.

_____, 1965: Structure of the ionosphere. In "Satellite Environmental Handbook" (Johnson, ed.), Stanford Univ. Press, Stanford, California, 155 pp.

Hanson, W.B. and Cohen, R., 1968: Photoelectron heating efficiency in the ionosphere. J. Geophys. Res. 73, 831.

Harris, I. and Priester, W., 1962: Time-dependent structure of the upper atmosphere. J. Atmos. Sci. 19, 286.

_____, 1965: Of the diurnal variation of the upper atmosphere. J. Atmos. Sci. 22, 3.

_____, 1969: On the semiannual variation of the upper atmosphere. J. Atmos. Sci. 26, 233.

Hildebrand, F.B., 1956: Introduction to numerical analysis. McGraw-Hill, 511 pp.

Hines, C., 1965: Dynamical heating of the upper atmosphere. J. Geophys. Res. 70, 177.

Hintereger, H.E., 1965: Absolute intensity measurements in the extreme ultraviolet spectrum of solar radiation. Space Sci. Rev. 4, 461.

Hinteregger, H.E., Hall, L.A. and Schmidtke, G., 1965: Solar XUV radiation and neutral particle distribution in July 1963 thermosphere. Space Research V, 1175. North-Holland Pub. Co.

Hough, S.S. 1897: On the application of harmonic analysis to the dynamical theory of the tides. Phil. Trans. Roy. Soc. London A. 189, 201.

_____, 1898: On the application of harmonic analysis to the dynamical theory of the tides: Part II, On the general integration of

Laplace's dynamical equations. Phil. Trans. A. 191, 139.

Hunt, D.C. and T.E. Van Zandt, 1961: Photoionization heating in the F-region of the atmosphere. J. Geophys. Res. 66, 1673.

Jacchia, L.C., 1965: The temperature above the thermopause. Space Res. V, 1152.

_____, 1967: Recent results in the atmospheric region above 200 km and comparison with CIRA 1965. Smithson. Astrophys. Obs. Spec. Rept., No. 245, 25 pp.

Jacchia, L.G. and Slowey, J.W., 1967: The shape and location of the diurnal bulge in the upper atmosphere. Space Res. VII, Part 2, Amsterdam, North-Holland Publ. Co., 1077.

Karplus, R., Francis, W.E. and Dragt, A.J., 1962: Attenuation of hydromagnetic waves in the ionosphere. Planet. Space Sci. 9, 771.

Kato, S., 1956: Horizontal wind systems in the ionospheric E regions deduced from the dynamo theory of the geomagnetic Sq variation. 2, Rotating earth. J. Geomagnet. Geoelec., Kyoto, 8, 24.

_____, 1962: Joule heating and temperature in the upper atmosphere. Planet. Space Sci. 9, 939.

_____, 1966: Diurnal atmospheric oscillation, 1, eigenvalues and Hough functions. J. Geophys. Res. 71, 3, 201.

Keating, G.M. and Prior, E.J., 1967: The winter helium bulge, paper presented at the 1967 IQSY/COSPAR Assembly, London, England, July 17-29, 1967.

King-Hele, D.G. and Allan, R.R., 1966: The rotational speed of the upper atmosphere: a review. Space Sci. Rev. 6, 248.

King-Hele, D.G. and Scott, D.W., 1966: A revaluation of the rotational speed of the upper atmosphere. Planet. Space Sci. 14, 1339.

Konowalow, D.D., Hirschfelder, J.O. and Linder, B., 1959: Low-temperature, low-pressure transport coefficients for gaseous oxygen and sulfur atoms. J. Chem. Phys. 31, 1575.

Krasovskij, V.I. and Sefov, N.N., 1965: Airglow. Space Sci. Rev. 4, 176.

Kuhn, W.R. and London, J., 1969: Infrared radiative cooling in the middle atmosphere (30-110 km). J. Atmos. Sci. 26, 189.

Lagos, C.P., 1967: On the dynamics of the thermosphere. Rept. No. 20,

Dept. of Meteor., M.I.T., 134 pp.

_____, 1968: The role of vertical motions in the thermospheric dynamics. Trans. American Geophys. Union, 49, 181.

Lagos, C.P. and Mahoney, J.R., 1967: Numerical studies of seasonal and latitudinal variability in a model thermosphere. J. Atmos. Sci. 24, 88.

Laplace, P.S., 1799, 1825: Mècanique Cèleste, Paris.

Lasorev, V., 1964: Ionizing radiation and heating of the upper atmosphere. Space Res. IV, 516.

Lindzen, R.S., 1966a: Crude estimate for the zonal velocity associated with the diurnal temperature oscillation in the thermosphere. J. Geophys. Res. 71, 865.

_____, 1966b: On the theory of the diurnal tide. Mon. Wea. Rev. 94, 295.

_____, 1967a: Reconsideration of diurnal velocity oscillation in the thermosphere. J. Geophys. Res. 72, 1591.

_____, 1967b: Thermally driven diurnal tide in the atmosphere. Quart. J. Roy. Meteor. Soc., 93, 18.

Longuet-Higgins, M.S., 1967: The eigenfunctions of Laplace's tidal equations over a sphere. Private Communication.

Lorenz, E.N., 1967: The nature and theory of the general circulation of the atmosphere. World Meteor. Organization, No. 218, TP, 115.

Mahoney, J.R., 1966: A study of energy sources for the thermosphere. Rept. No. 17, Dept. of Meteor., M.I.T., 218 pp.

Matsushita, S., 1967: Lunar tides in the ionosphere. In "Handbuch der Physik" (Flugge, ed.), 59/2, p. 547-602.

May, B.R., 1966: The effect of a rotation of the atmosphere on the calculated diurnal variation of upper-air density and temperature. Planet. Space Sci. 14, 657.

McClure, J.P., 1969: Diurnal variation of neutral and charged particle temperatures in the equatorial F region. J. Geophys. Res. 74, 279.

Moe, K., 1963: Dependence on latitude of atmospheric heating during magnetic storms. Nature 201, 481.

Nagy, A.F., Fontheim, E.G., Stolarska, R.S., and Beutler, A.E., 1969: Ionospheric electron temperature calculations including protonospheric and conjugate effects. To be published in J. Geophys. Res.

Newell, R.E. 1966: Thermospheric energetics and a possible explanation of some observations of geomagnetic disturbances and radio aurorae, Nature 211, 700.

_____, 1967: The semi-annual variation in thermospheric density. Nature 217, 150.

_____, 1968: The general circulation of the atmosphere above 60 km. In "Meteorological Investigations of the Upper Atmosphere" (Quiroz, ed.). Meteorological Monographs, Vol. 9, No. 31, p 98-113.

Nicolet, M., 1960: The properties and constitution of the upper atmosphere. In "Physics of the Upper Atmosphere" (Ratcliff, ed.), Academic Press.

_____, 1965: Ionospheric processes and nitric oxide. J. Geophys. Res. 70, 691.

Nisbet, J.S., 1968: Photoelectron escape from the ionosphere. J. Atmos. Terr. Phys. 30, 1257.

O'Brien, B.J., Allum, F.R. and Goldwire, H.C., 1965: Rocket measurement of midlatitude airglow and particle precipitation. J. Geophys. Res. 70, 161.

Pedlosky, J., 1964: The stability of currents in the atmosphere and the ocean: Part I. J. Atmos. Sci. 21, 201.

Phillips, N.A., 1963: Geostrophic motion. Rev. Geophys. 1, 123.

Piddington, J.A., 1954: The motion of ionized gas in combined magnetic, electrical and mechanical fields of force. Mon. Not. Roy. Astronomical Soc. 114, 651.

Priester, W., Roemer, M. and Volland, H., 1967: The physical behavior of the upper atmosphere deduced from satellite drag data. Space Sci. Rev. 6, 707.

Rishbeth, H., 1967: The effect of winds on the ionospheric F2-peak. J. Atmos. Terr. Phys. 29, 225.

Rishbeth, H., Megill, L.R. and Cahn, J., 1965: The effect of ion-drag on the neutral air in the ionospheric F-region. Annales de Geophysique 21, 235.

Sharp, R.D., Evans, J.E. and Johnson, R.G., 1966: Measurements of particle precipitation at the South Pole. Planet. Space Sci. 14, 85.

Sharp, R., Evans, J. Imhof, W., Johnson, R.G., Reagan, J.B. and Smith, R.V., 1964: Satellite measurements of low energy electrons in the northern auroral zone. J. Geophys. Res. 69, 2721.

Sharp, R., Evans, J., Johnson, R. and J. Reagan, 1965: Measurement of total energy flux of electrons precipitating on auroral zones. Space Res. V, 282.

Sharp, R.D., Johnson, R.G., Shea, M.F., and Shook, G.B., 1967: Satellite measurements of precipitating protons in the auroral zone. J. Geophys. Res. 72, 227.

Siebert, M., 1961: Atmospheric tides. Advance Geophys. 7, 105.

Spreiter, J.R., Summers, A.L. and Alksne, A.Y., 1966: Hydromagnetic flow around the magnetosphere. Planet. Space Sci. 14, 223.

Starr, V.P., 1968: Physics of negative viscosity phenomena. McGraw-Hill, Inc., New York.

Volland, H., 1966: A two-dimensional dynamic model of the thermosphere, Part I. Theory, J. Atmos. Sci. 23, 799.

_____, 1967: On the dynamics of the upper atmosphere. Space Res. VII, North-Holland Publ. Co., Amsterdam.

Wallace, L. and McElroy, M.B.M., 1966: The visual dayglow, Planet. Space Sci. 14, 677.

Wilkes, M.V., 1949: Oscillations of the earth's atmosphere. Cambridge Univ. Press, Cambridge.

Wright, J.N., 1962: Dependence of the ionospheric F region on the solar cycle. Nature 194, 461.

Yanowitch, M., 1967: Effect of viscosity on gravity waves and the upper boundary condition. J. Fluid Mech. 29, 209.

Appendix I: Energy Equation for a Single Fluid Plasma Approximation

The energy equation of a single fluid plasma under the action of mechanical and magnetic changes for the special case of low frequency oscillations of a conducting fluid are derived in this appendix. It is shown that when an external magnetic field is applied the pressure, the internal energy and the reversible work done on a fluid have two components, the mechanical and magnetic parts. When these modifications are considered together the thermodynamic equations for gas dynamics remain unaltered except with the additional heat source due to Joule

The usual hydromagnetic approximation amounts to the omission of the displacement current in Ampere's law and consequently neglect Coulomb's law, thus Maxwell's equations are

$$\nabla \times \underset{\sim}{E} = -\frac{\partial \underset{\sim}{B}}{\partial t} \quad , \quad \nabla \times \underset{\sim}{B} = \underset{\sim}{J}$$
$$\nabla \cdot \underset{\sim}{B} = 0 \qquad\qquad \underset{\sim}{J} = \sigma \cdot (\underset{\sim}{E} + \underset{\sim}{V} \times \underset{\sim}{B}) \tag{I.1}$$

where the symbols are defined in section 2.1.

The fluid is supposed to be non-magnetic and hence its permeability is taken as unity. The hydrodynamic equations are (2.1) - (2.4).

In addition to the above equations, we have the following relations: The electromagnetic energy per unit volume

$$M = 1/2\ B^2 \tag{I.2}$$

The energy flow which is the Poynting vector

$$\underset{\sim}{N} = \underset{\sim}{E} \times \underset{\sim}{B} \tag{I.3}$$

and the Maxwell stress tensor

$$T_{ij} = B_i\ B_j - 1/2\ \delta_{ij}\ B^2 \tag{I.4}$$

In a moving fluid with velocity $\underset{\sim}{v}$ the relationship between the electromagnetic field vectors $\underset{\sim}{E}^*$, $\underset{\sim}{B}^*$ and the current density $\underset{\sim}{J}^*$ in the local frame, and $\underset{\sim}{E}$, $\underset{\sim}{B}$ and $\underset{\sim}{J}$ in the laboratory frame are given by

$$\begin{aligned} \underset{\sim}{E}^* &= \underset{\sim}{E} + \underset{\sim}{V} \times \underset{\sim}{B} \\ \underset{\sim}{B}^* &= \underset{\sim}{B} - \underset{\sim}{V} \times \underset{\sim}{E} \\ \underset{\sim}{J}^* &= \underset{\sim}{J} \end{aligned} \tag{I.5}$$

and the Poynting vector is similarly transformed according to (I.5).

The derivation of the energy equation here follows closely the analysis by Chu (1959), who has discussed the thermodynamics of a general electrically conducting fluid including the displacement current and the dependence of dielectric constant and the permeability on the state of the fluid.

The thermodynamic pressure due to the joint action of the mechanical and magnetic changes can be written as the sum of two parts

$$p = p^{(o)} + p^{(m)} \tag{I.6}$$

where

$$p^{(o)} = R\rho T \ , \qquad p^{(m)} = 1/2 \ B^2 \tag{I.7}$$

Similarly the internal energy U due to the joint action of the mechanical and magnetic changes can be written

$$U = U^{(o)} + U^{(m)} \tag{I.8}$$

where

$$U^{(o)} = C_v T \ , \qquad U^{(m)} = 1/2 \ B^2/\rho \tag{I.9}$$

and the stress tensor

$$\tau_{ij} = \tau_{ij}^{(o)} + \tau_{ij}^{(m)} \tag{I.10}$$

where

$$\tau_{ij}^{(o)} = - p^{(o)}\delta_{ij} + \pi_{ij} \tag{I.11}$$

$$\tau_{ij}^{(m)} = - p^{(m)}\delta_{ij} + B_i B_j \tag{I.12}$$

and where the viscous stress tensor π_{ij} is given by (cf. equation (2.7))

$$\pi_{ij} = \mu\left(\frac{\partial v_i}{\partial x_j} + \frac{\partial v_j}{\partial x_i}\right) - \frac{2}{3}\mu \frac{\partial v_k}{\partial x_k}\delta_{ij} \tag{I.13}$$

The momentum equation for the single mechanical and electromagnetic system can be rewritten (omitting the coriolis force, see equation (2.1))

$$\rho \frac{dv_j}{dt} = \frac{\partial \tau_{ij}}{\partial x_i} + \rho F_j \tag{I.14}$$

where F_j is the external body force per unit mass acting on the fluid. The electromotive force $\underset{\sim}{J} \times \underset{\sim}{B}$ is included in τ_{ij}. This can be see as follows,

$$\begin{aligned} \underset{\sim}{J} \times \underset{\sim}{B} &= \underset{\sim}{B}(\nabla \cdot \underset{\sim}{B}) - \underset{\sim}{B} \times (\nabla \times \underset{\sim}{B}) \\ &= \underset{\sim}{B}(\nabla \cdot \underset{\sim}{B}) + (\underset{\sim}{B} \cdot \nabla)\,\underset{\sim}{B} - 1/2\ \nabla\, \underset{\sim}{B}^2 \end{aligned} \tag{I.15}$$

which can be identified as the divergence of a dyadic:

$$\begin{aligned} \underset{\sim}{B}\,(\nabla \cdot \underset{\sim}{B}) + (\underset{\sim}{B} \cdot \nabla)\,\underset{\sim}{B} - 1/2\ \nabla\, B^2 &= \nabla \cdot (\underset{\sim}{B}\underset{\sim}{B} - 1/2\ \overleftrightarrow{I}\, B^2) \\ &= \nabla \cdot \overleftrightarrow{T} \end{aligned} \tag{I.16}$$

where $\overleftrightarrow{T}$ is the tensor-dyadic, the magnetic part of Maxwell's stress

tensor. The elements of this tensor are

$$T_{ij} = B_i B_j - 1/2\ \delta_{ij}\ B^2 = -\ p^{(m)}\delta_{ij} + B_i B_j$$
$$= \tau_{ij}^{(m)} \tag{I.17}$$

Hence

$$\underset{\sim}{J} \times \underset{\sim}{B} = \frac{\partial}{\partial x_i}\ \tau_{ij}^{(m)}$$

The continuity equation (2.2) will be sued in the form

$$\frac{dv_j}{dx_j} = \rho\ \frac{d}{dt}\ (\frac{1}{\rho}) \tag{I.18}$$

The equation of energy balance for a mass of fluid may be written as

$$W_s + W_b + C + Q + N = K + U \tag{I.19}$$

where W_s is the rate of work done by the surface stresses, W_b the rate of work done by external body forces, C the rate of heat energy conducted, Q the rate of heat energy added by radiation and chemical action N the rate of energy radiated, and K and U are the rate of increase of kinetical and internal energy of the mass. That is,

$$\int \tau_{ij}\ v_j\ d\underset{\sim}{s} + \int \rho\ F_j\ v_j\ dv + \int (KV\ T) \cdot d\underset{\sim}{s}$$
$$+\ \int \rho Q\ dv - \int (\underset{\sim}{E}^* \times \underset{\sim}{B}^*) \cdot d\underset{\sim}{s} = \frac{d}{dt} \int \rho\ (1/2V^2 + U)\ dv \tag{I.20}$$

and making use of Gauss's theorem, (I.20) becomes

$$\rho\ \frac{d}{dt}\ (\frac{1}{2}\ V^2 + U) = \frac{\partial \tau_{ij} V_j}{\partial x_i} + \rho \underset{\sim}{F} \cdot \underset{\sim}{V} + \nabla\cdot(KV\ T) + \rho Q - \nabla\cdot\ (\underset{\sim}{E}^* \times \underset{\sim}{B}^*)$$

(I.21)

Next we derive an expression for the work done by the stresses and body forces. Using (I.14) and (I.18) we can write

$$\frac{\partial \tau_{ij} V_j}{\partial x_i} + \rho F_j V_j = V_j \left(\frac{\partial \tau_{ij}}{\partial x_i} + \rho F_j\right) + \gamma_{ij} \frac{\partial V_j}{\partial x_i}$$

$$= V_j \left(\rho \frac{dV_j}{dt}\right) - p \frac{\partial V_j}{\partial x_i} + B_i B_j \frac{\partial V_i}{\partial x_i} + \pi_{ij} \frac{\partial V_j}{\partial x_i}$$

$$= \rho \left[\frac{d}{dt}\left(\frac{V^2}{2}\right) - p \frac{d}{dt}\left(\frac{1}{\rho}\right)\right] + \underset{\sim}{B} \cdot (\underset{\sim}{B} \cdot \nabla)\underset{\sim}{V} + \Phi \tag{I.22}$$

Now

$$\underset{\sim}{B} \cdot (\underset{\sim}{B} \cdot \nabla)\underset{\sim}{V} = (\underset{\sim}{B} \cdot \nabla)(\underset{\sim}{V} \cdot \underset{\sim}{B}) - \underset{\sim}{V} \cdot (\underset{\sim}{B} \cdot \nabla)\underset{\sim}{B}$$
$$= \nabla \cdot [\underset{\sim}{B} (\underset{\sim}{V} \cdot \underset{\sim}{B})] - \underset{\sim}{V} \cdot (\underset{\sim}{B} \cdot \nabla)\, \underset{\sim}{B} \tag{I.23}$$

$$\underset{\sim}{E}^* \times \underset{\sim}{B}^* = \underset{\sim}{E} \times \underset{\sim}{B} - \underset{\sim}{B} \times (\underset{\sim}{V} \times \underset{\sim}{B}) = \underset{\sim}{B} (\underset{\sim}{V} \cdot \underset{\sim}{B}) - \underset{\sim}{V} (\underset{\sim}{B} \cdot \underset{\sim}{B}) \tag{I.24}$$

$$\nabla \cdot (\underset{\sim}{E}^* \times \underset{\sim}{B}^*) = \nabla \cdot (\underset{\sim}{E} \times \underset{\sim}{B}) + \nabla \cdot [\underset{\sim}{B} (V \cdot \underset{\sim}{B})] - \nabla \cdot [\underset{\sim}{V} (\underset{\sim}{B} \cdot \underset{\sim}{B})] \tag{I.25}$$

$$\nabla \cdot (\underset{\sim}{E} \times \underset{\sim}{B}) = - \underset{\sim}{E} \cdot \nabla \times \underset{\sim}{B} + \underset{\sim}{B} \cdot \nabla \times \underset{\sim}{E} = - \underset{\sim}{J} \cdot \underset{\sim}{E} - \underset{\sim}{B} \cdot \frac{\partial \underset{\sim}{B}}{\partial t} \tag{I.26}$$

thus (I.23) can be rewritten

$$\underset{\sim}{B} \cdot (\underset{\sim}{B} \cdot \nabla)\underset{\sim}{V} = \nabla \cdot (\underset{\sim}{E}^* \times \underset{\sim}{B}^*) + (\underset{\sim}{B} \cdot \underset{\sim}{B}) \nabla \cdot \underset{\sim}{V} + \underset{\sim}{B} \cdot (\underset{\sim}{V} \cdot \nabla)\underset{\sim}{B} + \underset{\sim}{J} \cdot \underset{\sim}{E}$$
$$+ \underset{\sim}{B} \cdot \frac{\partial \underset{\sim}{B}}{\partial t} - \underset{\sim}{V} \cdot (\underset{\sim}{B} \cdot \nabla)\underset{\sim}{B}$$
$$= \nabla \cdot (\underset{\sim}{E}^* \times \underset{\sim}{B}^*) + (\underset{\sim}{B} \cdot \underset{\sim}{B}) \nabla \cdot \underset{\sim}{V} + \underset{\sim}{B} \frac{\partial \underset{\sim}{B}}{\partial t} + \underset{\sim}{B} \cdot (\underset{\sim}{V} \cdot \nabla)\underset{\sim}{B} \tag{I.27}$$
$$+ \underset{\sim}{J} \cdot \underset{\sim}{E} - \underset{\sim}{V} \cdot (\underset{\sim}{J} \times \underset{\sim}{B})$$

or

$$\underset{\sim}{B}\cdot(\underset{\sim}{B}\cdot\nabla)\underset{\sim}{V} = \nabla\cdot(\underset{\sim}{E}^{*}\times\underset{\sim}{B}^{*}) + \underset{\sim}{J}\cdot\underset{\sim}{E} - \underset{\sim}{V}\cdot(\underset{\sim}{J}\times\underset{\sim}{B}) + \rho[\underset{\sim}{B}\cdot\frac{d}{dt}(\frac{\underset{\sim}{B}}{\rho})] \tag{I.28}$$

Hence (I.22) becomes

$$\frac{\partial\tau_{ij}V_j}{\partial x_i} + \rho F_j V_j = \rho[\frac{d}{dt}(\frac{V^2}{2}) - p\frac{d}{dt}(\frac{1}{\rho}) + \underset{\sim}{B}\cdot\frac{d}{dt}(\frac{\underset{\sim}{B}}{\rho})] + \nabla\cdot(\underset{\sim}{E}^{*}\times\underset{\sim}{B}^{*}) + \underset{\sim}{J}\cdot\underset{\sim}{E} - \underset{\sim}{V}\cdot(\underset{\sim}{J}\times\underset{\sim}{B}) + \Phi \tag{I.30}$$

therefore the energy equation (I.21) becomes

$$\rho[\frac{dU}{dt} + p\frac{d}{dt}(\frac{1}{\rho}) - \underset{\sim}{B}\cdot\frac{d}{dt}(\frac{\underset{\sim}{B}}{\rho})] = \nabla\cdot(K\nabla T) + \underset{\sim}{J}\cdot\underset{\sim}{E} - \underset{\sim}{V}\cdot(\underset{\sim}{J}\times\underset{\sim}{B}) + \Phi + \rho Q \tag{I.29}$$

where again p and U are the pressure and internal energy due to the joint action of mechanical and electromagnetic effects.

Using the second law of thermodynamics, we see that

$$\begin{aligned} Tds &= dU + pd(\frac{1}{\rho}) - \underset{\sim}{B}\cdot\frac{d}{dt}(\frac{\underset{\sim}{B}}{\rho}) \\ &= dU^{(o)} + p^{(o)}d(\frac{1}{\rho}) \\ &= Tds^{(o)} \end{aligned} \tag{I.31}$$

where $s^{(o)}$ is the mechanical entropy.

Hence (I.30) the energy equation becomes, dropping the upperscript on s,

$$\rho T\frac{ds}{dt} = \nabla\cdot(K\nabla T) + \underset{\sim}{J}\cdot(\underset{\sim}{E} + \underset{\sim}{V}\times\underset{\sim}{B}) + \Phi + \rho Q \tag{I.32}$$

Appendix II: Pondermotive Force and Ion Drag

The basic effect of a magnetic field on the dynamics of a conducting fluid is accounted for by the pondermotive force per unit mass, which in our fluid is the magnetic component of the Lorentz force,

$$\underset{\sim}{F}_I = \frac{1}{\rho} (\underset{\sim}{J} \times \underset{\sim}{B}) \tag{II.1}$$

where $\underset{\sim}{J}$ is the current density, $\underset{\sim}{B}$ the magnetic induction, and ρ the density of the fluid. The current density, in turn, is related to the electric and magnetic fields by

$$\underset{\sim}{J} = \boldsymbol{\sigma} \cdot \underset{\sim}{E}' = \quad \cdot(\underset{\sim}{E} + \underset{\sim}{V} \times \underset{\sim}{B}) \tag{II.2}$$

where $\underset{\sim}{E}$ is the polarization electric field, $\underset{\sim}{v}$ the velocity and $\hat{\boldsymbol{\sigma}}$ the anisotropic electric conductivity tensor.

Substitution of (II.2) in the formula for $\underset{\sim}{F}_I$, give the expression for this vector as

$$F_{iI} = \sum_{jmk} \varepsilon_{ijk} \boldsymbol{\sigma}_{jm} E'_m B_k \tag{II.3}$$

This expression is simplified by assuming that the vertical current flow can be neglected and by expressing $\underset{\sim}{B}$ in the form

$$\underset{\sim}{B} = (- \cos I \hat{j} - \sin I \hat{K})B \tag{II.4}$$

where I denotes the magnetic dip angle. The λ and ϕ - components of $\hat{F}_I$ are

$$\begin{aligned} F_{\lambda I} &= \sigma_{\lambda\lambda} (U_d - U)B^2\sin^2 I + \sigma_{\lambda\phi} (v_d - v)B^2\sin^2 I \\ F_{\phi I} &= \sigma_{\phi\phi} (v_d - v)B^2\sin^2 I - \sigma_{\lambda\phi} (U_d - U)B^2\sin^2 I \end{aligned} \tag{II.5}$$

where U_d and v_d are the components in the λ and ϕ directions of the drift velocity $\underset{\sim}{E} \times \underset{\sim}{B}/|\underset{\sim}{E}|^2$ and the components of the conductivity tensor are given by (Chapman 1956)

$$\sigma_{\lambda\lambda} = K^{-1}\sigma_1 \sigma_o$$

$$\sigma_{\lambda\phi} = K^{-1}\sigma_2 \sigma_o \sin I$$

$$\sigma_{\phi\phi} = K^{-1}(\sigma_1 \sigma_o \sin^2 I + \sigma_1 \sigma_3 \cos^2 I) \qquad \text{(II.6)}$$

$$\sigma_3 = \sigma_1 + \sigma_2^2 / \sigma_1$$

$$K = \sigma_1 \cos^2 I + \sigma_o \sin^2 I$$

and where σ_o, σ_1 and σ_2 are given by (Chapman and Bartels, 1940)

$$\sigma_o = (n_i e/B)[(\omega_i/\nu_i) + (\omega_e/\nu_e)]$$

$$\sigma_1 = (n_i e/B)[\omega_i\nu_i/(\omega_i^2 + \nu_i^2) + \omega_e\nu_e/(\omega_e^2 + \nu_e^2)] \qquad \text{(II.7)}$$

$$\sigma_2 = (n_i e/B)[\omega_e^2/(\omega_i^2 + \nu_i^2) - \omega_i^2/(\omega_i^2 + \nu_i^2)]$$

where n_e, n_i and n_n are the number densities of electrons, ionized and neutral molecules, e is the absolute value of their charge, $\omega_i = n_i eB/\rho_i$, $\omega_e = n_e eB/\rho_e$ are gyrofrequencies, ρ_e and ρ_i are the densities of electrons and ionized molecules, ν_e and ν_i are the electron-neutral and ion-neutral collision frequencies. In the middle and upper thermosphere the following inequalities $\sigma_o >> \sigma_1 > \sigma_2$, $\omega_e >> \omega_i$ $\omega_e >> \nu_e$ and $\nu_i >> \nu_e$ are satisfied. Hence the expressions for $F_{\lambda I}$ and $F_{\phi I}$ are

$$F_{\lambda I} = \frac{n_i \nu_i / n_n}{1 + \rho_+^2} [(U_d - U) + \rho_+ (v_d - v) \sin I$$

$$F_{\phi I} = \frac{n_i \nu_i / n_n}{1 + \rho_+^2} [(v_d - v) \sin^2 I - \rho_+ (U_d - U) \sin I \qquad \text{(II.8)}$$

where $\rho_+ = \nu_i / \omega_i$. A somewhat similar analysis has been given by Piddington (1954).